The Pennsylvania State University

The Graduate School

College of Earth and Mineral Sciences

ELECTROPHORETIC DEPOSITION: FUNDAMENTALS, MECHANISMS AND EXAMPLES WITH AN IN DEPTH EXAMINATION OF THE ION DEPLETION EFFECT

A Thesis in

Materials Science and Engineering

by

Jonathan J. Van Tassel

Submitted in Partial Fulfillment
of the Requirements
for the Degree of

Doctor of Philosophy

May 2004

ABSTRACT

The research and analysis for this thesis have been directed toward two major goals: to better understand the process of electrophoretic deposition (EPD) and to demonstrate its utility. This is also the order in which these two topics are addressed in the writing of this thesis.

In order to define the limits of the problem, the first chapter is devoted to a description and definition of what is, and is not, EPD. Here EPD is defined as consisting of three steps. The first is the creation of a charge balanced suspension of electrostatically charged particles in a solvent where some mechanism acts to keep the particles from flocculating together during the time necessary to perform EPD. The second step is to create and maintain a DC electric field within the bulk of the solvent causing the electrostatically charged particles to move by electrophoresis toward an electrode. The final step is then to induce a change the nature of the suspension next to the electrode so that particles come into contact with each other and form a rigid deposition.

Chapter 2 then gives an outline of the scientific background necessary for understanding each of the three steps defined in Chapter 1. In order to make the complexity of the EPD system intellectually manageable, it is broken down into three components; solvent, particles, and electric field. Even though the scientific literature specifically on EPD is relatively modest, the literature on the binary interactions between each of these components (solvent-electric field, solvent-particle, etc.) is both extensive and elucidating. Previous reviews on EPD have concentrated almost exclusively on solvent-particle interactions. This thesis shows the vital importance of electrochemical reactions at the deposition electrode in understanding the mechanisms of deposition.

This approach also allows the categorization of mechanisms of EPD already demonstrated in the literature as well as the prediction of new mechanisms not previously demonstrated. To do this a list of mechanisms to prevent particles from flocculating in the bulk suspension is compared to a list of effects that can be induced in the suspension at the deposition electrode. The list of specific near-electrode effects that can cause particles from specific types of suspensions to floc or coagulate at the electrode then becomes a list of the possible mechanisms of EPD. One of the most interesting of these mechanisms, ion depleted enhanced - automatic leveling deposition, was chosen for in-depth analysis.

The first step in this analysis is to obtain a complete understanding of the suspension from which the particles are to be deposited. This is done in Chapter 3 for alumina powder in ethanol with added HCl. Here it is shown that in the absence of dissolved ions alumina develops a significant positive surface charge in ethanol by the dissociative adsorption of ethanol molecules to the surface and the preferential desorption of ethoxide ions from the surface. The addition of HCl leads to a large rise in surface charge due initially to the reduction in ethoxide activity. After this initial rise the surface charge is set by a competitive adsorption equilibrium of chloride and ethoxide ions to positive surface sites on the powder.

Chapter 4 is then devoted to analyzing the deposition of alumina from this system. The first part of this chapter is detailed analysis of the conduction layer next to the cathode, the deposition electrode for the positively charged particles. The development of ionic and charge gradients, and the inevitability of a transition to convective transport at the electrode is shown for the electrolyte in the absence of particles. It is then shown that the dramatic change in conduction behavior in the presence of particles can be accounted for by the stabilization of an ion depleted, unbalanced charge conduction layer. Extremely high voltage gradients in this layer then exert a strong consolidating force on the positively charged alumina particles, compacting them into a densely packed deposited layer. This high gradient also leads to a strong equilibrating force to maintain a uniform thickness of the compact deposited layer, the automatic leveling effect.

The second objective here has been to demonstrate the potential utility of EPD in addressing current problems in the manufacture of electroceramic devices. This is undertaken in Chapter 5 with a complete description of the process to form suspensions, deposit particles, process these depositions into final form and to characterize the component created. The direct electrostatic deposition of silver/palladium powder is used to demonstrate the ability of EPD to create both very thin layers and very narrow conductor lines that can be measured on the scale of the particles used to create them. The electrophoretic deposition of PZT is used to demonstrate the formation of an intermediate thickness film with well controlled stoichiometry.

In the final chapter the thesis concludes with a discussion of what still needs to be done to advance the understanding and application of EPD.

TABLE OF CONTENTS

LIST OF FIGURES

LIST OF TABLES

Symbols used in Chapter 3

Fundamental constants

e Elementary charge (1.602E-19 C)

k Boltzman Constant (1.381E-23 J/K)

ε_o Permitivitty of free space (8.854E-12 C^2/J·m)

General symbols

a Particle radius (m)

a_O Geometric mean distance of closest approach of ions in solution (nm)

E Reduced electrophoretic mobility (non-dimensional)

EtO$^-$ Ethoxide ion

HEtO Ethanol molecule

K_S Solvent autoprotolysis equilibrium constant

pa_{H^+}* -Log$_{10}$ a_{H^+}* where $a_{H^+}^* \equiv \frac{[H_+]}{[H_+^\circ]}$ at infinite dilution in the solvent.

pHi Indicated pH (pH meter display)

pH* Operational pH (equal to pa_{H^+}* in dilute solutions.)

q Surface charge density (C/m^2)

Ss Surface adsorption site

T Temperature (K)

u_E Particle electrophoretic mobility (μm·cm/V·s)

z Ion valence

f_- Activity coefficient for negative ion at particle surface

f_+ Activity coefficient for positive ion at particle surface

$f_\pm$ Activity coefficient for ions in bulk solution

δ Conversion constant between pHi and pH* for a given solvent and reference electrode combination.

ε_r Relative dielectric constant

η Solvent Viscosity (Poise)

κ Inverse Debye length (m^{-1})

ρ_∞ Density of dissociated molecules of a binary salt in bulk solution (m^{-3})

ζ Particle Potential at Shear Layer (mV)

$\tilde{\zeta}$ Reduced particle potential at shear layer (non-dimensional)

$[x]$ Molar concentration of chemical species x

$[x^\circ]$ Standard concentration of chemical species x (usually 1 molar)

Conductivity

Λ Molar conductivity (μS·dm^3/cm·Mol)

Λ_O Molar limit conductivity (μS·dm^3/cm·Mol)

c Molar concentration of dissolved salt (Mol/dm^3)

α Dissociated fraction of dissolved salt

K_A Association constant for oppositely charged ions in solution

Electroacoustics

δ Pressure wave decay parameter for acoustophoresis

ω Measurement frequency in acoustophoresis (s^{-1})

ρ Solvent density in acoustophoresis

Chapter 3

Surface Chemistry and Surface Charge Formation for an Alumina Powder in Ethanol

3.1 Introduction

As has been mentioned in previous chapters, there have been relatively few studies that have attempted to analyze the deposition process in a quantitative manner. This due in large part to the complex, dynamic and non-equilibrium electrochemical environment near the deposition electrode. References (**1-3**) are some of the most notable exceptions to this rule.

To venture a quantitative analysis of a particular deposition requires a quantitative knowledge of the interaction between the particles, the suspending solvent and the ions dissolved in that solvent. Therefore, the objective of this chapter is to develop a model of the surface chemical reactions on the depositing powder sufficient to predict its behavior in the unique chemical environment near the deposition electrode. This means developing mathematical models of the particle adsorption isotherms for individual ions, independent of the activity of their co-ions. These adsorption isotherms are then critical for the deposition analysis presented in Ch.4.

The alumina-ethanol system analyzed here was chosen for simplicity, stability and the level of information available in the literature on the system components. Alumina was chosen as the powder component for its low solubility and our own experiments showing that it could be washed easily to remove surface contaminants. Ethanol was chosen as a readily available, non-toxic solvent. Because ethanol is very hydrophilic, making and maintaining completely anhydrous ethanol is quite difficult. Therefore, ethanol with a known water content was used. Hydrochloric acid is a simple acid that is almost fully dissociated in low concentrations in ethanol, has been shown to raise the surface potential of alumina in ethanol, and has been used previously for EPD. (**4**)

3.2 Materials

Alumina - The powder used in this study is AKP-50, Sumitomo Chemical Co., Osaka, Japan. For particle size measurement the powder was dispersed in water using an ultrasonic horn, and size was measured by laser light scattering (Mastersizer, Malvern Instruments Ltd., Worcestershire, UK). The particle size distribution was bi-modal with 90 vol.% having an average size of 0.27μm and 10% an average 3μm. 10 vol.% of the powder was less than 130 nm. Surface area as measured by single point BET (Monosorb, Quantachrome Corp., Boynton Beach, Florida) is 10.0m^2/g. The powder is 100% α-phase by X-ray diffraction. The particles have an axisymmetric but angular morphology.

Ethanol - The ethanol used in this study is from Pharmco, Inc., Brookfield, Connecticut. The as-received water content is 0.045 wt.% as determined by Karl Fischer titration. The conductivity of the ethanol prior to water addition is less than 0.1 μS/cm. Deionized water, conductivity $\approx$ 0.5 μS/cm, was added to adjust the water content to 0.5 wt.%. The density of this mixture is 0.7866 g/cc by linear interpolation of literature data at 100% and 95% ethanol. This gives a 0.218 molar water concentration. The conductivity measured at the beginning of each of the titrations was less than 0.1 μS/cm.

It should be noted that the water content of the ethanol is very significant for the measurements made here. Small quantities of water will affect both the mobility of H^+ ions as well as level of association between the positive and negative ion.

In the pure solvent the ion is able to hop from molecule to molecule, passing through the solvent much more quickly than ordinary ionic migration. This is referred to as either anomalous proton conduction or the Grotthus mechanism. However if there is water present the proton can jump to a water molecule:

$$C_2H_5OH_2^+ + H_2O \Leftrightarrow C_2H_5OH + H_3O^+$$

De Lisi et al. have calculated the free energy of this reaction to be -14.01 kJ/mol. (**10**) Because of the strong forward bias of this reaction, protons will be trapped by water molecules in the ethanol and have to migrate through the solvent as hydronium ions significantly reducing the H^+ mobility. This is shown in Fig 1 from where the molar limit conductivity for HCl in ethanol drops by nearly fifty percent with the addition of the first 1 % of water added to the ethanol.

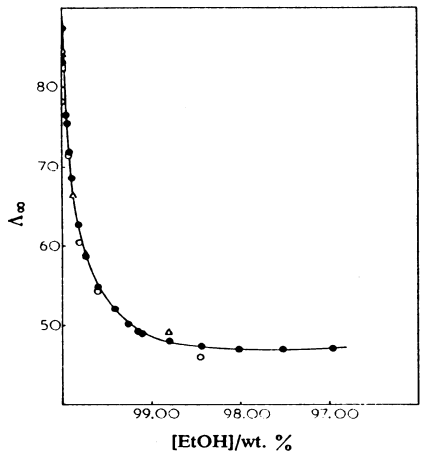

Fig. 3.1 Molar limit conductivity of HCl as a function of ethanol concentration with water. (**10**)

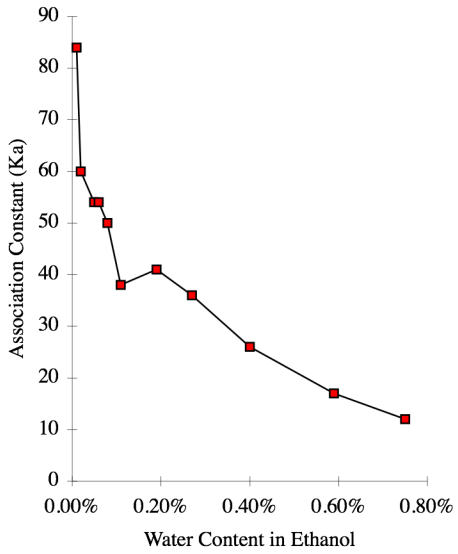

Fig. 3.2 Association constant of H^+ and Cl^- in ethanol as a function of water content. (**10**)

The second chart is a graph of data also from De Lisi et al. for the association constant between the positive ion and the chloride ion in solution as a function of water content:

$$Cl^- + H_3O^+ \Leftrightarrow Cl^-\bullet H_3O^+ \quad \text{or} \quad Cl^- + H_2EtO^+ \Leftrightarrow Cl^-\bullet H_2EtO^+$$

When the positive and negative ions are associated there will be no net migration in an electric field, therefore associated ions will not show up in a conductivity measurement.

The effect of these small quantities of water on the dielectric constant of the medium is small, therefore, this dramatic effect would not be predicted by a solvation model that considers the solvent as a continuous dielectric medium. A reasonable explanation is that water makes a solvation shell around the ions which has an effective dielectric constant much higher than the bulk of the solvent. The water molecules are attracted to the vicinity of the ions both by their higher dipole moment and by the break in the ethanol structure caused by the ions.

HCl - Hydrochloric acid was titrated from 0.103 and 0.0103 wt.% solutions in ethanol prepared by dilution of a 37 wt.% HCl/water azeotropic solution (Fisher Chemical Co., Pittsburgh, Pennsylvania) into ethanol. The HCl content was verified by pH titration in water against the KOH standard solution below. Water contents as calculated from

component compositions were 0.11 and 0.05 wt. % for the 0.1 and 0.01 wt. % solutions respectively.

KOH - 0.098 molar potassium hydroxide standard solution in ethanol (J. T. Baker Co., Phillipsburg, NJ.) was used for titration both in as-received form and diluted by a factor of ten using as-received ethanol above. Density of the 0.098 molar solution at 25.0°C was measured as 0.7887 g/cc. Water content was 0.45 wt.% as determined by Karl Fisher Titration. This equals a 0.197 molar water concentration.

3.3 Experimental Methods

3.3.1 Washing and Hydration of Powder Surface

To prevent the introduction of unknown ionizable compounds into the system, the alumina powder was washed thoroughly prior to use. 150 g of powder was placed into a 0.5 liter HDPE bottle and filled with de-ionized (D.I.) water. The bottle was heated to ≈60°C in a commercial microwave and shaken for ≈ 1 minute. The powder was allowed to sediment out for varying lengths of time, usually overnight. The conductivity of the supernatant was measured, the supernatant poured off, and the bottle refilled with D.I. water. This procedure was repeated until the room temperature conductivity of the supernatant was equal to or less than the conductivity of the D.I. wash water (≈0.5 μS/cm). For the powder used in this study this required nine rinsing cycles.

To verify that the powder lost when pouring off the supernatants did not affect the specific surface area, the surface area was re-measured after washing and was found to be unchanged at 10.0 m^2/g.

Thermal gravimetric analysis (TGA) of the powder after exposure to liquid water showed a discrete weight loss as it was heated from 220° to 260°C in flowing dry air. The magnitude of this weight loss increased with time held in room temperature water and did not reach a saturation value over three days. (Fig. 3.3) However, by holding the powder in water at 80°C, it was found that the weight loss reached a maximum value of 0.20% in two days. (Fig. 3.3) Powder held for three days showed a slightly lower weight loss. No additional runs were made to determine if this is a real effect or due to experimental error.

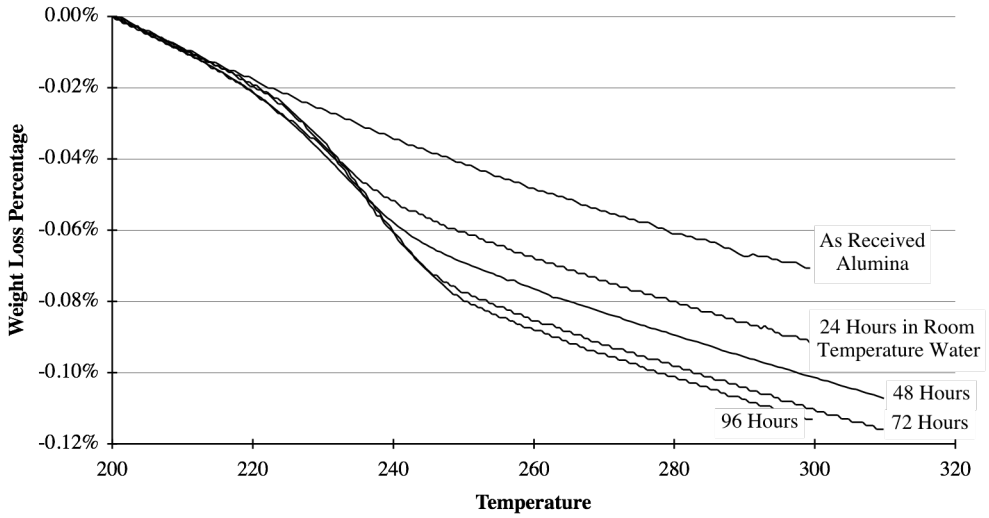

Fig. 3.3 Weight loss for alumina powder as a function of temperature for powders held in water at room temperature for 0, 1, 2, 3, and 4 days, all weights normalized to 0 at 200°C.

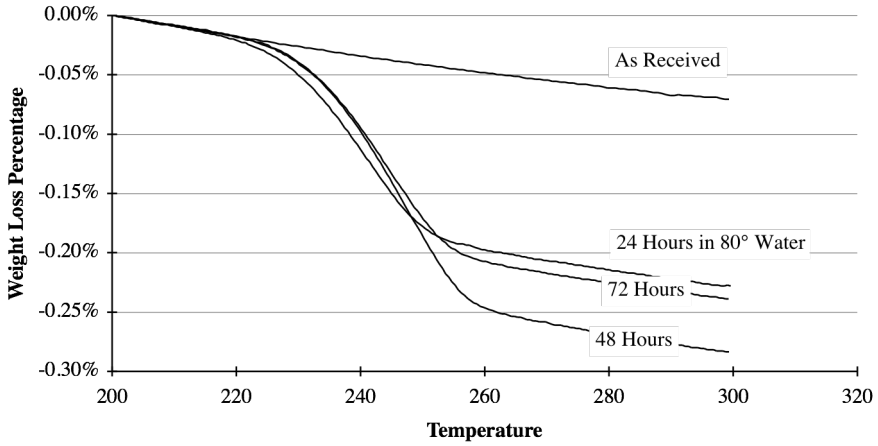

Fig. 3.4 Weight loss for alumina powder as a function of temperature for powders held in water at 80°C for 0, 1, 2, and 3 days, all weights normalized to 0 at 200°C.

It has been reported previously that the point of zero charge of α-alumina powders in room temperature water can drift over several days from a pH of 6.7 to 9.2. (**5**) Water has been shown to actually reverse the charge on very well dried α-alumina in longer chain alcohols. (**6**) To standardize the alumina surface all powder was equilibrated in 80°C water for two days after washing.

3.3.2 Conductivity Measurements

Conductivity was measured using a rectangular parallel plate conductivity probe having a cell constant of 0.22. The plates were of polished platinum 2.6 mm apart. The voltage across the conductivity probe was measured using a voltage divider circuit. A sine wave input signal of ≈ 1V rms was provided by an HP 33120A signal generator. The voltage across the conductivity probe was reduced to ≈ 0.5 V rms using a resistance decade box. The total input voltage and voltage across the decade box were measured using an HP 54645A oscilloscope and used to calculate the resistance across the conductivity probe.

A simple equivalent circuit for the for the conductivity measurement setup used is shown in Fig. 3.4. V_i is the test signal input; R_r is the reference resistance which must be close to the R_{cp}, the resistance of the conductivity probe, in order to generate accurate results; C_{cp} is the capacitance of the test cell, which is a constant as long as the test cell geometry and the solvent remain the same; C_{sc} and $R_{cp\ lim}$ are the space charge capacitance and limiting resistance. The voltage output, V_o, is measured with the oscilloscope which has an input capacitance, C_o, of 13 pF and an input resistance, R_o, of 1.00 MΩ. The behavior of the conductivity probe in regions where significant space charge accumulates is considerably more complex than is suggested by this simple parallel capacitor/resistor, however, in the range where charge only begins to accumulate this is a reasonable approximation.

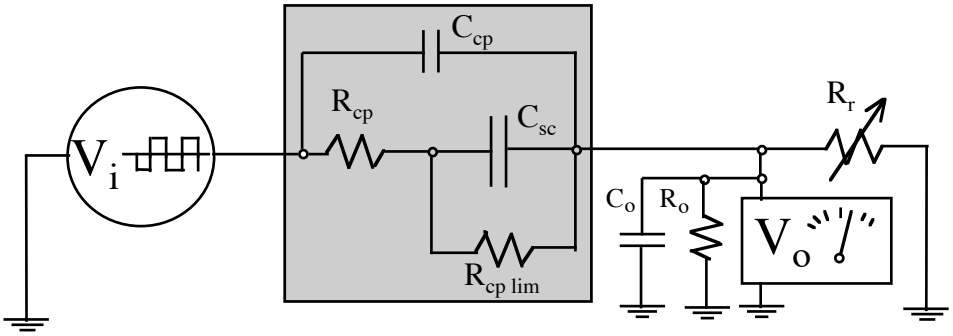

Fig. 3.4 Equivalent circuit for conductivity measurement setup. The area in the gray box is a simplified equivalent circuit for the conductivity probe.

Frequency was adjusted as a function of conductivity from 20 Hz to 20 kHz to remain between double layer capacitance effects in the conductivity cell and capacitance effects in the measuring circuit. At low frequencies the voltage across the conductivity probe includes components due to both the resistance of the fluid and space charge build up at the electrodes. As the frequency is raised the voltage alternates faster than the space

charge can form, and the voltage across the cell will be due only to the resistance of the fluid. At higher frequencies the resonance of the input capacitance of the oscilloscope will begin to short circuit the oscilloscope. Therefore the measurement procedure is to scan a set of frequencies, each time adjusting the reference resistance to divide the signal voltage evenly between the conductivity cell and the measurement circuit. The resistance of the conductivity cell is then calculated at each frequency assuming that $C_o = 0$. The minimum calculated resistance is then taken as the resistance value for the conductivity probe.

$$R_{cp} = \left[\left(R_r\right)^{-1} + \left(R_o\right)^{-1} \right]^{-1} \frac{V_i - V_o}{V_o} \qquad \text{Conductivity Probe Resistance Calc.}$$

Calibration of the test cell and determination of absolute accuracy of the measurement procedure was performed by comparison of measurements to previously published data. Calibration was performed by titration of KCl into water using as a standard the equation of Lind, et al. (**7**) This was verified and measurement accuracy estimated by titration of LiCl into ethanol compared to the data of Graham, et al. (**8,9**) and HCl into ethanol containing 0.5 wt.% water compared to the data of De Lisi et al. (**10**) Measurement accuracy was within ±1% over the range from 4 μS/cm to 120μS/cm and within ±2% from 1 to 4 μS/cm. Percentage accuracy declined rapidly below 1 μS/cm, however, absolute accuracy above 0.3 μS/cm is estimated to be within ±0.05μS/cm.

The conductivity test cell was held in the suspension with the plates aligned vertically. The bottom edge of the cell, 5.9 mm wide, was open so that powder sedimenting out of the suspension would not accumulate in the test cell. The surface conductivity of the powder can be significantly higher than that of the bulk solution. If sedimented powder is allowed to accumulate between the plates, the higher conductivity of the sediment will short circuit the cell. A small hole in the top of one side of the cell allowed for free circulation of suspension through the cell.

3.3.3 Titration Procedure

Conductumetric and pH titrations were performed in a jacketed beaker maintained at 25 ± 0.02°C by a circulating isothermal bath. Titrants were added manually by weight. Where alumina was added, it was first held in a drying oven at 135°C for at least 2 hours to standardize the quantity of adsorbed water. In all cases alumina was added to yield an approximately 1 vol.% suspension.

The solution was mixed using a magnetic stirrer. The powder was sufficiently flocced from the washing process that it rapidly sedimented out at all conditions when the stirrer was turned off. Conductivity measurements made with the powder held in

suspension by stirring and in the quiescent supernatant after sedimentation were identical within the measurement error of the apparatus and technique.

3.3.4 Electrophoretic Mobility

Mobility was measured using a Delsa 440 laser Doppler velocimeter (Beckman Coulter, Inc., Fullerton, California). This instrument measures particle velocity in suspension within a rectangular capillary. An electric field of 57 V/cm is applied across the capillary for 2.5 seconds, turned off for 2 sec., and a reverse field is applied for 2.5 seconds. This is repeated 12 times and the results are averaged. Reversing the field is intended to minimize the electrochemical boundary layer formation at the electrodes. If the velocity measured in each polarization direction was not the same, the measurement was rejected.

To separate the electro-osmotic flow of the fluid in the capillary from the electrophoretic motion of the particles, particle velocity was measured at nine points across the capillary, the results fitted to a parabola, and the particle velocities at the theoretical stationary levels calculated from the parabola. For all of the data points reported here the r^2 fit of the parabola was better than 98%.

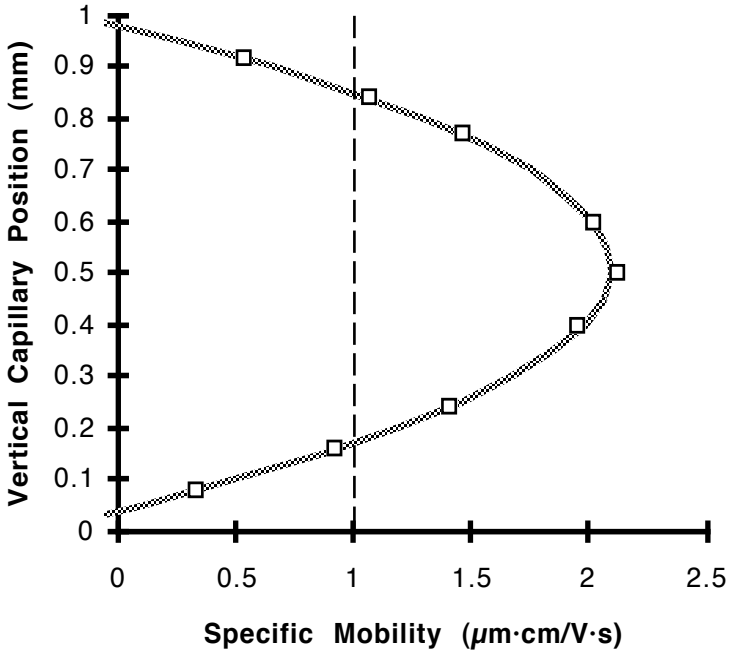

Fig. 3.5 Specific mobility vs. vertical position in measurement capillary. Squares are data points, gray line is parabola fitted by least squares. Vertical dashed line intersects parabola at theoretical stationary layers. This is the data for one of two measurements made for the 1.23 μS/cm case in table 3.1. Cell center calculated to be at 0.51 mm, r^2 fit for parabola 0.999, specific mobility 1.00 μm•cm/V•s.

For a significant signal to be generated by the instrument the laser must be able to propagate across the capillary with only modest scattering. This requires that the sample have a volume density of particles in suspension of 0.01% vs. 1% in the standard working suspensions used here. To prepare samples for measurement a 1% suspension was prepared in a centrifuge tube. HCl solution was added, the suspension mixed, and conductivity was measured to determine the ionic strength in the solvent. The suspension was centrifuged at 3,600 m/s^2 for 3 minutes. This usually left enough particles suspended in the supernatant for an electrophoretic measurement. If there were too few particles in the supernatant, some of the clear supernatant was drawn into a syringe, the remaining material was resuspended and a small amount was drawn into the same syringe and mixed. Volume density was judged visually.

We were only able to produce credible measurements using this instrument for very stable suspensions that were also stabilized against floccing to the quartz capillary wall. Although there was no attempt to quantify the surface charge on the capillary walls, in all of the measurements where a stable, symmetric, parabolic electroosmotic flow developed the flow indicated that there was a significant positive charge on both the capillary walls and the particles. Without this stability, the horizontal capillary is susceptible to sedimentation of particles onto the bottom surface. This gives the bottom a different surface charge from the top and prevents the development of a symmetric parabolic flow. As a result we were unable to make any valid measurements in suspensions with added KOH.

3.3.5 Electroacoustic Measurement

These measurements were made using an ElectroAcoustic Spectrometer DT-1200 with automatic titrator (Dispersion Technology, Inc., Mt. Kisco, New York). This instrument uses a piezoelectric actuator to apply a 1 MHz acoustic signal to a particulate suspension. Because of the density difference between the particles and solvent, there will be a relative motion between the two in the acoustic wave. This relative motion polarizes the electrostatic double layer around the particles. This polarization is detected as a current at an electrode on the face of the acoustic actuator.

To prepare the suspensions for electroacoustic measurement the alumina powder was placed in a 135°C oven for 2 hours to standardize the adsorbed water. This was added to the 99.5/0.5 wt.% ethanol/water solvent to produce a 1.00 vol. % alumina suspension. The mixture was placed on a vibratory mill for ≈ 6 hours with 2mm spherical alumina milling media. The HCl titration was performed the next day and the KOH titration was

performed on a portion of the same suspension one day later. The suspension was very stable and the initial zeta potential reading for each titration was within ±1 mV.

The instrument was calibrated with a 10 vol. % silica Ludox suspension with a zeta potential of -38 mV in water measured independently with an optical zeta potential instrument. Readings were made in a partially covered beaker rapidly and continuously stirred with a magnetic stir bar at ambient temperature, 25° ± 3°C. An automatic titrator was used to inject fixed volumes of titrant. In the titration with HCl, the suspension was allowed to equilibrate for 5 minutes after each injection of HCl solution before two zeta potential readings were made, each 40 seconds apart. In the KOH titration the equilibration time was reduced to two minutes.

3.3.6 pH

The pH numbers reported here are the direct numerical reading measured using a Fisher Accumet 20 pH meter (Fisher Scientific, Pittsburgh, Pennsylvania). An Accumet combination probe was used consisting of a general purpose glass sensing membrane and a Ag/AgCl reference electrode with a porous plug junction. The meter was calibrated using aqueous standard buffers at pH 4.00, 7.00, and 10.00. This direct readout of the pH meter in ethanolic solutions using a probe calibrated in aqueous standard solutions will be referred to here as the 'Indicated pH' or pHi.

In ethanolic solutions with a conductivity of ≈ 1μS/cm or less, pHi readings were not stable. Above this conductivity and below readings of ≈ pHi 9, stable reproducible readings were produced within three minutes of immersion in the ethanol while stirring. When the probe was replaced in the aqueous standard it returned within one minute to the standard value. Above readings of ≈ pHi 9 there was considerable drift in the readings and when the probe was returned to an aqueous standard up to 20 minutes could elapse before the probe returned to the correct reading for the standard.

To verify the validity of this measurement a titration was performed in the 99.5/0.5 wt. % ethanol/water solvent used in this study. A forward titration was performed with HCl, and a reverse titration performed using NH_4OH. The concentration of protonated ions was calculated as the sum of moles of HCl added minus the number of moles of NH_4OH added where this yielded a positive number. Where this yielded a negative number, indicating a preponderance of ethoxide/hydroxide ions, the concentration of protonated ions was calculated by dividing the equilibrium constant for the autoprotolysis reaction in this solvent by the absolute value of this number. A constant pK_s of 13 was determined by iteration to achieve the best fit of a straight line connecting the pHi readings in the acidic and basic solvent. This is shown in Fig. 3.6.

$$HEtO + H_2O \Leftrightarrow EtO^- + H_3O^+$$

$$or \quad 2HEtO \Leftrightarrow EtO^- + H_2EtO^+$$ Autoprotolysis Reactions in Ethanol/Water

$$or \quad 2H_2O \Leftrightarrow OH^- + H_3O^+$$

$$K_s = \left[H_2EtO^+ + H_3O^+\right] \bullet \left[EtO^- + OH^-\right] \bullet f_{\pm}^2$$

Autoprotolysis Equilibrium in Ethanol/Water

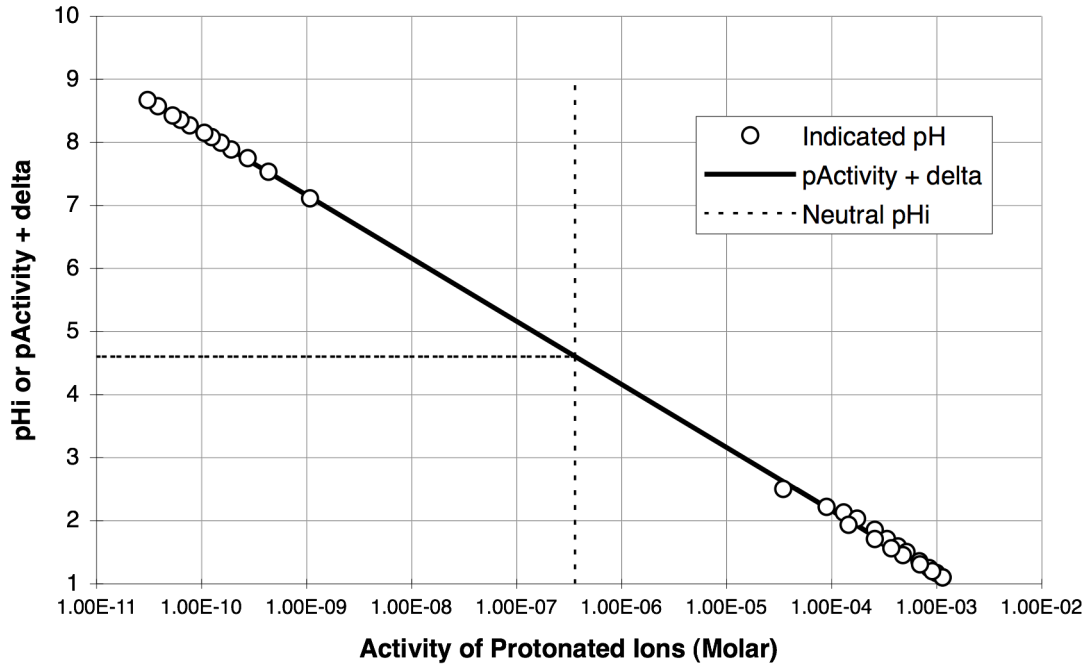

Fig. 3.6 pHi titration in 99.5/0.5 wt. % ethanol/water; forward titration with HCl, reverse titration with NH_4OH. Activity of H^+ ions (a_{H+} *) calculated using an autoprotolysis constant of 1.3e-13. Circles indicate pHi readings, the solid black line is the $-Log_{10}\, a_{H+}$ * + δ, where δ is -1.84. Neutral pHi is 4.6.

To further verify these measurements the pa_{H+}* was calculated where a_{H+}* is the activity of the protonated ions in the solvent where activity is equal to concentration at infinite dilution. This activity was calculated as the product of the concentration of protonated ions in the solvent and the activity correction factor, $f_{\pm}$, calculated using the Debye-Hückel formula [7] below. At the low ionic concentrations used here the pa_{H+}* scale will be essentially congruent with the pH*, or operational pH scale for this solvent. To convert from the operational pH (pH*) to the indicated pH (pHi) requires the addition of a correction factor δ. This factor compensates for the liquid junction potential between aqueous reference electrode and the ethanol/water solvent as well as the medium activity effect for the transference of the positive ion from water to the ethanol/water solvent. A δ

of -1.84 produced the very good fit shown in Fig. 3.6 where the circles are the pHi readings and the straight line is the calculated pa_{H^+}* + δ. This titration and activity fitting demonstrate that pHi readings can be reproducible and can be interpreted quantitatively.

A summary of the relevant proton exchange reactions in ethanol with very low concentrations of water (<1%)is as follows:

Proton Distribution (**10**):

$C_2H_5OH_2^+ + H_2O \Leftrightarrow C_2H_5OH + H_3O^+$ K_+=285

Ethoxide/Hydroxide Equilibrium (**18**):

$C_2H_5OH + OH^- \Leftrightarrow C_2H_5O^- + H_2O$ K_-=2

Pure Ethanol Autoprotolysis (**17**):

$2\ C_2H_5OH \Leftrightarrow C_2H_5OH_2^+ + C_2H_5O^-$ pK_{SEtO}=19

Pure Water Autoprotolysis (**17**):

$2\ H_2O \Leftrightarrow H_3O^+ + OH^-$ pK_{SW}=14

Autoprotolysis of combined solvent (0.995/0.005 wt. ethanol/water):

$C_2H_5OH + H_2O \Leftrightarrow C_2H_5O^- + H_3O^+$

and $2C_2H_5OH \Leftrightarrow C_2H_5O^- + C_2H_5OH_2^+$ pK_S=13

and $2H_2O \Leftrightarrow OH^- + H_3O^+$

3.4 Surface Charge Development of Alumina in Ethanol

3.4.1 Surface Charge with the Addition of HCl

3.4.1.1 Zeta Potential

Mobilities measured by electrophoresis are given in table 1 below. Without an independent mobility standard in ethanol the accuracy of the measurements could not be estimated, however, when a symmetric electroosmotic flow profile was established in the measurement capillary, reproducibility was within ±5%.

The conductivity was measured using a commercial parallel plate conductivity cell with a cell constant of $0.107 cm^{-1}$. The edges of the cell were open and, therefore, due to edge effects there is a great deal of uncertainty in the conductivity measurements below $4\mu S/cm$. Above this the estimated accuracy is ±10%. The first point represents only the washed alumina in ethanol with no added HCl and no conductivity measurement was made. Previous measurements of this concentration of alumina in ethanol have shown conductivity less than $0.05\mu S/cm$.

The molar ionic concentration in the bulk solution was then calculated with the Fuoss and Onsager equation (**11**) using values for HCl in 99.5wt.% ethanol linearly interpolated from the data of DeLisi, et al. (**10**) taken at 99.60 and 99.41 wt.% ethanol: $\Lambda_O = 53.40$, $a_O = 3.64$ and $K_A = 21$.

The bulk molar ionic strength was then used to calculate the Debye length, κ^{-1} eq. [3.1]. The relative double layer thickness, κa, was calculated using the average particle radius of 150nm. The non-dimensional reduced mobility **E** was calculated from the electrophoretic mobility, u_E eq. [3.2]. These values were then used to find the reduced potential, $\tilde{\xi}$, graphically from the charts for a 1:1 electrolyte published by O'Brien and White. (**12**) The zeta potential was then calculated in millivolts using eq. [3.3]. (Definitions of the terms used in these and all subsequent equations can be found at the head of the chapter.)

$$\kappa = \left[\frac{2e^2\rho_\infty z^2}{\varepsilon_o\varepsilon_r kT}\right]^{\frac{1}{2}} \qquad [3.1]$$

$$\mathbf{E} = \frac{3\eta e}{2\varepsilon_r\varepsilon_o kT}\cdot u_E \qquad [3.2]$$

$$\tilde{\xi} = \frac{ez\zeta}{kT} \qquad [3.3]$$

Table 3.1
Calculation of zeta potential from electrophoretic mobility.

Conductivity (μS/cm)	Bulk Molarity (mMol)	Debye Length	κa	Mobility (μm·cm/V·s)	Reduced Mobility	Reduced Potential	Zeta Potential
< 0.1			< 1	0.81	2.27	2.36	61 mV
0.46	0.009	58.5 nm	2.6	1.00	2.80	3.55	91 mV
1.23	0.023	36.0 nm	4.2	1.00	2.80	3.38	87 mV
4.91	0.095	17.7 nm	8.5	0.88	2.46	2.28	59 mV
12.02	0.242	11.1 nm	13.5	0.84	2.35	1.97	51 mV
19.81	0.400	8.6 nm	17.4	0.74	2.07	1.65	42 mV

Zeta potential was also measured using an electroacoustic instrument that measures the colloid vibration current and calculates the particle zeta potential based on a thin double layer assumption. The inputs to this instrument are the suspension volume fraction, solvent and particle densities, and average particle size. The instrument controls an automatic titrator and its output is the volume of an HCl solution titrated into the suspension and the calculated zeta potential.

The quantity of acid titrated into the suspension was first converted into bulk concentration of HCl by interpolation of the raw adsorption data as shown in the section on acid adsorption below. Using the resulting zeta potential vs. bulk ionic strength a chloride adsorption isotherm was calculated and used to recalculate the bulk ionic strength from the quantity of acid titrated in. This data was then used as the bulk free molarity of HCl on the horizontal axis in Fig. 1.

Concurrent with the calculation of bulk ionic strength, the zeta potential must be adjusted for double layer thickness effects. The zeta potential reported by the instrument is calculated based on a thin boundary layer assumption (**13**) and significantly underestimates the actual zeta potential for the range of double layer thicknesses considered here ($\kappa a \approx 1$ to 20). Sawatzky and Babchin (**14**) have developed theory for arbitrary double layer thickness. A key component of this theory is a function, not reproduced here, $f_1(\kappa a, a/\delta)$ which gives the ratio of the actual dynamic electrophoretic mobility to the mobility calculated assuming a thin double layer. The parameter δ, eq. [3.4], is a characteristic distance related to the distance over which the pressure waves generated by an oscillating particle decay. As the parameter $a/\delta \rightarrow 0$ the function f_1 goes to the function $f(\kappa a)$ of Henry (**15**) for calculating the DC electrophoretic mobility of particles with intermediate thickness double layers. The electroacoustic measurements used here were performed at a frequency of 1 MHz, which for ethanol will give a value for δ of 1.65 μm. Using the average particle radius, a, of 0.15μm and evaluating f_1 at its limits shows that the error in using the adjustment factor of Henry over the more complex formulation of Sawatzky and

Babchin is everywhere less than 10%. Therefore the adjustment of zeta potential values was done using values for the Henry formula interpolated from tabulated values. The resulting values are shown in Fig. 3.7, showing the agreement between the different zeta potential measurement methods.

$$\delta = \left(\frac{2\eta}{\rho\omega}\right)^{\frac{1}{2}} \qquad [3.4]$$

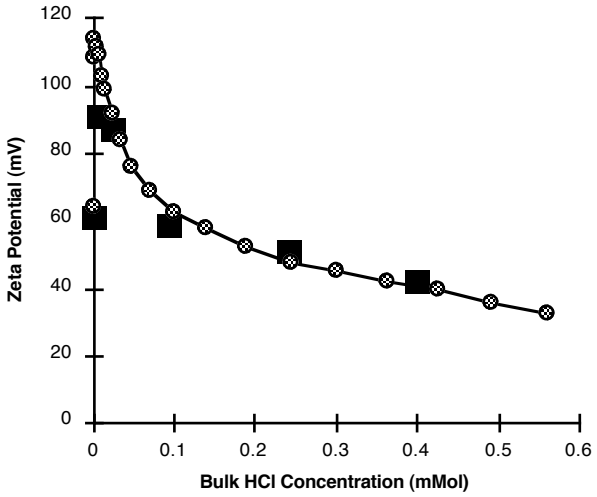

Fig. 3.7 Solid squares are zeta potentials calculated from electrophoretic mobility, circles are calculated from electroacoustic current using thin boundary layer theory and adjusted using the correction factor of Henry· (**12**)

When this data is replotted as a function of $-\log_{10}$ of the concentration of HCl in the bulk solution it appears reasonable that for bulk molar concentrations of HCl greater than 10μMol the zeta potential can be modeled as a straight line. Since the deviation between the straight line model and the data is less than the expected error in measuring and calculating the zeta potential (≈10%), values from the straight line approximation will be used in the subsequent calculations.

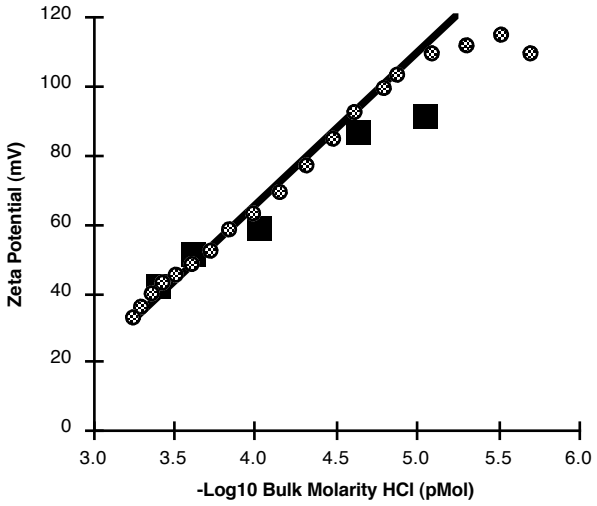

Fig. 3.8 Solid squares are zeta potentials calculated from electrophoretic mobility, circles are calculated from electroacoustic current using thin boundary layer theory and adjusted using the correction factor of Henry (**12**).

3.4.1.2 Surface Charge

Given the surface potential and the bulk ionic strength of the solvent, the surface charge density can be calculated. Loeb, et al. (**16**) used a numerical algorithm to calculate the surface charge density of a spherical colloid particle for a range of potentials and double layer thicknesses. They also presented an empirical formula, eq. [3.5], that can be used to estimate the results of their numerical calculations for surface charge density in a 1-1 electrolyte system to within 1% for the range of potential and double layer thickness values being considered here. We have used this equation to calculate the particle surface charge density, q, in milliCoulombs/meter^2 for the zeta potentials shown in Fig. 3.8 above. The results are shown in the graph in Fig. 3.9. These values were calculated using the linear zeta potential approximation except for the three data points below 10μMol HCl which diverge from the linear model. These points were calculated directly from the adjusted electroacoustic data and are shown as circles on the graph in Fig. 3.9.

$$q = \frac{\varepsilon_o \varepsilon_r kT}{e} \kappa \left(2\sinh\left(\tfrac{1}{2}\tilde{\xi}\right) + \frac{4}{\kappa a}\tanh\left(\tfrac{1}{4}\tilde{\xi}\right)\right) \qquad [3.5]$$

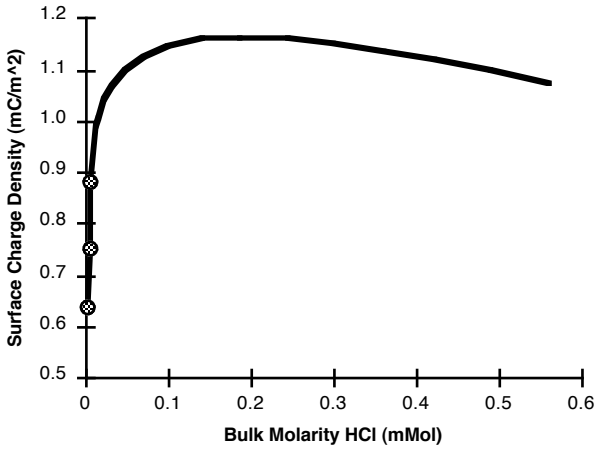

Figure 3.9 Surface charge density milliCoulombs/m^2. Circles are data points for bulk molarity less than 10μMol that do not correspond to the linear approximation shown in figure 2.

3.4.1.3 Acid Adsorption

Adsorption of HCl to the powder surface was determined using conductivity measurements. HCl was titrated into the 99.5/0.5 wt. % ethanol/water solvent mixture without alumina. This conductivity as a function of HCl addition is shown as round points in Fig. 4. The line labeled (1) superimposed on these points is the predicted conductivity/concentration curve using the Fuoss and Onsager (**11**) equation for an associated electrolyte, eq. [3.6] (see also Appendix A). It is calculated using values for HCl in 99.5wt.% ethanol linearly interpolated from the data of DeLisi, et al. (**10**) taken at 99.60 and 99.41 wt.% ethanol: $\Lambda_O = 53.40$, $a_O = 3.64$Å and $K_A = 21$.

$$\Lambda = \Lambda_o - S(c\gamma)^{1/2} + E'c\gamma\ln(6E_1'c\gamma) + Lc\gamma - K_A c\gamma f^2\Lambda \qquad [3.6]$$

The square data points are for the same conditions with the addition of 1 vol% alumina powder. The molarity of HCl in the solution is calculated from the conductivity. The difference between the HCl in solution and the total HCl titrated is taken to be the surface adsorption of the powder.

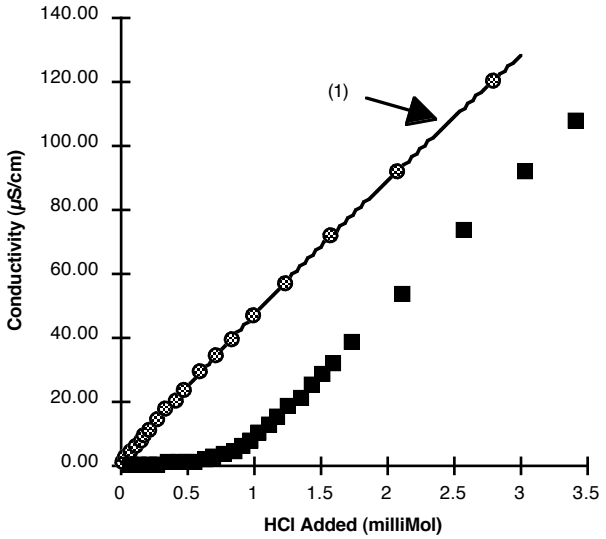

Figure 3.10 Solution conductivity with and without alumina powder present. Line labeled (1) is Fuoss and Onsager (**11**) equation plotted based on data from DeLisi and Goffredi (**10**).

3.4.1.4 Reversibility of Adsorption

Although the disappearance of HCl from solution in the presence of alumina can be measured accurately by conductometry, the question remains whether this is by surface adsorption or by an irreversible chemical reaction either changing the composition of the surface or converting the HCl to non-ionizing species in solution.

The reversibility of the adsorption was tested by pHi titration as shown in Fig. 3.11. HCl was titrated into ethanol with and without alumina. pHi readings were unstable until a concentration of HCl in solution of 0.02 mMol was reached (Conductivity $\approx 1\ \mu$S/cm). Above that the difference between the HCl titrated with and without alumina at equal pHi readings confirms the adsorption of HCl as determined by conductivity. Back titration of the solutions with KOH then shows the buffering of the pHi change in the alumina suspension due to the adsorbed HCl.

As a further check for other chemical reactions, the supernatants of alumina suspensions were checked by plasma spectroscopy for dissolved species containing aluminum. Suspensions of alumina in ethanol were prepared in ethanol alone, ethanol with up to 0.5 mMol KOH, and ethanol with up to 2.5 mMol added HCl. Supernatant was removed from the samples two hours, one day and ten days after preparation for analysis. No aluminum was detected in the solvent from any of the samples above a 90% confidence level minimum detection limit of 0.05 mMol aluminum. This indicates that the adsorption

does not involve reactions leading to a significant dissolution of aluminum from the surface.

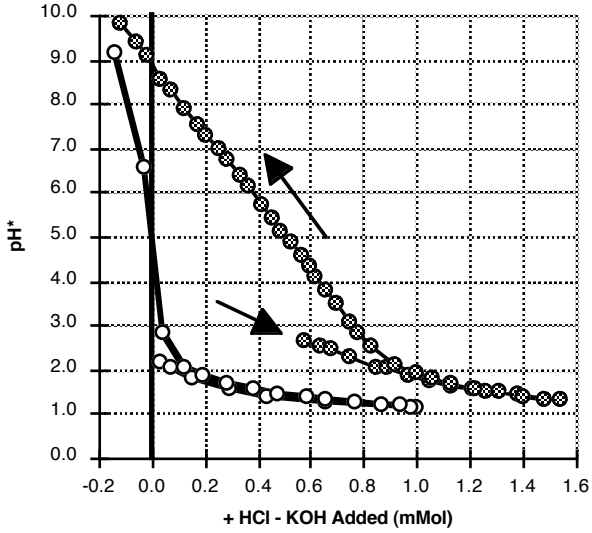

Fig. 3.11 Indicated pH, pHi, in ethanol + 0.5 wt. % water. Forward titration with HCl, back titrated with KOH. Open circles ethanol only, filled circles ethanol plus 1 vol. % alumina powder, surface area ≈320m^2/liter.

3.4.1.5 Notes on Concepts and Terminology

Before beginning further analysis of the data it will be useful to define some of the basic concepts used here regarding the surface, diffuse layer and solution chemistry in an ethanol-water solvent.

The particle is presumed to have a fixed number of surface sites which are either unoccupied, occupied by a proton, or occupied by a proton and negative ion. There are no assumptions about the nature of the bonding nor the invocation of an electrostatically bonded Stern or Helmholtz layer. All ions that are not adsorbed to a surface site are presumed to be in solution and outside the shear plane. Thus the terms 'on the surface' or 'adsorbed to the surface' imply ions that are rigidly attached to the particle surface and are inside the shear plane for electrophoretic measurement. The term 'at the surface' is then used to imply activities and potentials immediately adjacent to the surface but still dissolved and moving freely in the solvent, therefore outside the shear plane. As a result, the zeta potential, the potential measured at the shear surface, will be assumed to be equal to the surface potential.

The standard continuum assumptions are made, first that the surface charge is continuous across the surface and second that the solvent is a continuous dielectric medium

with the ions behaving as point charges. The second assumption seems reasonable given that at the maximum ionic strength where we have measured a zeta potential in this study the Debye length is 7.3 nm, about twenty times the 3.65 Å distance of closest approach of oppositely charged ions in solution determined by conductometry. The assumption that is likely to be violated first is that of a uniform, continuous surface charge. For the measurements with HCl the calculated surface charge of ≈ 1 mC/m^2 translates to one positive charge per 160 nm^2 or a uniformly distributed charge-charge separation distance of 13 nm. This is close to two times the Debye length mentioned above.

Notation in square brackets indicates either volume concentration in Mol/m^3 (milliMolar) or surface concentration in Mol/m^2. Activity of ions in the bulk solution is calculated as the product of the concentration and the Debye-Hückel mean molar activity correction factor, $f_{\pm}$, calculated using eq. [3.7]. Where the concentration is multiplied by an activity correction factor it is implicitly divided by the standard concentration to give a unitless activity. It is assumed that where the solution is charge balanced the activity correction factors for the positive and negative ions are equal. Where the solution is not charge balanced, such as in the particles electrostatic boundary layer, the activity correction factors for positive and negative ions, $f_+ f_-$, cannot be asumed to be equal, however, there will be no attempt to calculate either these correction factors or the surface ionic concentrations. Only the product of the two, the surface activity, will be calculated from the bulk activity using the Boltzmann relation, eq. [3.11].

$$-\ln f_{\pm} = \frac{\kappa e^2}{8\pi\varepsilon_o\varepsilon_r kT\left(1+\kappa a_o\right)} \qquad [3.7]$$

Finally, a note on the behavior of acids and bases in ethanol-water solvents. In the case of a Brønsted acid, the proton will have a greater affinity for water molecules in the solvent. Based on the equilibrium constant calculated in (**10**), in a 99.5/0.5 wt. % ethanol/water solvent mixture the protonated species will be 70 wt. % H_3O^+ and 30 wt. % H_2EtO^+. For a Brønsted base such as KOH in the same solvent mixture the negative ions will be greater than 99.9 wt. % ethoxide and the balance hydroxide, based on the equilibrium constant in (**18**). In the following discussion references to hydronium and ethoxide ions will implicitly include equilibrium concentrations of the ethoxonium and hydroxide ions, respectively.

3.4.1.6 Modeling Adsorption and Surface Charge with HCl

When the alumina powder is first put into the ethanol it develops a significant surface charge. The hypothesis for the development of this charge is that sites on the

alumina surface acts as a Lewis base, an electron donor. Ethanol molecules are adsorbed to these sites by their polar hydroxyl group.

$$Ss + HEtO \Leftrightarrow Ss\cdot H^+ \cdot EtO^-$$

There is then a equilibrium dissolution of ethoxide ions from the surface leaving protonated surface sites and a positive surface charge. The equilibrium for this reaction is given in eq. [3.8].

$$Ss\cdot H^+ \cdot EtO^- \Leftrightarrow Ss\cdot H^+ + EtO_S^-$$

$$\mathbf{K}_1 = \frac{\left[Ss\cdot H^+\right] f_-\left[EtO_S^-\right]}{\left[Ss\cdot H^+ \cdot EtO^-\right]} \qquad [3.8]$$

As HCl is added to the suspension there is a very rapid rise in the surface charge and zeta potential. This is likely due to a sharp reduction of ethoxide concentration in the bulk of the solvent due to reaction with the added HCl.

$$EtO_B^- + H_B^+ \Leftrightarrow HEtO$$

As shown in §3.3.6 the -$\log_{10}$ of the equilibrium constant for this reaction, pK_S, is 13 for the 99.5/0.5 ethanol/water misture used here.

Simultaneously there is an adsorption of chloride ions to the surface by substitution of chloride for the ethoxide ions at the surface. Surface charge now becomes principally a function of the equilibrium dissolution of chloride ions from the surface.

$$Ss\cdot H^+ \cdot Cl^- \Leftrightarrow Ss\cdot H^+ + Cl_S^-$$

$$\mathbf{K}_2 = \frac{\left[Ss\cdot H^+\right] f_-\left[Cl_S^-\right]}{\left[Ss\cdot H^+ \cdot Cl^-\right]} \qquad [3.9]$$

Equations [8] & [9] can be combined to yield eq. [10], showing that the adsorption of chloride can be modeled as a substitution of a chloride ion for an ethoxide ion on the surface, with the adsorption ratio determined by the ratio of dissolved chloride to ethoxide at the surface.

$$\frac{\left[Ss\cdot H^+ \cdot Cl^-\right]}{\left[Ss\cdot H^+ \cdot EtO^-\right]} = \frac{\mathbf{K}_1}{\mathbf{K}_2}\frac{f_-\left[Cl_S^-\right]}{f_-\left[EtO_S^-\right]} \qquad [3.10]$$

From conductivity measurements we know the bulk activity of the chloride ion, and with the zeta potential, the surface activity of chloride can be calculated using the Boltzman relationship and the bulk activity coefficient.

$$f_{-}\left[Cl_S^-\right] = f_{\pm}\left[Cl_B^-\right]\exp\left(\frac{e\zeta}{kT}\right) \qquad [3.11]$$

Then it will be assumed *a posteriori* that the surface ethoxide concentration can be estimated as a constant multiplied by an exponential of the zeta potential.

$$f_{-}\left[EtO_S^-\right] = \boldsymbol{K}_{EtO}\exp\left(\frac{e\zeta}{2kT}\right) \qquad [3.12]$$

Substituting [3.11] and [3.12] into [3.10] we generate an equilibrium equation in which the ratio of chloride to ethoxide adsorbed to the surface is a function of a constant and a lumped parameter which is the bulk chloride concentration times an exponential of the zeta potential, as shown in eq. [3.13].

$$\frac{\left[Ss\cdot H^+\cdot Cl^-\right]}{\left[Ss\cdot H^+\cdot EtO^-\right] f_{\pm}\left[Cl_B^-\right]\exp\left(\frac{e\zeta}{2kT}\right)} = \frac{\mathbf{K}_1}{\mathbf{K}_2\boldsymbol{K}_{EtO}} \qquad [3.13]$$

To simplify the following equations all of the constants will be collected into one lumped parameter and a simplified expression for the chloride dependence is given, eq.s [3.14] and [3.15] respectively. Note that the function *f*(Cl) depends on both the bulk chloride concentration and the zeta potential.

$$\mathbf{K}_{\mathbf{L}} = \frac{\mathbf{K}_1}{\mathbf{K}_2\boldsymbol{K}_{EtO}} \qquad [3.14]$$

$$f(\mathrm{Cl}) = \left[Cl_B^-\right]\exp\left(\frac{e\zeta}{2kT}\right) \qquad [3.15]$$

Assuming that there are a fixed number of surface sites and that these can be broken down into sites occupied by an ethanol molecule, HCl, a proton or unoccupied, the total surface site concentration is given by eq. [3.16].

$$\left[Ss_{Tot}\right] = \left[Ss\cdot H^+\cdot EtO^-\right] + \left[Ss\cdot H^+\cdot Cl^-\right] + \left[Ss\cdot H^+\right] + \left[Ss\right] \qquad [3.16]$$

A further approximation can be made assuming that the number of surface sites that are only occupied by a proton or are unoccupied are small relative to the total number of surface sites. With these approximations eq.s [3.14], [3.15], [3.16] can be substituted into

eq. [3.13] and algebraically manipulated to obtain an equation in the form of a Langmuir adsorption isotherm, eq. [3.17].

$$\left[Ss\cdot H^{+}\cdot Cl^{-}\right] = Ss_{Tot}\frac{\mathbf{K}_{\mathrm{L}} f(\mathrm{Cl})}{\mathbf{1}+\mathbf{K}_{\mathrm{L}} f(\mathrm{Cl})} \qquad [3.17]$$

By plotting the inverse of this equation, which is linear, eq. [3.18], the values for the total number of surface sites and the lumped equilibrium parameter $\mathbf{K}_{\mathrm{L}}$ can be estimated by a least squares fitting. This is plotted in Fig. 3.12(a) for data points taken at conductivities above 2 μS/cm ($\approx$ 0.04 mMol bulk molar concentration). The resulting values are Ss_{Tot} = 3.48 μMol/m^2 and $\mathbf{K}_{\mathrm{L}}$ = 7.7. The direct form of the equation, eq. [3.17], is plotted using these parameters and is shown in Fig. 3.12(b). The actual adsorption data points are superimposed on this curve showing the level of fit.

$$\left[Ss\cdot H^{+}\cdot Cl^{-}\right]^{-1} = Ss_{Tot}{}^{-1} + \left(\mathbf{K}_{\mathrm{L}} Ss_{Tot} f(\mathrm{Cl})\right)^{-1} \qquad [3.18]$$

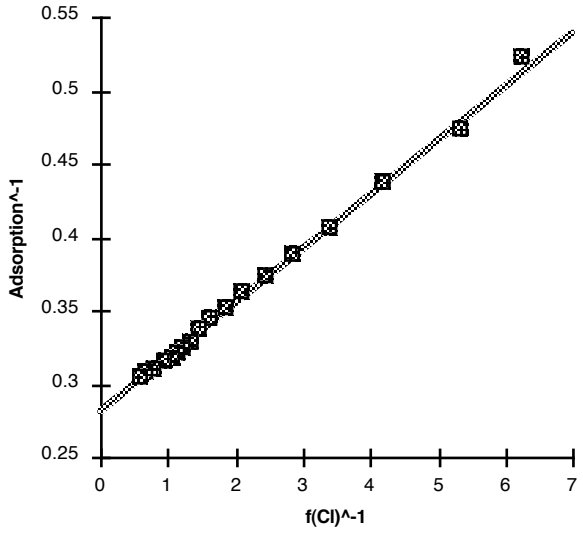

Fig. 3.12(a) Inverse of surface adsorption data for bulk molar HCl concentrations above 0.04 mMol plotted as a function of inverse of eq. [3.15]. Straight line fitted by least squares.

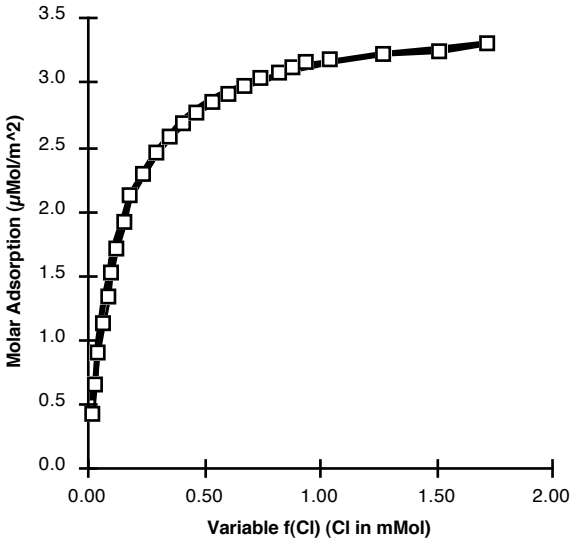

Fig. 3.12(b) Surface adsorption data plotted as a function of Eq. [3.14] superimposed on a fitted plot of the adsorption isotherm, Eq. [3.17].

Having developed an equation which accurately describes the chloride adsorption, it is now necessary to review the assumptions that were made in the derivation.

The assumption that the number of surface sites occupied only by a proton is small relative to the total number of surface sites does appear reasonable. The maximum surface charge density measured here is 1.14 mCoulombs/m^2 or 11.8 nanoMol/m^2. This is 0.34% of the total number of surface sites estimated by the chloride adsorption isotherm.

The assumption that the number of unoccupied surface sites is small is more difficult to address as there is no direct measurement of empty surface sites. However, if the equilibrium constant for the dissolution of an ethanol molecule from a surface site, eq. [19], is significantly larger than the equilibrium constant for the removal of a proton from a surface site by either an ethanol or water molecule, eq. [3.20], it can be shown that the concentration of empty surface sites will not affect the results derived here.

$$Ss\cdot H^{+}\cdot EtO^{-} \Leftrightarrow Ss + HEtO \qquad [3.19]$$

$$Ss\cdot H^{+} + H_2O \Leftrightarrow Ss + H_3O^{+} \qquad [3.20]$$

The assumption that there are a fixed number of surface sites is supported by the excellent fit of the adsorption data to a standard isotherm model.

It was also assumed that there is an equilibrium between the surface charge, free chloride ion concentration at the surface, and the total adsorbed chloride. If this is true the value of $\mathbf{K}_2$ calculated from eq. [3.9] should be a constant over the range where there is a significant level of chloride adsorbed to the surface.

$$\mathbf{K}_2 = \frac{\left[Ss{\cdot}\ H^+\right] f_-\left[Cl_S^-\right]}{\left[Ss{\cdot}\ H^+ \cdot\ Cl^-\right]} \qquad [9]$$

As can be seen from the plot in Fig. 3.13, the calculated value of $\mathbf{K}_2$ varies by ≈ ±10%, however, although the denominator is known to within a percent over most of the range, the numerator is the product of two values that are an exponential function of the zeta potential. This makes the calculated value of this function very sensitive to the magnitude of the zeta potential. A change of 5% in the value of the zeta potential at 100 mV leads to a 30% change in the calculated value of $\mathbf{K}_2$. This sensitivity to a ±5% change in the zeta potential is also plotted in Fig. 3.13. While the data does not conclusively prove that $\mathbf{K}_2$ is a constant, this assumption seems reasonable and is well within the limits of measurement error for the data used here.

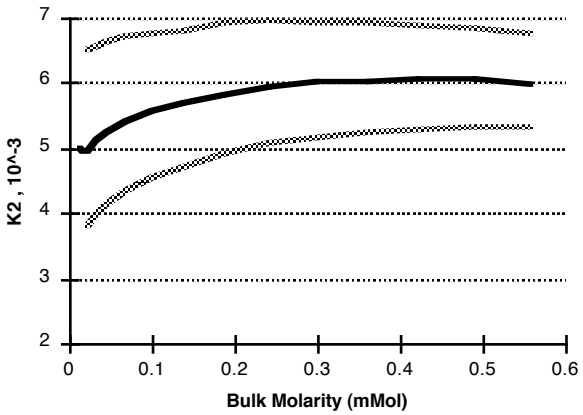

Fig. 3.13 Plot of $\mathbf{K}_2$ from Eq. [9]. Quantities are in Moles or Mol/m^2, as appropriate. Gray lines show the sensitivity of the calculation to a ±5% change in zeta potential.

Justification of the next two assumptions is somewhat more involved, and they will be treated together. The first is that there is an equilibrium between surface adsorbed ethanol, protonated surface sites and dissolved ethoxide ions at the surface eq. [3.8]. The second is that the concentration of the ethoxide ion at the surface changes in proportion to the square root of the Boltzmann relation of the zeta potential eq. [3.12].

$$\mathbf{K}_1 = \frac{\left[Ss{\cdot}\ H^+\right] f_-\left[EtO_S^-\right]}{\left[Ss{\cdot}\ H^+ \cdot\ EtO^-\right]} \qquad [3.8]$$

$$f_-\left[EtO_S^-\right] = \boldsymbol{K}_{EtO} \exp\left(\frac{e\zeta}{2kT}\right) \qquad [3.12]$$

One way of testing these assumptions is to substitute eq. [3.12] into eq. [3.8] and calculate the value $\mathbf{K}_1/\boldsymbol{K}_{EtO}$ to see how closely this approximates a constant over the range of HCl concentrations used here. The result of this calculation as shown in Fig. 3.14 is within ±8% of a constant. As with $\mathbf{K}_2$ above, this is a very sensitive function of zeta potential and the assumption that the value $\mathbf{K}_1/\boldsymbol{K}_{EtO}$ is a constant does not appear unreasonable.

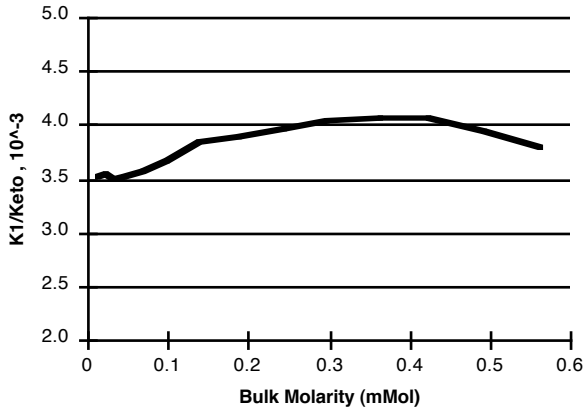

Fig. 3.14 Plot of $\mathbf{K}_1/\boldsymbol{K}_{EtO}$ from equations [8] & [12]. Variation around the average value is ±8%.

Although a theoretical justification can be made for why the surface concentration of the ethoxide ion should be approximated by eq. [3.12], the best test of this assumption is to return to eq. [3.10], substitute eq. [3.8] for the surface ethoxide concentration, and recalculate the adsorption isotherm. Although there is insufficient data to estimate the absolute ethoxide concentration at the surface, and therefore a value for $\mathbf{K}_1$, the adsorption can be plotted as a function of the surface chloride concentration divided by the ethoxide concentration over $\mathbf{K}_1$. To do this, eq. [3.18] is replotted replacing f(Cl) with f'(Cl) below where f'(Cl) is given by eq. [3.21] and plotted in Fig. 3.15. The fit to a straight line is slightly worse than shown in Fig. 3.12, particularly at the extrema, however, the assumption embodied in eq. [3.12] has been eliminated and it has been shown that surface charge and the adsorption of HCl to the surface can be modeled using only the very basic equations [3.8], [3.9] and [3.16].

$$f'(\mathrm{Cl}) = \frac{f_{\pm}\left[Cl_B^-\right]\exp\left(\frac{e\zeta}{kT}\right)}{\left(f_-\left[EtO_S^-\right] \Big/ \mathbf{K}_1\right)} = \frac{\left[Ss\cdot H^+\right] \times f_{\pm}\left[Cl_B^-\right]\exp\left(\frac{e\zeta}{kT}\right)}{\left[Ss_{Tot}\right] - \left[Ss\cdot H^+\cdot Cl^-\right]} \qquad [3.21]$$

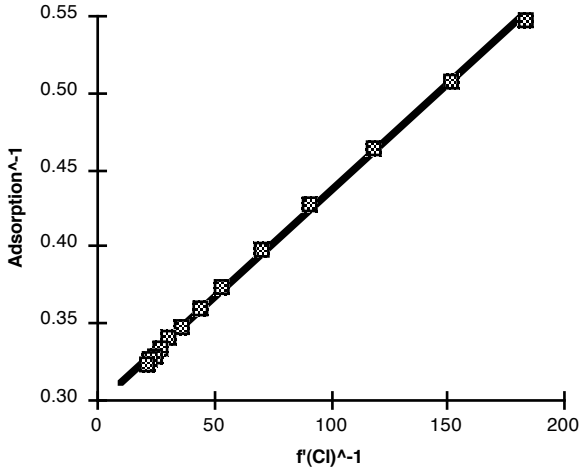

Fig. 3.15 Inverse of surface adsorption data for bulk molar HCl concentrations above 0.04 mMol plotted as a function of inverse of Eq. [321]. Straight line fitted by least squares.

The one significant reaction that has not yet entered into the discussion is the autoprotolysis equilibrium for ethanol, eq. [3.22]. This controls the ethoxide ion concentration given the concentration of the protonated species and vice versa. If the surface proton activity is calculated from the bulk concentration and zeta potential using the Boltzmann relation, eq. [3.23], this activity would be expected rise by four orders of magnitude over the measurement range, as plotted in Fig. 3.16. If the autoprotolysis equilibrium eq. [3.22] is valid at the surface, then the activity of the ethoxide ion at the surface would be expected to decline proportionally by four orders of magnitude.

$$HEtO \Leftrightarrow EtO_B^- + H_B^+$$

$$\mathbf{K_S} = \frac{f_{\pm}^2\left[H^+\right]\left[EtO^-\right]}{\left[HEtO\right]} \qquad [3.22]$$

$$f_+\left[H_S^+\right] = f_{\pm}\left[H_B^+\right]\exp\left(\frac{-e\zeta}{kT}\right) \qquad [3.23]$$

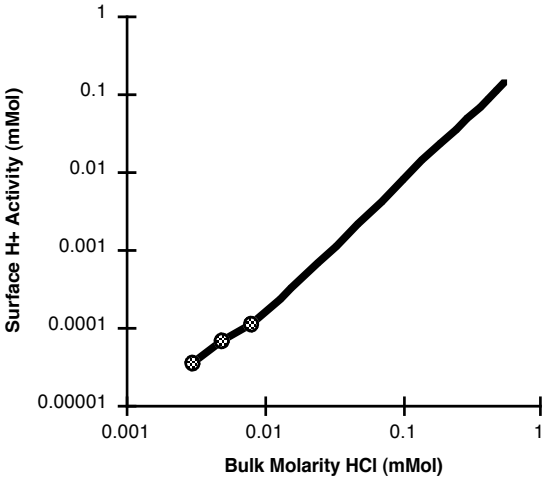

Fig. 3.16 Log/Log plot of surface activity of H^+ ion calculated from bulk concentration using the Boltzmann relation.

That, however, contradicts the model developed above where the ethoxide concentration at the surface is set by a surface equilibrium reaction. When the relative change in ethoxide concentration is plotted using equations [3.8] & [3.16] in Fig. 3.17, the ethoxide concentration is seen to change by only one order of magnitude. Even further, over the range of bulk HCl concentrations from 0.01 to 0.56 milliMolar, the predicted concentration of the proton at the surface is seen in Fig. 3.16 to increase by a factor of more than one thousand while the relative ethoxide concentration as shown in Fig. 3.17 declines by less than a factor of 7.

$$\frac{f_{-}\left[EtO_S^-\right]}{\mathbf{K}_1} = \frac{\left[Ss_{Tot}\right] - \left[Ss{\cdot}\ H^+ {\cdot}\ Cl^-\right]}{\left[Ss{\cdot}\ H^+\right]} \qquad [3.8, 3.16]$$

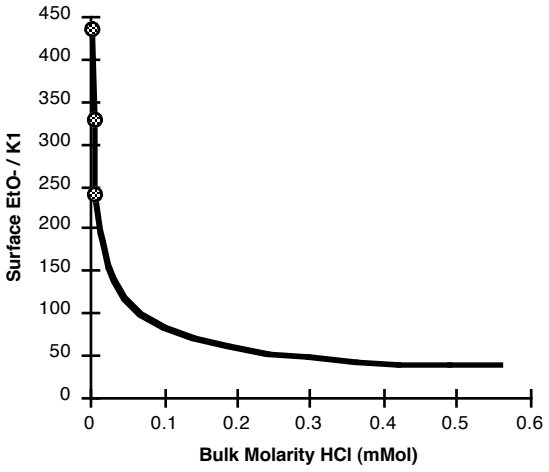

Fig. 3.17 Relative surface activity of EtO^- ion calculated from surface equilibrium equations [3.8], [3.16].

This contradiction only exists if the autoprotolysis equilibrium constant is taken to be constant. If this constant is higher at the surface than in the bulk by three orders of magnitude or more, then this contradiction disappears. In other words, our model of surface adsorption and charge formations remains consistent if the surface also acts to catalyze the autoprotolysis reaction of ethanol.

This is not a large jump to make given that the first step of the catalysis reaction has already been proposed as the charging mechanism for the alumina surface in the pure solvent. As proposed above, an ethanol molecule adsorbs to the surface and desorbs as an ethoxide ion leaving a proton on the surface. This gives the particles their positive surface charge. The next step would be for some of the protons on the surface to desorb as either a hydronium or protonated ethanol ion. These two ions would then diffuse outward a finite distance from the surface and react in solution, re-forming a neutral ethanol molecule. The voltage gradient in the double layer around the particle would accelerate the outward diffusion of the positive ions while retarding the outward diffusion of the ethoxide ions. The outward flux of positive ions from the surface would balance the inward flux of positive ions being consumed by reaction with ethoxide near the surface. The result is that the particle would be able to maintain a layer containing a significant concentration of ethoxide ions even when the bulk solution has a significant proton activity, and therefore an effectively zero concentration of ethoxide.

3.4.2 Behavior with Added KOH

Having examined the behavior with the addition of a simple acid, the next step is the addition of a simple base. Potassium hydroxide was chosen because it was readily available in a low water content ethanol solution. As was mentioned above, potassium hydroxide will react with ethanol, and in a 99.5/0.5 wt. % ethanol/water solvent it will convert to more than 99% potassium ethoxide. (**18**)

3.4.2.1 Conductivity

In order to measure ionic strengths in solution it is necessary to know the conductivity function for KOH in this concentration of ethanol. Lacking literature data, our first step was to measure the molar conductivity and fit this to the Fuoss & Onsager equation [3.6]. The curve was fitted to data points taken between concentrations of 1 and 6 milliMolar which lie in the most accurate measurement range for our system. An iterative fitting algorithm was used which converged unambiguously to the following values: Molar limit conductivity, $\Lambda_o = 40.75$; ionic distance of closest approach, $a_o = 3.50$; and ionic

association constant, $K_A = 0$. The result is plotted in Fig. 3.18 below along with the data points below 1 milliMolar not used in the fitting.

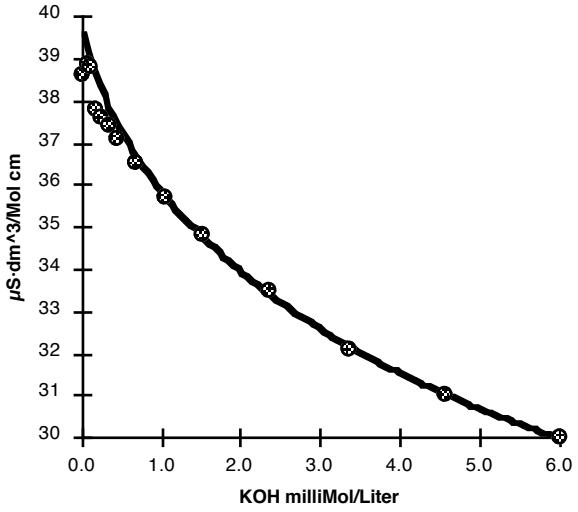

Fig. 3.18 Molar conductivity of KOH in 99.5/0.5 wt. % ethanol/water solvent. Circles are measured data points. Curve is Fuoss and Onsager equation fitted to data points between 1 and 6 milliMolar.

3.4.2.2 Adsorption

Adsorption data was obtained by measuring conductivity changes as KOH was titrated into a stirred 1 vol. % suspension of alumina powder. Concentration of KOH in solution was determined from conductivity measurements using the Fuoss-Onsager equation with the parameters fitted above. The difference between the KOH in solution and the total KOH added was taken as the powder surface adsorption.

Fig. 3.19 shows the molar conductivity as a function of the total KOH addition to the alumina suspension. This highlights the counterintuitive behavior of adsorption below an addition of 0.4 milliMolar. In this initial region the more KOH that is adsorbed the larger the proportion of additional KOH that will be adsorbed. This is exactly the opposite of what would be expected from a normal adsorption isotherm, and can be explained by first understanding the surface charging of the particles.

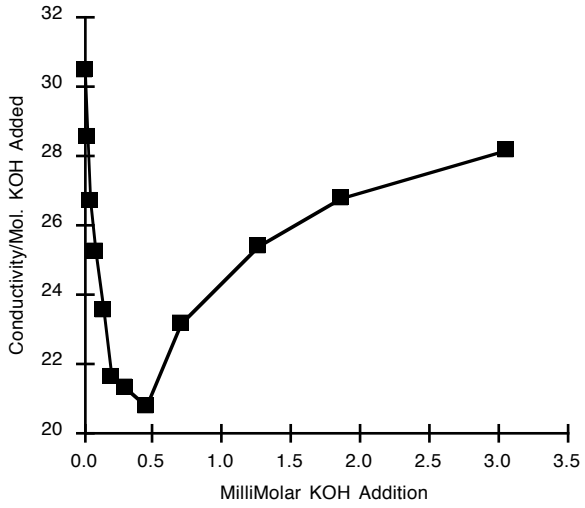

Fig. 3.19 Conductivity per molar addition of KOH to a 1 vol. % alumina suspension.

3.4.2.3 Zeta Potential

As a result of the low surface potentials and consequently low stabilities of alumina suspensions with added KOH, zeta potentials were measured only electroacoustically. Electroacoustic measurements were made in a continuously stirred suspension of 1 vol. % alumina powder. An automatic titrator was used to inject a solution of 0.1 molar KOH in 12 μl increments. An unadjusted zeta potential of 44.6 mV was measured before the titrator tip was inserted into the solution.

The bulk ionic strength was used to calculate the Debye length and Henry correction factor for the zeta potential as in the measurements with HCl above. The corrected zeta potential values as a function of bulk KOH concentration are shown in Fig. 3.20. At a bulk molar concentration of approximately 0.2 milliMolar the indicated zeta potential dropped below zero and went to -1.4 mV at the maximum KOH concentration measured.

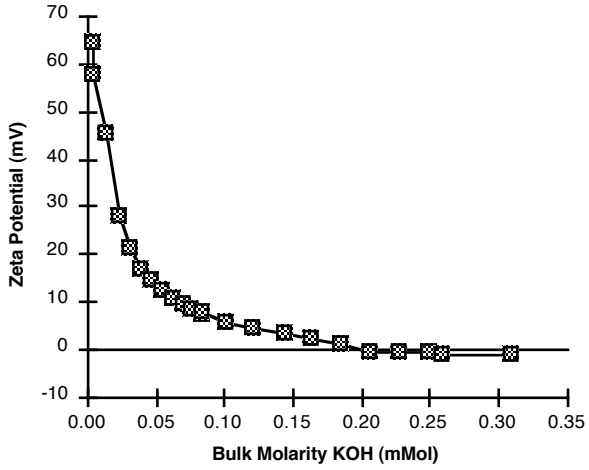

Fig. 3.20 Zeta Potential as a function of molarity of KOH in bulk solution.

3.4.2.4 Surface Charge

With the zeta potential and the bulk ionic strength, the surface charge density can be calculated using eq. [3.5]. The results are shown in Fig. 3.21. The zeta potential is again assumed to be the same as the surface potential.

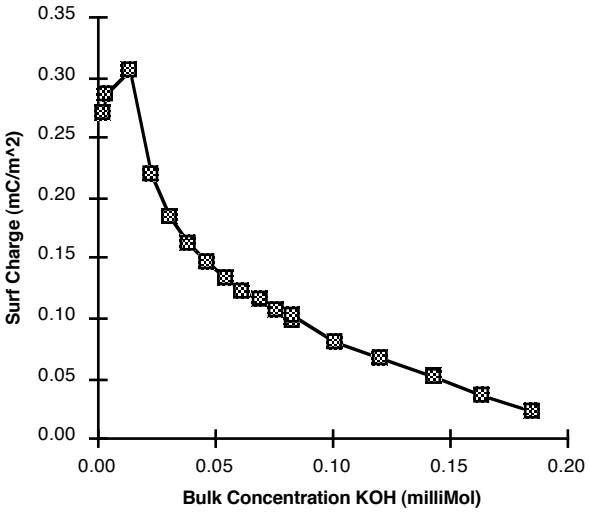

Fig. 3.21 Surface charge density in milliCoulombs per square meter.

3.4.2.5 Modeling Surface Charge with KOH

Returning to the model for surface charge of alumina in pure ethanol above, ethanol molecules adsorbed to the surface dissociate, and ethoxide ions desorb from the surface leaving a positive surface charge. Knowing the bulk ethoxide activity and zeta

potential, the surface ethoxide activity can be calculated using the Boltzmann relation, eq. [3.11]. With this it is now possible to plot $\mathbf{K}_1$ from eq. [3.8], and this is shown in Fig. 3.22.

$$Ss\cdot H^+\cdot EtO^- \Leftrightarrow Ss\cdot H^+ + EtO_S^-$$

$$\mathbf{K}_1 = \frac{\left[Ss\cdot H^+\right] f_-\left[EtO_S^-\right]}{\left[Ss\cdot H^+\cdot EtO^-\right]} \qquad [3.8]$$

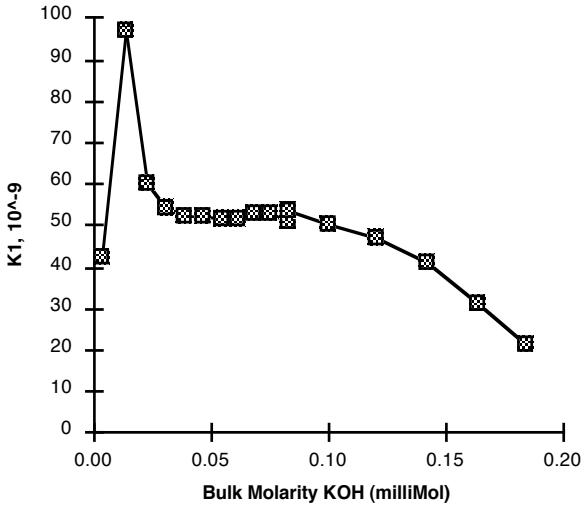

Fig. 3.22 Plot of $\mathbf{K}_1$ from Eq. [3.8]. Quantities are in Moles or Mol/m^2, as appropriate.

Looking at this plot more closely, it can be seen that if the first three points at the lowest KOH concentrations and the last four points at the highest KOH concentrations can be neglected, then the remaining data points are well within 5% of a constant, as shown in Fig. 3.23. Moreover, there are very reasonable bases for believing that these points at the extremes can be neglected.

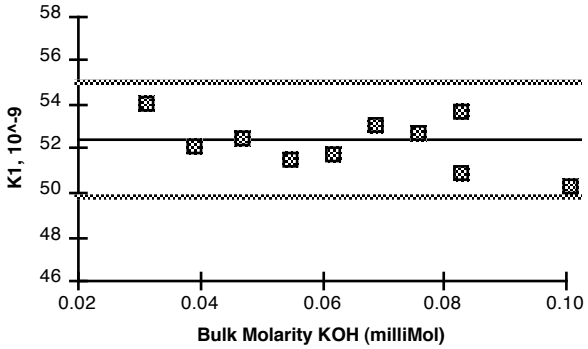

Fig. 3.23 Plot of $\mathbf{K}_1$ from Eq. [3.8]. Range of zeta potentials from 21 to 5.7 mV, bulk conductivities from 1.3 to 4.1 μS/cm. Dashed line is average value of 5.25E-8. Gray lines indicate ± 5% from average.

The first three points in Fig. 3.22 have a relatively high degree of uncertainty both because of uncertainty of the exact quantity titrated in the initial injections of KOH titrant and the uncertainty of the interpolation of free molarity from adsorption data taken in a region where the conductivity is less that 1 μS/cm. Furthermore, if the hypothesis that the surface catalyzes the autoprotolysis of ethanol is correct, then at low ionic strengths in the bulk, the ionic strength at the surface cannot be calculated from the bulk. This adds an additional uncertainty to the surface charge density calculation which depends on knowing the ionic strength near the surface.

The final four data points plotted in Fig. 3.22 represent data points where the measured zeta potential is less than 5 mV. There are two easily identifiable sources of error in surface potential measurement at values this low; floccing of the particles, and the nature of the surface charge. DLVO calculations indicate that the interparticle repulsion goes to zero at a bulk molarity of 0.06. Therefore as zeta potential continues to drop and ionic strength to rise with further additions of KOH, it is reasonable to expect that floccing of the particles would cause the measured zeta potential to deviate from the actual value beyond this point. Furthermore, at the highest ionic strength/ lowest zeta potential point in Fig. 3.23, the uniform surface charge assumption implicit in the calculations performed here becomes questionable. At this point the zeta potential is 5.7mV and the bulk ionic strength 0.10 mMol, this gives a surface charge density of 8.1×10^{-5} C/m^2 and a Debye length of 17nm. If the charge sites are uniformly distributed across the surface, this gives a charge-charge separation distance of 46 nm, almost three times the Debye length.

So if the hypothesis is that the equilibrium of eq. [3.8] describes the particle surface charge, the test of this hypothesis is whether the value of $\mathbf{K}_1$ calculated from measured data is a constant. Given the above arguments, the range of data that supports the contention that $\mathbf{K}_1$ is a constant, as shown in Fig. 3.23, is actually better than might be expected.

3.4.2.6 Adsorption of KOH

As can be seen from Fig. 3.19 above, the marginal adsorption of KOH increases with increasing KOH concentration. This is only possible if adsorption is mediated by the positive K^+ ion. With the initial small additions of KOH, the positive surface potential repels the positive ions and little adsorption occurs. As more KOH is added, the surface potential drops and the surface concentration of K^+ rises many times faster than the concentration in the bulk. This leads to the inverse marginal adsorption behavior in the region where the particles have a positive and declining surface charge, illustrated in Fig. 3.19.

Without making any assumptions about the nature of the surface adsorption site for the potassium ion, the adsorption can be written as an equilibrium with a generic surface site Ss' as shown in eq. [3.24].

$$Ss' + K_S^+ \Leftrightarrow Ss' \cdot K^+$$
$$\mathbf{K}_{\mathrm{K}} = \frac{\left[Ss \cdot K^+\right]}{\left[Ss'\right] f_+ \left[K_S^+\right]} \qquad [3.24]$$

This can be rewritten in the form of a standard Langmuir adsorption isotherm, eq. [3.25].

$$\left[Ss \cdot K^+\right] = Ss_{Tot} \frac{\mathbf{K}_{\mathrm{K}} \, f_+ \left[K_S^+\right]}{1 + \mathbf{K}_{\mathrm{K}} f_+ \left[K_S^+\right]} \qquad [3.25]$$

As above in the case of Cl^- adsorption, the inverse of eq. [3.25] is plotted and a straight line is fitted to the data by least squares. The result is a total surface adsorption of 2.4 μMol/m^2 and an adsorption equilibrium constant $\mathbf{K}_{\mathrm{K}}$ of 1.8 with quantities in millimolar or millimoles/m^2.

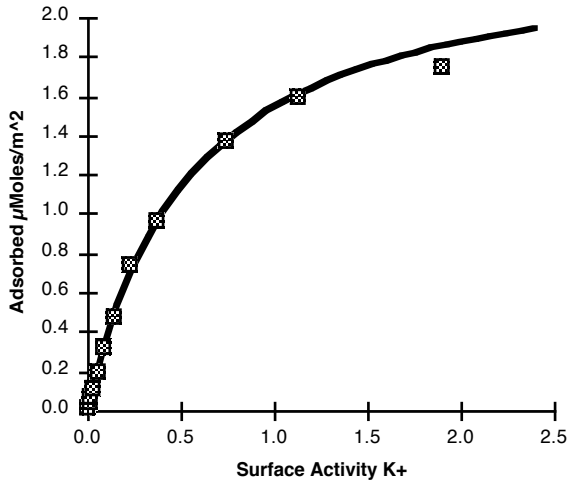

Fig. 3.24 Surface adsorption as a function of surface K^+ activity.

What is interesting about this adsorption isotherm is that it appears to be a function only of the surface activity of the positively charged potassium ion, yet has no effect on the surface charge density. Over the concentration range shown in Fig. 3.23 where surface charge appears to be only a function of ethoxide concentration, the adsorption of K^+ goes up from 2% to 60% (0.047 to 1.4 μMol/m^2) of total surface sites, and the surface activity goes up by a factor of 70, from 0.011 to 0.75 mMolar. From this it is clear that the adsorption of K^+ must be by some charge neutral mechanism. The adsorption of a K^+ ion must either be accompanied by the adsorption of a negative ion or the desorption of a

positive ion and must occur in such a manner that it does not affect the ethoxide adsorption equilibrium.

One possible explanation for the absence of an effect of the K^+ adsorption on surface charge would be that the K^+ could only stably adsorb along with a negative ethoxide or hydroxide ion, eq. [3.26].

$$Ss' + K_S^+ + EtO_S^- \Leftrightarrow Ss' \cdot K^+ \cdot EtO^- \qquad [3.26]$$

However this implies a dependency of adsorption on the ethoxide activity at the surface which is not supported by the data.

Another charge neutral mechanism would be the substitution of a potassium ion for the proton from a surface adsorbed ethanol molecule.

$$Ss \cdot H^+ \cdot EtO^- + K_S^+ \Leftrightarrow Ss \cdot K^+ \cdot EtO^- + H_S^+ \qquad [3.27]$$

An argument against this mechanism would be that there should be an effect of the activity of the proton in the solution at the surface. This means that the adsorption should be a function of both the K^+ activity and the inverse of the ethoxide activity, but here again there is no indication of an ethoxide dependency in the data.

However, if we accept the hypothesis that the surface acts as a catalyst to dissociate ethanol molecules into adsorbed protons and ethoxide ions, then the adsorbed proton concentration will be a function of ethanol activity, which is effectively constant. This mechanism can then fulfill the two seemingly contradictory conditions that: 1) adsorption is only a function of activity of the positive potassium ion, and 2) the adsorption of the K^+ ion have no effect on the surface charge, which remains only a function of the ethoxide activity.

A second possible argument against this adsorption mechanism is that the number of sites does not match the number of sites determined by Cl^- adsorption. The total K^+ adsorption is 2.4 μMol/m^2 vs. a Cl^- adsorption of 3.5 μMol/m^2. This can potentially be explained by the size difference of the proton and the K^+ ion. An adsorption site density of 3.5μMol/m^2 would give a site-site spacing of 7.4 Å assuming a uniform hexagonal spacing of sites across the surface. Given that the sites are likely not uniformly spaced, it seems reasonable that there would be sites that would not fit the 3.0 to 3.3 Å diameter K^+ ion.

An implication of this adsorption mechanism and the lack of an effect of K^+ adsorption on the surface charge is that the positive and negative surface adsorption sites are separate sites and do not interact. There has to be a significant physical separation between positive and negative sites for the substitution of the much larger potassium ion to have no effect on the ethoxide adsorption. This in turn implies that surface adsorbed ethanol is completely dissociated into ethoxide and a proton adsorbed to different sites.

This again supports the picture of the alumina surface as a catalyst for the autoprotolysis of the ethanol-water solvent.

3.4.3 Conclusions Regarding Alumina Surface Charging

The picture of the behavior of the alumina surface in ethanol that emerges from the data above is as follows.

When the alumina powder is put into ethanol it adsorbs a coating of ethanol molecules. This is a dissociative adsorption process where a proton is adsorbed to a Lewis base site and an ethoxide ion is adsorbed to an adjacent Lewis acid site. Of the two ions, the ethoxide ion is more readily dissolved from the surface. This leaves behind a net positive charge on the particles in pure ethanol.

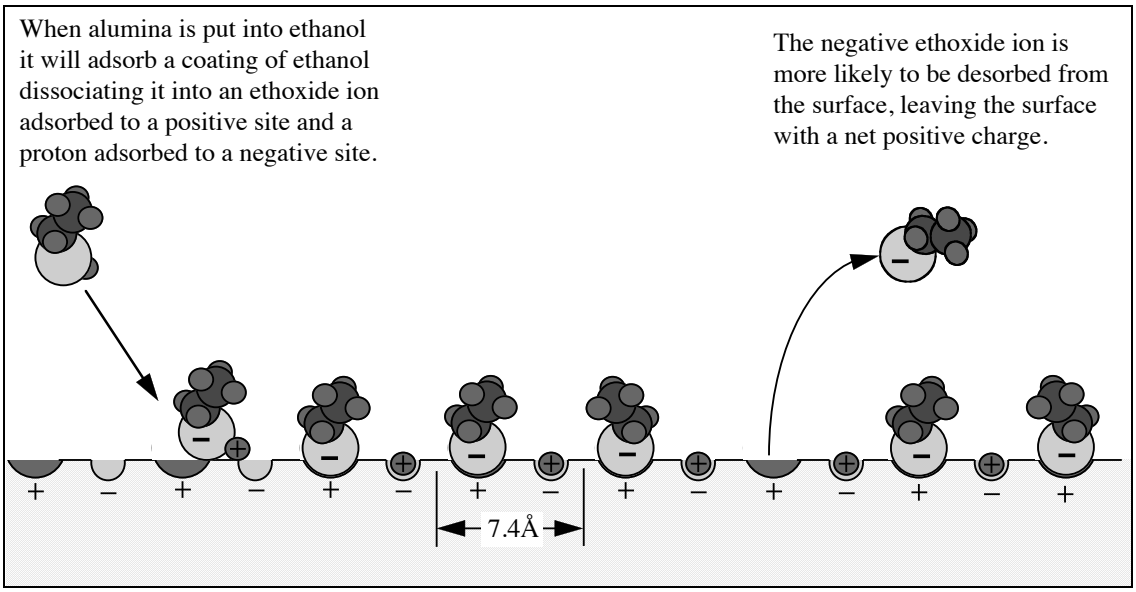

Fig. 3.25 Development of surface charge in pure ethanol.

The dissociated ethanol will also desorb from the surface as negative ethoxide ions and protons in the form of hydronium or protonated ethanol ions. The alumina surface therefore acts as a catalyst for the autoprotolysis reaction of ethanol, eq. [3.22]. (Hydroxide and protonated ethanol molecules exist but solvent ions will primarily be hydronium and ethoxide.)

$$HEtO + H_2O \Leftrightarrow EtO^- + H_3O^+ \qquad [3.22]$$

As the two types of ion diffuse outward from the surface they will recombine to form neutral ethanol molecules until at some distance from the particle they reach the equilibrium prevailing in the bulk solution. The effect of this is that the particle surrounds

itself with its own ionic atmosphere. At the particle surface there can be significant concentrations of ethoxide ions even when they are virtually non-existent in the bulk solution. This behavior is critical in understanding the surface adsorption and surface charging of the alumina powder.

When HCl is titrated into the suspension the activity of the ethoxide in the bulk drops effectively to zero due to reaction with the acid. This reduces but does not eliminate the ethoxide in solution at the surface. The reduction of ethoxide in solution at the surface does mean that more ethoxide desorbs from the surface and the net positive charge on the surface increases.

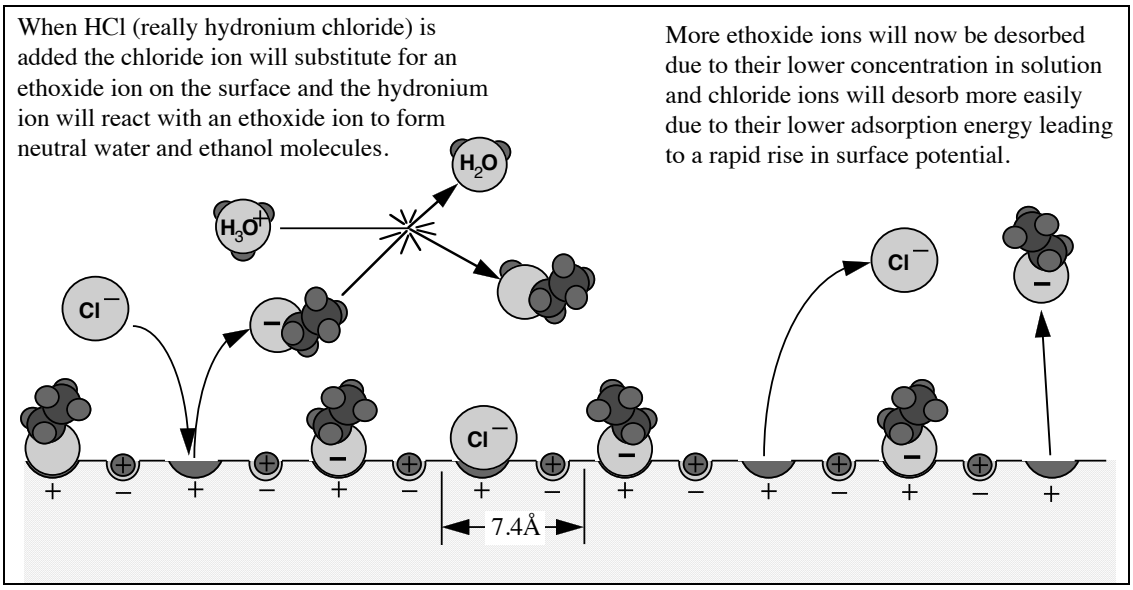

Fig. 3.26 Surface charge formation in ethanol/water with added HCl.

The Cl^- ions are adsorbed at the same Lewis acid sites as the ethoxide ions on the surface. This leads to a competitive adsorption process where the ratio of Cl^- to EtO^- adsorbed to a fixed number of sites on the surface is determined by the activity ratios of the two ions in solution at the surface.

The adsorption energy of the Cl^- ion to these sites is lower than that of the EtO^- ion. Therefore the number of unoccupied sites, which determines surface charge, will be higher at a given concentration of Cl^- compared to the EtO^- ion. The positive charge increases with the reduction of ethoxide and the substitution of Cl^- on the surface sites until the concentration of Cl^- at the surface is sufficient to begin to suppress the desorption of Cl^- from the surface.

The strongest base in ethanol is the ethoxide ion. Any stronger base will react with the ethanol solvent to form ethoxide ions. In the titration of potassium hydroxide/ethoxide,

the increased concentration of ethoxide in solution suppressed the dissociation of ethoxide from the surface, rapidly eliminating the net positive charge on the particle surface. However, despite a significant concentration of free ethoxide in the solvent, the desorption of protons from the surface never significantly exceeded the desorption of ethoxide and no net negative charge formed within the probable margin of error of the measurements made here. Thus it appears unlikely that in the absence of specific adsorption this hydrated alumina will develop a negative surface charge in this solvent.

If this model of surface chemistry, adsorption and charge formation can be extended to pure aqueous solutions, it would explain two frequently observed experimental phenomena. The first is the large difference between the surface charge density determined by titration and that determined by electrokinetic measurements. (**18**) This is explained here by the very large ratio between the number of active surface sites and the number of unoccupied sites necessary to generate the kinetically observed surface charge. The second is the nature of the surface charge. The second is the measured force between two approaching charged surfaces. It has been observed that the force falls between that predicted by a constant surface charge and a constant surface potential model. (**20**) If the surface charge was independent of ionic composition of the bulk solution then constant surface charge behavior would be expected. If the surface charge was only a function of the ionic composition of the bulk solution then the constant surface potential model would be correct. In the theory put forward here the surface charge is set in part by the activity of the solvent at the surface, which is a constant, and in part by ionic activities at the surface, which is a function of surface potential and composition of the bulk solvent. This leads to a behavior which will be in between constant charge and constant potential.

The objective of this chapter is to better understand the surface chemical behavior of an oxide powder in a particular system for electrophoretic deposition, with the ultimate goal of being able to quantitatively predict adsorption and surface charge in an arbitrary chemical environment. Based on the formulas and quantities developed here, it is possible to make quantitative estimates of the particle-electrode double layer interaction for many conditions during electrophoretic deposition, and at least qualitatively describe the interactions at all times and positions in the depositing layer. With a modest amount of additional work this information could be adapted for computational modeling of the deposition process. In the following chapter the surface adsorption quantities developed here are a vital component of an analytic description of the ionic flux at the deposition electrode. The data in this chapter provides a foundation for a very compelling analytic demonstration in Ch. 4 of the existence, nature and scale of what is referred to here as the Ion Depletion Augmented Electrostatic deposition mechanism.

Symbols used in Chapter 4

Abbreviations

DEBL — Diffuse electrostatic boundary layer

EHD — Electrohydrodynamic

EPD — Electrophoretic Deposition

Symbols

a	Particle radius (m)
c_o	Ionic concentration in bulk solution (Mol/m^3 or milliMolar)
c	Ionic concentration (Mol/m^3 or milliMolar)
d	Distance between parallel electrodes (m)
D_{Cl}	Chloride ion diffusion coefficient (m^2/s)
D_H	Hydrogen ion diffusion coefficient (m^2/s)
E	Electric field (V/m)
F	Faraday Constant
$\boldsymbol{F}$	Force (N)
I	Current Density (A/m^2)
J	Ionic flux (Mol/s•m^2)
k	Boltzmann Constant
q	Solution net specific electrostatic charge (C/m^3)
T	Temperature (K)
u_{Cl^-}	Chloride ion electrophoretic mobility (m/s)
u_∞	Particle velocity (m/s)
x	Distance parallel to electric field (m)

ε	Relative dielectic constant
ε_o	Permittivity constant
κ^{-1}	Debye length (m)
κa	Diffuse layer thickness index
$\boldsymbol{\kappa}$	Conductivity (μS/cm)
Λ	Molar conductivity (cm^2/Ω•Mol)
μ	Solvent viscosity (cP or mPa•s)
$\boldsymbol{\nu}_{Cl}$	Chloride ion mobility (m^2/V•s)
$\boldsymbol{\nu}_H$	Hydrogen ion mobility (m^2/V•s)
ϕ	Electrostatic potential (V)

Chapter 4
Electrophoretic Deposition of an Electrostatically Stabilized Alumina Powder Suspension

4.1 Introduction

Having developed in Ch. 3 a fairly complete picture of the solution and surface chemistry of alumina in ethanol, this chapter now undertakes an analysis of the electrophoretic deposition (EPD) of alumina particles from these suspensions.

The chapter begins with the description of a simple EPD experiment in which a series of twenty one deposition trials were performed on a suspension of alumina particles in ethanol with increasing quantities of added HCl. Of these twenty one trials, three trials showing different types of behavior were chosen for detailed analysis.

Unfortunately, even the simplest EPD experiment is a complicated event. To break this process down into components the explanation will follow the same 4-C pattern used in Ch. 2: chemistry, conduction, convection, and colloid. Chemistry — what ions are created or consumed at the electrodes during conduction. Conduction — what ionic concentration and voltage gradients form in the solution due to diffusion and migration of ions between the electrodes. Convection — some of the gradients that develop are unsustainable in a conducting liquid medium and additional ionic transport must be provided by electrically driven convection (electrohydrodynamic or EHD convection). Colloid — only after describing behavior of the solvent alone are the effects of the suspended particles introduced.

A large portion of this chapter is devoted to analysis of conduction in the solvent in the absence of particles. It is only after understanding the behavior of the solvent in conduction without particles is it possible to understand the effects of particles on the system. The apparently contradictory result of this analysis is that, while particle electrophoresis has a negligible effect on conduction, it has a decisive effect on ionic transport. Secondly, once the particle electrophoresis is stopped at the deposition electrode, the physical effect of an accumulation of solid, non-conducting particles is again negligible compared to the ionic buffering effect of particle surface adsorption. Only once the complex interactions of conduction in a colloid suspension are understood and how voltage and concentration gradients are suppressed or stabilized at the deposition electrode, does it become possible to describe how stably suspended particles can be deposited and consolidated to form a dense deposition.

Of the many effects and concepts discussed in this chapter, the concept of primary importance is that of 'Ion Depletion Enhanced' electrostatic deposition. This is one of the most important practical mechanisms for EPD both because it is one of the few mechanisms that can produce a dense deposition prior to drying and because it has an effective, inherent automatic leveling effect. This means that uniformly packed, uniform thickness depositions can be reliably and repeatably produced even without perfect conditions of electric field or suspension density. The information in this chapter should allow the careful reader to direct research on deposition systems to try to induce this effect, to recognize this mechanism of deposition when it occurs, and to optimize conditions when this mechanism of deposition is used.

4.2 Procedure

4.2.1 Suspension Preparation

The Al_2O_3 powder was washed and hydrated as detailed in Ch. 3. Prior to mixing the Al_2O_3 powder was placed in a 135°C drying oven for at least 1 hour to remove excess condensed moisture. 7.988 g of this powder was added to 155.42 g of 99.5/0.5 wt. % ethanol/water in a HDPE bottle. This yields a 1.01 vol. % suspension of alumina particles based on an α-alumina density of 3.97 g/cc. 1 mm diameter alumina milling media was added to $\approx$ 50 vol. % of the mixture (filling the bottle to 1 cm below the surface of the ethanol-alumina suspension). This bottle was placed on a vibratory mill for 20 hours to de-agglomerate the alumina particles. The suspension was then poured into another HDPE bottle through a sieve to remove the milling media prior to deposition trials. There was no evidence of remaining alumina sediment.

4.2.2 Deposition Device

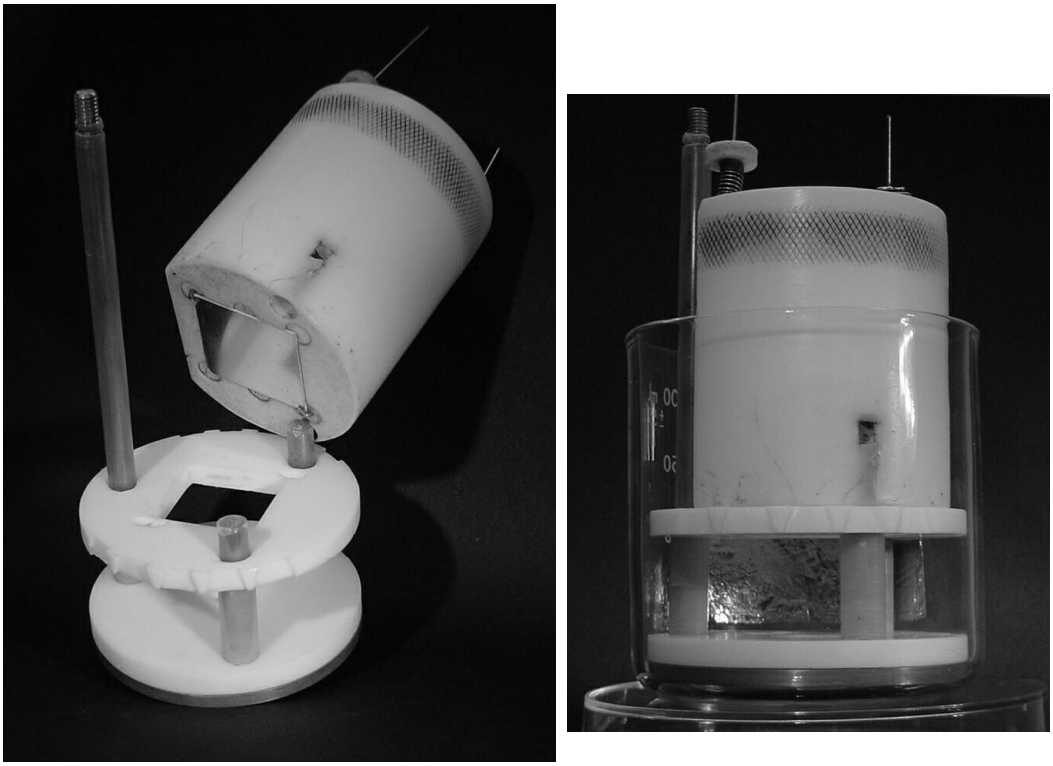

(a) (b)

Fig. 4.1 Deposition Cell; (a) Device with holder block (upper) lifted from stand and masking disk (lower). Reflective square on the bottom of the holding block is the deposition electrode. (b) Assembled deposition device. One counter electrode is removed for clarity, second counter electrode is visible behind device stand.

The deposition trials were performed using a deposition device designed to be immersed in suspension in a 250 ml, 6.2 cm inside diameter Pyrex beaker. The deposition electrode is a 25.4 x 25.4 x 0.5 mm alumina circuit substrate with a sintered platinum coating on one side which was polished to a mirror finish. The deposition substrate is clipped to a PTFE holder block by two spring loaded stainless steel hooks which also serve to provide electrical connection to the platinum surface. The holder block is placed onto a 5 mm thick PTFE masking disk with a square cut out which exposes a 5.2 cm^2 area of the deposition electrode. The mask disk is mounted horizontally on three posts above a cylindrical volume 1.5 cm high and 6 cm in diameter. The counter electrodes are two platinum foils which each cover one quadrant of the sides of this cylindrical volume.

During a deposition trial particles will move away from the counter electrodes. This creates an area of lower density fluid at the surface of the electrodes. The cell is designed so that this lower density, particle depleted fluid can rise to the surface of the suspension well above the electrophoresis zone. Undepleted fluid from below the surface

of the suspension can then flow back down into the electrophoresis zone in the two quadrants not covered by the counter electrodes, replacing the depleted fluid. This flow pattern prevents gravitational convection or particle depleted solvent from the anode from affecting the deposition behavior at the cathode. In the center of the cylindrical volume the electrophoretic motion of the particles will become vertical, moving into the square mask cut-out toward the deposition electrode. Constant voltage/current is provided by a Keithly 2410 power supply which also provided voltage/current measurements.

4.2.3 Conductivity Measurement

Conductivity was measured using a voltage divider circuit with a 0.5 V oscillating current at the conductivity probe. Oscillation frequency ranged from 100 Hz at the lowest conductivity to 2 kHz at the highest. The conductivity probe was a shiny platinum parallel plate design with a cell constant of 0.107 cm^{-1} (Orion Research, Inc., Beverly, MA). Accuracy is estimated to be the larger of ± 0.2 μS/cm or ± 3%.

4.2.4 Deposition Procedure

The following is the step by step procedure for each deposition trial:

- 1 wt. % HCl solution in ethanol, if any, is added using a transfer pipette. The quantity is determined by the weigh of the pipette before and after the acid solution is added.
- Suspension is stirred for at least 30 sec. to assure suspension uniformity, regardless of whether acid solution is added.
- Measure Conductivity.
- Deposition substrate is mounted on holding block and holding block placed on deposition device in the suspension.
- The power supply is turned on for approximately 1 sec. at 20 V and the current is recorded. The power supply is then switched to constant current mode and this current is entered.
- The power supply is then turned on for 120 sec. at constant current and the voltage recorded manually every 15 sec.
- The mounting block and deposition substrate are then removed from the suspension and observed for deposition. The deposition substrate is removed from the mounting block with tweezers for rinsing. The deposition is exposed to air for approximately 30 sec. during this step. Although some evaporation occurs, no area of the deposition or substrate becomes dry prior to rinsing.

- The deposition substrate is rinsed in clear, as-received ethanol.
- The deposition is then allowed to dry and the weight is measured.
- The deposition substrate is then cleaned and the procedure is repeated.

The procedure for determining the set point for the constant current deposition trials proved to be a useful shortcut for determining a current which generates a uniform electric field at different conductivities. The relationship between conductivity and current setting is shown in Fig. 4.2.

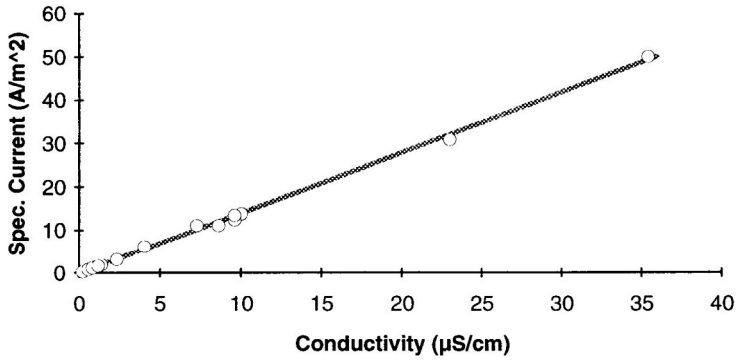

Fig. 4.2 Relation between current set point and conductivity.

4.3 Data

This chapter will analyze a series of twenty one deposition trials performed on a single alumina suspension with increasing additions of HCl. As shown in Fig. 4.3 these depositions can be separated into three groups: depositions that occurred with no added acid, trials with small amounts of added acid where no depositions occurred, and trials at higher conductivities marked by significant voltage rises and dense deposition layers.

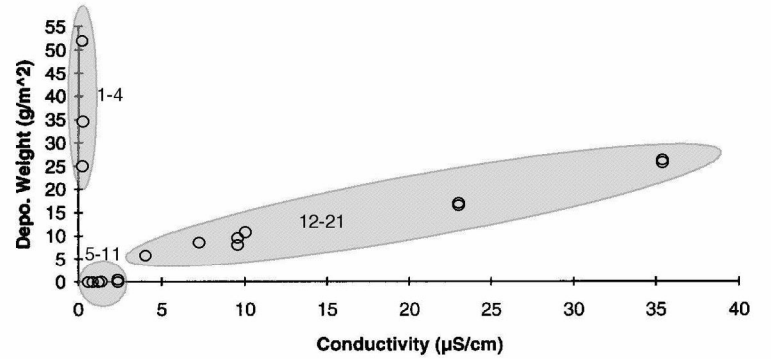

Fig. 4.3 Relationship between conductivity and deposition weight. Deposition trials can be separated into three groups.

Deposition Trials 1-4 — The first four deposition trials were performed on the as-prepared suspension containing only ethanol solution and alumina powder. Measured conductivity was 0.2 μS/cm. The current setting for deposition was 32.7 mA/m^2.

Although depositions resulted from these trials, the results were very non-uniform. The voltage rises during deposition were 0.5, 2.0, 0.8 and 0.7 V. The first trial resulted in a thick, fluffy deposition covering most of the center of the electrode. The deposited area had irregular edges. Near the boundaries of the masked area there was no deposition. The unrinsed average deposition weight was 24 g/m^2. The second deposition covered the entire deposition area, however the entire deposition was removed by rinsing. During rinsing a distinct flow pattern was observable. The third deposition was very thick and appeared uniform prior to rinsing, however rinsing revealed a distinct flow pattern. Weight after rinsing was 53 g/m^2. The final deposition in this set again yielded a fairly uniform, low density deposition. When the deposition was removed from the holder block and held at an angle the surface of the deposition was observed to flow off. The deposition weight without rinsing was 34 g/m^2.

Deposition Trials 5-11 — Deposition trials in this set were conducted with progressively higher additions of HCl yielded no significant deposition. The first five trials in this set covered a conductivity range from 0.6 to 1.2 μS/cm and showed voltage rises from 0.2 to 0.7 V. The final two deposition trials were conducted at a conductivity of 2.3 μS/cm and showed voltage rises of 1.0 and 1.1 V. A very small deposition of particles was observed as a slight fogging of the reflective platinum surface. The deposition weight of 0.6 g/m^2 is only slightly above the estimated accuracy of the scale used here of $\pm$0.2 g/m^2 , however this deposition appears to correspond to a uniform, well packed monolayer of particles. The final deposition trial of this set, #11, was chosen for detailed analysis in the following sections. The data for this trial is given in Table 4.1 and the voltage rise is shown in Fig. 4.5.

Depositions 12-21 — This set of trials was marked by significant voltage rises during deposition, an overlayer of particles which rinse off the substrate, and a uniform, dense deposition layer which does not rinse off. Conductivities range from 4.4 to 35.4 μS/cm. Voltage rises increased with conductivity from 2.0 to 18.9 V. Deposition weights also increased with conductivity from 5.8 to 26.1 g/m^2.

Depositions in this set were rinsed by dipping the substrate into the rinse ethanol and moving it back and forth at several tens of centimeters per second until no further alumina was seen to rinse off. The remaining deposited layers did not show evidence of any large scale convection patterns.

Two depositions in particular, #'s 16 and 20, were chosen from this set for detailed analysis. The data from these depositions are listed in Table 4.1 and their voltage rise profiles are shown in Fig. 4.5.

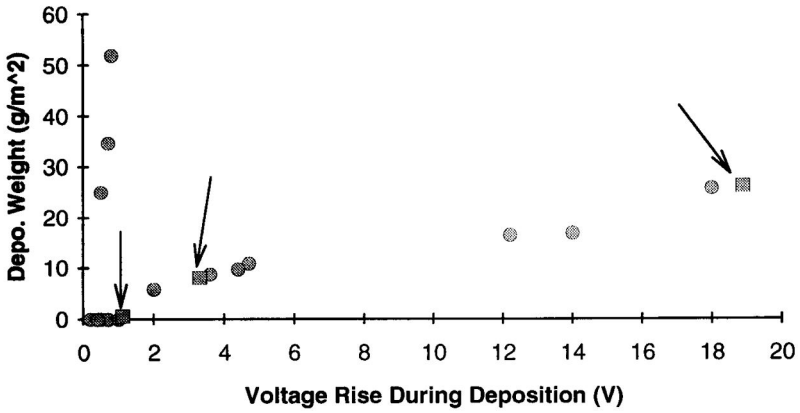

Fig. 4.4 Relationship between voltage rise and deposition weight. Deposition trial #'s 11, 16 & 20 are square markers indicated by arrows.

Table 4.1 Deposition Data

	Trial 11	Trial 16	Trial 20
Conductivity	2.31 μS/cm	9.58 μS/cm	35.4 μS/cm
Current density (I)	0.32 A/m^2	1.25 A/m^2	5.0 A/m^2
Total current	38.3 C/m^2	150 C/m^2	600 C/m^2
Voltage rise	1.0 V	3.3 V	18.9 V
Deposition weight	0.6 g/m^2	8.1 g/m^2	26.1 g/m^2
Deposit specific current	66 C/g	18 C/g	23 C/g
Deposition thickness at 60 vol. % density	0.24 μm	3.4 μm	11.0 μm

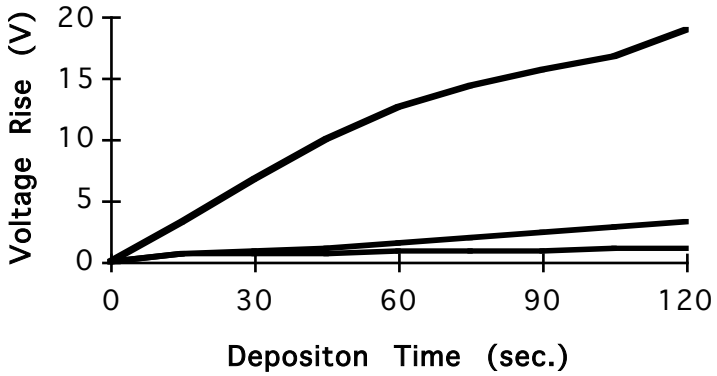

Fig. 4.5 Voltage rises in deposition trial #'s 11, 16 & 20 .

Data from Prior Experiments — Two facts used here result from prior experience with depositions of this type. The first is the density of the deposited layer. Density of the deposited layers was not measured in this experiment, however, previous measurements have shown that these types of depositions, marked by a rise of several volts during deposition and which cannot be removed even by vigorous agitation during rinsing, have a density between 50 and 65%. Based on this, a density estimate of 60 vol. % is used here. A lower actual density will not significantly affect the conclusions reached here.

The second fact used here is the location of the excess voltage that arises during deposition. Experiments using a platinum wire as a voltage probe have shown that the voltage rise during deposition is almost completely accounted for by a potential difference across the deposited layer. For example, a constant current deposition with an initial potential of 20 V shows a rise in voltage to 40 V over the course of the deposition. The final voltage breakdown will be approximately: 20 V due to resistance of the solution; 1 V to drive convection in solution due to concentration gradients, this is sometimes referred to a concentration potential; and 19 V across the deposited layer. The wire probe can be pressed against the deposited layer, and, as long as the deposited particles are not scraped away, a 19 V potential difference will be measured between the deposition electrode and the solvent side of the deposition. This was confirmed by the voltage measurements of Sarkar and Nicholson (**1**).

4.4 Analysis

The quantitative analysis of any of the mechanisms of EPD is not a simple prospect. Many reactions happen at one time in a very small space where particles, ions and solvent are all in relative motion due to diffusional gradients and electrostatic forces on several scales. Equilibrium is the exception — not the rule. Furthermore, of the various mechanisms of deposition the one featured here, Ion Depletion Enhanced Electrostatic, is likely the most complex and least intuitive.

To handle the complexity of this process a description is built up step-by-step with each step adding an element of complexity to make the description more complete. Before beginning on the EPD process a foundation for this step-by-step buildup is given in § 4.4.1. Using the data and analysis from Ch. 3, a complete, quantitative description is given of the three suspensions to be focused on here. The first step in understanding the EPD process, § 4.4.2, is a description of the electrochemical reactions involved in conduction in the solvent, ignoring all other effects. The next step, § 4.4.3, adds a significant level of complexity by analyzing the transport of ions through the solvent at the deposition electrode in the absence of convection. This analysis is then the basis for the next step, § 4.4.4, describing the initiation of convection in the solvent. It is only after this basic picture of conduction and convection in the solvent is drawn up that particles are first introduced. In § 4.4.5 it is shown that even though the particles do not contribute significantly to the conductivity of the solution, they have a dramatic impact on ionic transport and convection. Finally this is brought together in § 4.4.6 for a complete explanation of the deposition experiment.

4.4.1 Suspension Description

Molar Conductivity, Ionic Mobility & Diffusion — Using the Fuoss-Onsager equation as detailed in Ch. 3, from the conductivity it is possible to iteratively solve for the molar conductivity and ionic concentration in the solution. These are shown in Table 4.2. The molar limit conductivity for HCl in this ethanol/water mixture is 53.4 S•cm^2/Mol. This conductivity is the sum of the conductivity due to the mobility of the chloride and hydrogen ions in solution.

$$\Lambda_{o_{HCl}} = \lambda_{o_{Cl^-}} + \lambda_{o_{H^+}} \qquad [4.1]$$

Grahm et al. (**2**) measured the molar limit conductance for the chloride ion in anhydrous ethanol as 21.9 S•cm^2/mol. The mobility of the chloride ion will be relatively unaffected by water content therefore this can be taken as an estimate for the limit conductance of chloride in this solvent as well. This gives a molar limit conductance for the proton of

31.5 S•cm^2/mol. Since ionic strength effects will affect both positive and negative ions equally, this ratio is used to divide the molar conductivity at each concentration between chloride and proton components. This molar conductivity is converted to an ionic mobility by dividing by the Faraday constant:

$$\nu_i = \frac{\lambda_i}{F} \qquad [4.2]$$

The Einstein relation is then used to estimate the diffusion coefficients, D_i, from the ionic mobilities:

$$D_i = \frac{kT}{z_i e}\nu_i \overset{or}{=} \frac{RT}{z_i F}\nu_i \qquad [4.3]$$

These values are listed in Table 4.2 for the three deposition conditions to be analyzed here.

Table 4.2 Ionic Properties of Solution

	Trial 11	Trial 16	Trial 20
Conductivity	2.31 μS/cm	9.58 μS/cm	35.4 μS/cm
Molar conductivity (Λ)	51.3 cm^2/Ω•Mol	49.9 cm^2/Ω•Mol	47.1 cm^2/Ω•Mol
Bulk HCl Concentration (milliMolar or Mol/m^3)	0.045 mMolar	0.192 mMolar	0.751 mMolar
Chloride ion mobility (ν_{Cl})	2.19x10^{-8} m^2/V•s	2.13x10^{-8} m^2/V•s	2.01x10^{-8} m^2/V•s
Chloride ion diffusion coefficient (D_{Cl})	5.62x10^{-10} m^2/s	5.42x10^{-10} m^2/s	5.16x10^{-10} m^2/s
Hydrogen ion mobility (ν_H)	3.13x10^{-8} m^2/V•s	3.04x10^{-8} m^2/V•s	2.87x10^{-8} m^2/V•s
Hydrogen ion diffusion coefficient (D_H)	8.03x10^{-10} m^2/s	7.81x10^{-10} m^2/s	7.37x10^{-10} m^2/s

Mobility, Electrostatic Stability & Surface adsorption of particles — Table 4.3 gives some of the colloidal and electrochemical properties of the suspensions in the three deposition trials to be analyzed in detail. The diffuse layer thickness index is calculated using the average particle radius of 135 nm. For trials # 11 and 16 the mobility was interpolated from data collected in Ch. 3. For trial # 20 the mobility was extrapolated using the straight line fit shown in Fig. 3.8. Surface potential and particle charge were calculated using the procedure of § 3.4.1. The particle charge is calculated by multiplying the surface charge density with the surface area of an average size 270 nm dia. particle. The surface adsorbed quantity of HCl is calculated using Eq. [3.17].

Table 4.3 Surface and Colloid Properties

	Trial 11	Trial 16	Trial 20
Debye length (κ^{-1})	26 nm	12.5 nm	6.3 nm
Diffuse layer thickness index (κa)	5.24	10.8	21.4
Electrophoretic mobility	0.97 μm•cm/V•s	0.85 μm•cm/V•s	0.47 μm•cm/V•s
Surface potential	79 mV	51 mV	26 mV
Average Particle Electrostatic Charge	2.52×10^{-16} C	2.64×10^{-16} C	2.40×10^{-16} C
Surface adsorbed HCl	21.4 μMol/g	27.5 μMol/g	31.6 μMol/g

From the data above it is possible to estimate the interaction potential of two average diameter spherical particles. These are shown in Fig. 4.6. The attractive L-VdW force is calculated as outlined in § 2.4.3. This is adjusted for retardation of the interaction as separation distance increases using the estimation method of Russel, et al. (**3**, p155). The repulsive force that results from the overlap of the DEBL's is calculated using the Derjaguin approximation for constant potential $\Phi = 2\pi\varepsilon_r\varepsilon_o\psi_o^2 a \ln\left(1+e^{-\kappa h}\right)$. The total interaction energy is then the sum of these two forces.

To obtain an order-of-magnitude estimate of the electric field that would be necessary to bring two particles together, the maximum interparticle repulsion force was divided by the charge on a single average particle to obtain the voltage gradient that would produce an equivalent force on an isolated particle, independent of EHD effects.

Table 4.4 Particle Interaction Properties

	Trial 11	Trial 16	Trial 20
Max. Energy Barrier to Floccing	230 *kT*	70 *kT*	3.5 *kT*
Max. Interparticle Repulsion Force	28.2 pN	15.5 pN	1.42 pN
Electric Field to Produce an Equivalent Force	1,120 V/cm	590 V/cm	60 V/cm

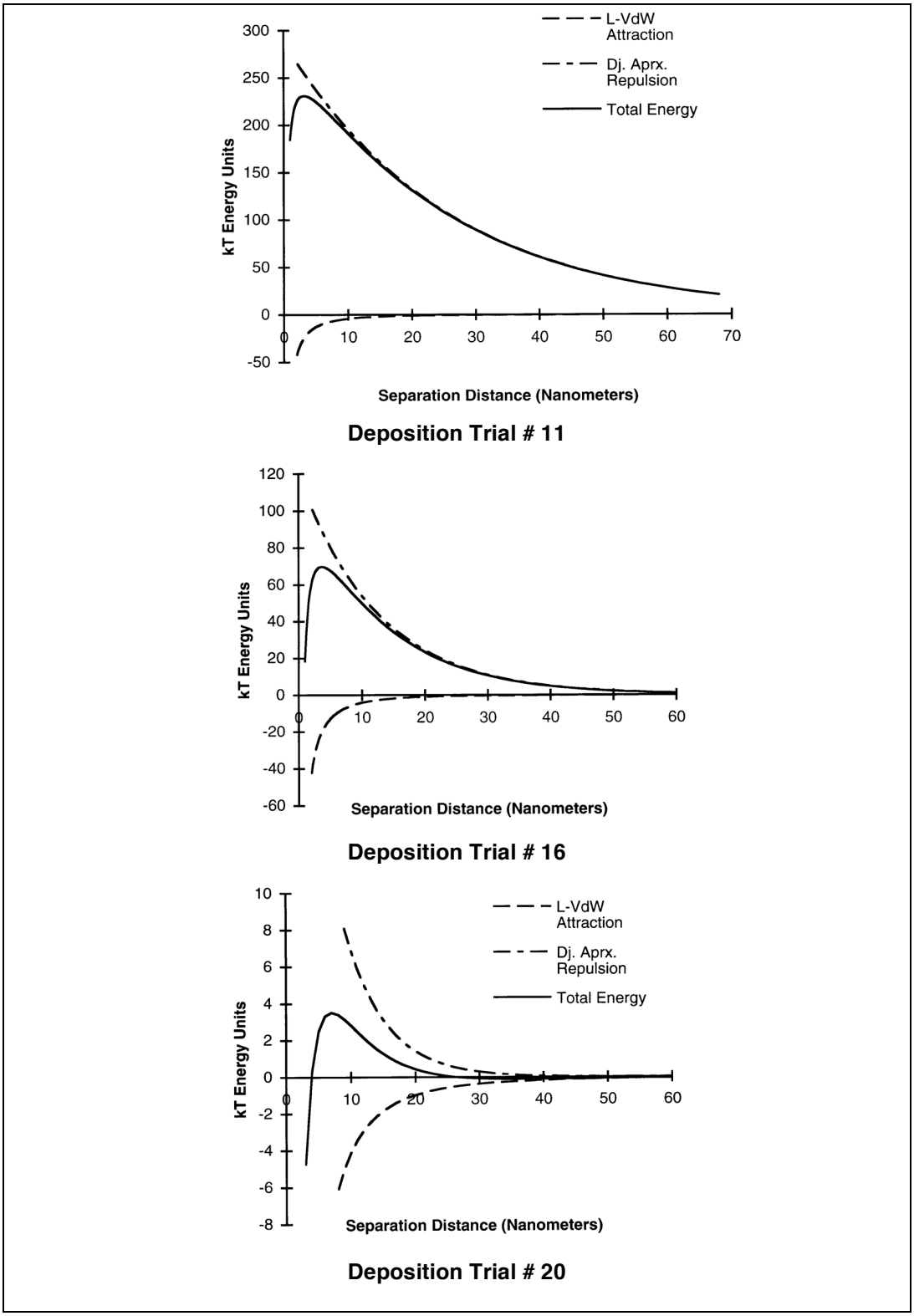

Fig. 4.6 Calculated electrostatic stabilization energies.

4.4.2 Chemistry of Conduction

There are three components to direct current conduction in a solution. Electrochemical reactions at the cathode transfer electrons to the solution to either reduce positive ions from solution or introduce negative ions into solution. At the anode electrons are removed from solution either by removing electrons from negative ions or the oxidation of neutral atoms or molecules to produce positive ions. Between these two electrodes conduction in solution consists of the motion of ions from one electrode to another, with the possibility of these ions participating in chemical reactions along the way. These components for the specific solution here are as follows:

Cathode Reactions — The cathode reaction in this system is fairly simple. Hydrogen ions arriving at the surface in the form of hydronium or ethoxonium ions are neutralized to form hydrogen gas and water or ethanol. In the absence of other positive ions which could form a soluble salt with hydroxide or ethoxide ions there will be no electrolysis of the solvent.

Anode Reactions — The chemistry at the anode is slightly more complex with several possible reactions. The primary reaction is presumably the electrolysis of water to produce hydronium or ethoxonium ions and oxygen gas. Other reactions that could be occurring are: the oxidation of chloride ions to form chlorine gas; the combination of the electrolysis of ethanol with the neutralization of a chloride ion to produce ethylene chloride; a combination of electrolysis reactions to produce ethane gas, and the possible formation of platinum chlorides. Reactions which produce hydronium or ethoxonium are essentially neutral. They generate ions which simply replace ions consumed at the cathode. These reactions are also essentially equivalent as the H_3O^+/H_2EtO^+ ratio will go to equilibrium in solution regardless of which ion is produced more rapidly at the electrode.

Reactions which consume chloride ions, either producing chlorine gas or ethylene chloride, will result in a net decrease in ionic concentration in solution. In an extended conduction test in 99.5% ethanol with added HCl there was a drop in ionic concentration equivalent to ≈ 20% of the total electron flux through the solution. This means that 80% of the current at the anode results in the formation of H_3O^+/H_2EtO^+. Over the time span of the depositions here the molar current flux is not significant in comparison to the total quantity of ions in the suspension.

Conduction Through the Solution — Since no ions or reactive chemical species are produced at the cathode, there are no neutralization reactions in the solution, and, although not in concentration equilibrium, the solution remains in chemical equilibrium during

conduction. Ions are only created and consumed at the electrodes and all conduction in the solution takes place by transport of these ions between the electrodes.

Independent of conduction, in ethanol with HCl the formation of ethylene chloride and water is energetically favorable. There is some indication that at sufficient concentration of HCl this mixture may become explosive.(4) However, at room temperature and at the concentrations used here this reaction is very slow. Stock solutions of HCl in ethanol showed no decrease in ionic concentration over several months.

4.4.3 Conduction in the Solvent - Without Convection

The Quasi Neutral Limit Current — A useful first step is to return to the concept of the quasi-neutral limit current outlined in Ch. 2. This can establish the scale on which the problem should be approached and thereby allows some simplifying assumptions.

In Ch. 2 the problem was analyzed for the maximum current that could be carried by a cell with given dimensions, ionic concentration and ionic mobility. For the deposition solutions considered here, the ionic mobilities, concentrations and current density are known, and the question can be re-framed to ask what is the maximum cell size which can conduct this current without convection. Assuming a simple parallel plate cell in which positive protonated ions are created at the anode and consumed at the cathode, the maximum thickness for a given current density will be a simple transposition of Eq. [2.42]:

$$d_{\lim} = 2\frac{FD_{H^+}}{I}c_o \qquad [4.4]$$

Taking c_o as the ionic concentration in the bulk solution and the proton diffusion rate at 0.8 x 10^{-10} m^2/s, the maximum distance between electrodes is 22, 23, and 21 μm using the bulk concentration and current density figures from deposition trials 11, 16 and 20 respectively. Because of the linear relation between concentration and conductivity these distance are similar for all three solutions. Further calculations show that this gradient will form in a fraction of a second.

Given that this thickness is three orders of magnitude lower than the scale of the deposition cell, it is clear that the applied currents in these depositions far exceed the ability of the solution to conduct without violating the assumptions of no convection and quasi neutrality, and these limits are exceeded in a fraction of a second.

To get a picture of what is going on it is helpful to start with a picture of the hypothetical limit current case. In this hypothetical 22 μm cell the ionic concentration will go from almost zero at the cathode to c_o at the anode. This situation is maintained in a steady state by the presence of the anode, which blocks the further migration of the

negative chloride ions. The chloride ion profile then remains stable as electrophoretic migration toward the anode is matched by concentration diffusion back toward the cathode. This is shown in Fig. 4.7 (a).

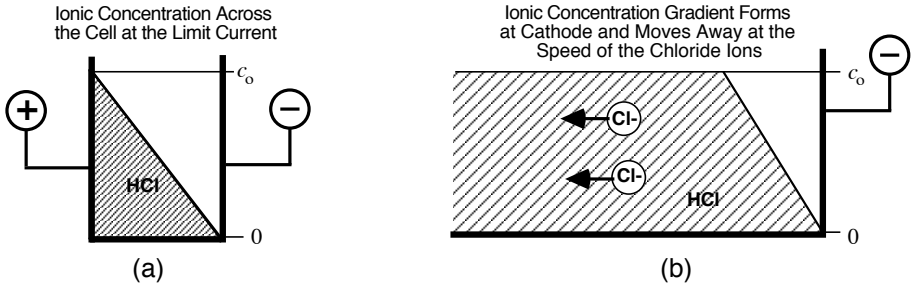

Fig. 4.7 (a) Ionic concentration across the cell at the equilibrium quasi-neutral limit current, (b) anions in the bulk continue to move away from the cathode gradient region.

Beyond the Limit Current- Layers of Conduction — In the actual cell there isn't an anode to block the motion of the chloride ions away from the cathode. At the high side of this concentration gradient, the chloride ions will be moving away from cathode at the same speed as the general migration of chloride ions in the bulk solution. This is shown in Fig. 4.7 (b). Since there is a constant current flux in this system the gradient layer cannot become significantly wider while transmitting the same current without violating quasi neutrality. This means that a moving gradient layer will be formed, slightly less steep than the static gradient layer, that moves away from the cathode at the same speed as the migration of chloride ions in the bulk. This opens up a region between the moving gradient region and the cathode where charge neutrality is completely violated, a very high voltage gradient is created, and conduction is primarily by unaccompanied positive ions. This is illustrated schematically in Fig. 4.8.

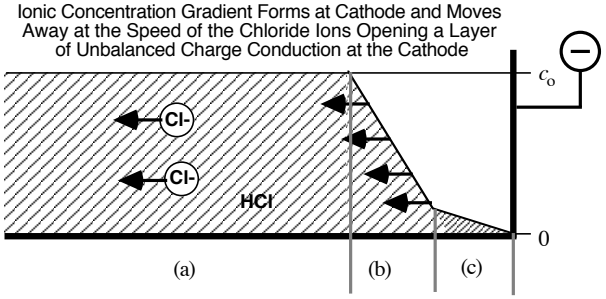

Fig 4.8 Electrochemical boundary region near the cathode without convection is divided into four zones; a) neutral region or bulk solution, b) quasi-neutral or gradient region, c) charged layer or unbalanced charge region, and d) diffuse boundary layer (not shown).

The above treatment shows that the electrochemical boundary layer that is of interest here is on the scale of microns. This justifies ignoring both the anode electrochemical layer and the cathode diffuse electrostatic boundary layer. At the anode chloride ions will be accumulating, the ionic concentration will be going up, and eventually this will cause bulk EHD convection in the cell. However, this is happening two centimeters away from the 20-30 μm cathode electrochemical layer that is analyzed here. The cathode diffuse electrostatic boundary layer (DEBL) will be on the scale of the Debye length prior to the beginning of deposition, 6 to 26 nm. When current begins to flow the ionic concentration outside the DEBL will go down, but this layer will remain well below 1 μm. This boundary layer does have an effect on how the very first layers of particles deposit and adhere to the electrode surface, but this is beyond the scope of the current analysis.

In the following quantitative analysis of the conducting gradient layers in regions A, B & C, the following coordinate system will be used:

- Positive points to cathode.
- A positive current is positive ions moving in a positive direction (toward the cathode) or negative ions moving in a negative direction.
- Concentration and electrostatic potential decline toward the cathode therefore $\frac{\partial c}{\partial x}$ and $\frac{\partial \phi}{\partial x}$ are negative quantities.

As ionic concentration declines in the gradient layer, ionic mobility will rise toward the limit value at zero concentration. To simplify the analysis, the mobilities and diffusion constants are assumed to be constant at their bulk values in the gradient layer, and are taken at their zero concentration limit values in the unbalanced charge layer.

The following analysis of the quasi neutral gradient region is extended from the work of Levich (**5**). The concept and equations for the unbalanced charge conduction layer are from Chazlaviel (**6**).

Region A - Bulk Conduction & Mobility — To calculate the electric field in the bulk solution near the cathode the specific current is divided by the conductivity to get the electric field gradient:

$$\frac{\partial \phi}{\partial x} = \frac{I}{\kappa} \qquad [4.5]$$

This gives voltage gradients of 13.9, 13.0 and 14.1 V/cm for the three cases considered here. The velocity of the chloride ions in the bulk is then the mobility times the field gradient:

$$u_{Cl^-} = \nu_{Cl^-} \frac{\partial \phi}{\partial x} \qquad [4.6]$$

The chloride ion velocities are then 30.3, 27.7 and 28.3 μm/s. Once a stable gradient layer is formed it will move away from the cathode at this velocity.

Region B - The Quasi-Neutral Moving Gradient Layer — The analysis of this layer is based on two assumptions: that of quasi neutrality and that of an equilibrium profile moving gradient layer.

Anywhere there is a concentration gradient in a conducting solution there will also be a change in the voltage gradient. The voltage gradient only changes where there is a net accumulation of positive or negative charge. The assumption of quasi neutrality is only that the difference between the concentration of positive and negative ions at any point is very small compared to the total number of ions present. This does not preclude large changes in voltage gradients, since even a small charge imbalance can create very large voltage gradients.

As the gradient layer moves away from the cathode there are three ways that the gradient profile can evolve. It can: 1) become continually steeper, 2) can achieve an equilibrium profile, or 3) it can grow as it moves with the same total concentration drop spreading over a wider distance. The first case is self limiting. The maximum possible gradient would be a discontinuous step in concentration, however, diffusion would provide a stricter limit on how steep the gradient can become. The gradient is also limited in how flat it can become. Similar to what was shown in the static limit current discussion, the current flux will set a minimum possible gradient through the layer. If the gradient profile is then limited both by how steep and how flat it can become, it must achieve some profile between the two extremes. Since there is no input that would cause it to oscilate, it must approach a steady, equilibrium profile.

Based on the assumption of quasi neutrality, as current flows through the solution there will be no net accumulations of either positive or negative charge. To obey this restriction the net ionic flux must be constant at all points through the gradient layer. This criterion can be expressed by:

$$\frac{I}{F} = J = -D_{H^+} \frac{\partial c_{H^+}}{\partial x} + D_{Cl^-} \frac{\partial c_{Cl^-}}{\partial x} - \nu_{H^+} \frac{\partial \phi}{\partial x} c_{H^+} - \nu_{Cl^-} \frac{\partial \phi}{\partial x} c_{Cl^-} \qquad [4.7]$$

The restriction that the profile of the gradient layer be stable implies that the net motion of the Cl^- ions at all points in the gradient layer will be the same as the migration of the Cl^- ions in the bulk. This can be expressed in terms of current by:

$$\frac{\nu_{Cl^-}}{\nu_{Cl^-}+\nu_{H^+}} J \frac{c_{Cl^-}}{c_{Cl^-_o}} = D_{Cl^-} \frac{\partial c_{Cl^-}}{\partial x} - \nu_{Cl^-} \frac{\partial \phi}{\partial x} c_{Cl^-} \qquad [4.8]$$

The right hand side of this equation is the flux of chloride ions. On the left $\frac{\nu_{Cl^-}}{\nu_{Cl^-}+\nu_{H^+}} J$ is the proportion of net ionic flux due to Cl^- ions in the bulk, and $\frac{c_{Cl^-}}{c_{Cl^-_o}}$ is the ratio of Cl^- ions at a point in the gradient layer to the concentration of Cl^- ions in the bulk.

Using the assumption of quasi-neutrality:

$$c_{Cl^-} \approx c_{H^+} = c \qquad [4.9]$$

where c is a function of position x, these equations can be simplified to:

$$J = \left(D_{Cl^-} - D_{H^+}\right)\frac{\partial c}{\partial x} - \left(\nu_{Cl^-} + \nu_{H^+}\right) c \frac{\partial \phi}{\partial x} \qquad [4.10]$$

$$\frac{\nu_{Cl^-}}{\nu_{Cl^-}+\nu_{H^+}} J \frac{c}{c_o} = D_{Cl^-} \frac{\partial c}{\partial x} - \nu_{Cl^-} c \frac{\partial \phi}{\partial x} \qquad [4.11]$$

Multiplying Eq.[4.21] by $\frac{\left(\nu_{H^+}+\nu_{Cl^-}\right)}{\nu_{Cl^-}}$ gives:

$$\frac{c}{c_o} J = \frac{\left(\nu_{Cl^-}+\nu_{H^+}\right)}{\nu_{Cl^-}} D_{Cl^-} \frac{\partial c}{\partial x} - \left(\nu_{Cl^-} + \nu_{H^+}\right) c \frac{\partial \phi}{\partial x} \qquad [4.12]$$

This can be subtracted from Eq. [4.20] to give:

$$\left(1 - \frac{c}{c_o}\right) J = \left[\left(D_{Cl^-} - D_{H^+}\right) - \frac{D_{Cl^-}\left(\nu_{Cl^-}+\nu_{H^+}\right)}{\nu_{Cl^-}}\right]\frac{\partial c}{\partial x} \qquad [4.13]$$

The term in square brackets can be simplified as follows:

$$\left(D_{Cl^-} - D_{H^+}\right) - \frac{D_{Cl^-}\left(\nu_{Cl^-}+\nu_{H^+}\right)}{\nu_{Cl^-}} = D_{Cl^-} - D_{H^+} - D_{Cl^-} - \frac{D_{Cl^-}}{\nu_{Cl^-}}\nu_{H^+} = -2D_{H^+} \qquad [4.14]$$

Substituting this into Eq. [4.13] and re-arranging gives:

$$\frac{-J}{2c_o D_{H^+}} dx = \frac{1}{c_o - c} dc \qquad [4.15]$$

Integrating both sides gives:

$$\frac{-J}{2c_o D_{H^+}} x + k_1 = -\ln\left(c_o - c\right) \qquad [4.16]$$

where k_1 is a constant of integration. By re-arranging terms, taking the exponential of both sides, and performing one more re-arrangement, a formula for the concentration is obtained:

$$c = c_o - k_1 \exp\left[\frac{J}{2c_o D_{H^+}} x\right] \qquad [4.17]$$

The value for the integration constant k_1 then must be determined by boundary conditions for the problem. Since c will only approach c_o asymptotically, there is no point x where c=c_o. On the other end, there is a theoretical point where c=0. If x is set equal to zero at this point the equation becomes:

$$c = c_o - c_o \exp\left[\frac{J}{2c_o D_{H^+}} x\right] \qquad [4.18]$$

In this equation J , D_{H^+} and c_o will be positive, therefore for increasing negative values of x, c will approach c_o. The value of $\left[J/2c_o D_{H^+}\right]^{-1}$ for the three cases analyzed here is 21.8, 23.1 and 21.4 μm. This number is a useful index of the thickness of the moving gradient layer. Once again because the current flux is proportional the concentration, the thickness of the moving gradient layers in all three cases is similar.

In a similar manner it is possible to solve for the potential, field and field gradient. The details of this are given in appendix B, the results are listed below.

$$\phi = \frac{-J}{c_o\left(\nu_{Cl^-} + \nu_{H^+}\right)} x + \frac{RT}{F} \ln\left(1 - \exp\left[\frac{J}{2c_o D_{H^+}} x\right]\right) + \phi_o \qquad [B.16]$$

$$\frac{\partial \phi}{\partial x} = \frac{-J}{c_o\left(\nu_{Cl^-} + \nu_{H^+}\right)} + \frac{-J}{2c_o \nu_{H^+}} \left[\left(1 - \exp\left[\frac{J}{2c_o D_{H^+}} x\right]\right)^{-1} - 1\right] \qquad [B.7]$$

$$\frac{\partial^2 \phi}{\partial x^2} = -\left(\frac{J}{c_o}\right)^2 \frac{\exp\left[-\frac{J}{2c_o D_{H^+}} x\right]}{4 D_{H^+} \nu_{H^+} \left(1 - \exp\left[-\frac{J}{2c_o D_{H^+}} x\right]\right)^2} \qquad [B.12]$$

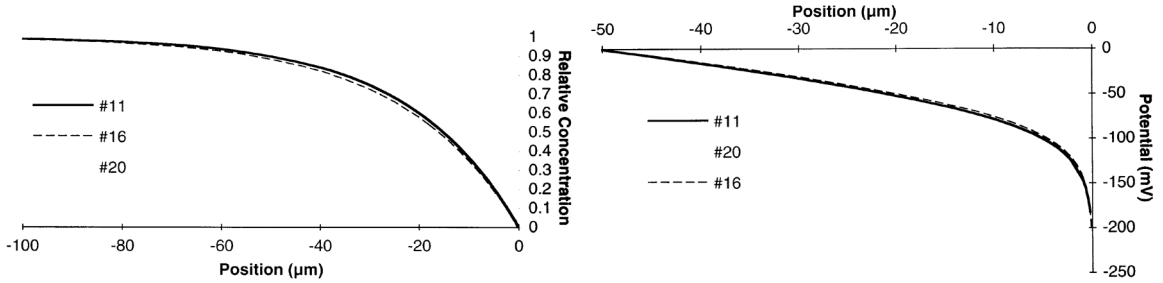

(a) (b)

Fig. 4.9 Equilibrium moving concentration gradient in quasi neutral region.

Table 4.5 Moving Gradient Layer Region

	Trial 11	Trial 16	Trial 20
Conductivity	2.31 μS/cm	9.58 μS/cm	35.4 μS/cm
Current density (I)	0.32 A/m^2	1.25 A/m^2	5.0 A/m^2
Limit current thickness	22 μm	23 μm	21 μm
Bulk voltage gradient	13.9 V/cm	13.0 V/cm	14.1 V/cm
Bulk Cl^- ion velocity	30.3 μm/s	27.7 μm/s	28.3 μm/s
$\left[J/2c_o D_{H^+}\right]^{-1}$	21.8 μm	23.1 μm	21.4 μm

This gradient layer will take approximately 1/2 second to form. This estimate is based on the ionic flux, and a full calculation is not made here. However, after this approximately 1/2 second inception time the gradient layer will begin to move away from the cathode at the migration velocity of the chloride ions in the bulk, ≈ 30 μm/s. This opens up a region of unbalanced charge conduction designated here as region C.

Region C - Unbalanced Charge Conduction Layer — The ionic concentration never actually becomes zero, but at some point it becomes so low and the voltage gradient so high that the assumption of quasi-neutrality will no longer be valid. Given the exponential decline in concentration and rise in voltage through the quasi-neutral gradient region, the edge of this region can be considered a point at which conduction changes to conduction purely by cations with a zero concentration of anions. Because of the very high voltage gradient in this region, migration will be so much higher than diffusion that diffusion can be ignored. This allows current flux to be written as a function only of electric field and cation concentration:

$$J = -\nu_{H^+} c_{H^+} \frac{\partial \phi}{\partial x} \qquad [4.19]$$

The electric field gradient will then be determined by the cation concentration:

$$\frac{\partial^2 \phi}{\partial x^2} = -\frac{F c_{H^+}}{\varepsilon \varepsilon_o} \qquad [4.20]$$

Combining these equations gives:

$$-\frac{F c_{H^+}}{\varepsilon \varepsilon_o} = \frac{\partial^2 \phi}{\partial x^2} = \frac{\partial}{\partial x}\left[-\frac{J}{\nu_{H^+} c_{H^+}}\right] = \frac{J}{\nu_{H^+}} \frac{1}{c_{H^+}^2} \frac{\partial c_{H^+}}{\partial x} \qquad [4.21]$$

Separating variables and integrating to determine concentration as a function of position gives:

$$c_{H^+} = \left[\frac{J\varepsilon\varepsilon_o}{2F\nu_{H^+}x}\right]^{\frac{1}{2}} \qquad [4.22]$$

The constant of integration is set to zero by taking a boundary condition of $c = \infty$ at $x = 0$.

This expression can be substituted into Eq. 4.40 and both integrated and disintegrated to give the potential, potential gradient, and the rate of change of the potential gradient:

$$\phi = \phi_o - \frac{2}{3}\left[\frac{2JF}{\nu_{H^+}\varepsilon\varepsilon_o}\right]^{\frac{1}{2}} x^{\frac{3}{2}} \qquad [4.23]$$

$$\frac{\partial\phi}{\partial x} = -\left[\frac{2JF}{\nu_{H^+}\varepsilon\varepsilon_o}\right]^{\frac{1}{2}} x^{\frac{1}{2}} \qquad [4.24]$$

$$\frac{\partial^2\phi}{\partial x^2} = -\frac{1}{2}\left[\frac{2JF}{\nu_{H^+}\varepsilon\varepsilon_o}\right]^{\frac{1}{2}} x^{-\frac{1}{2}} \qquad [4.25]$$

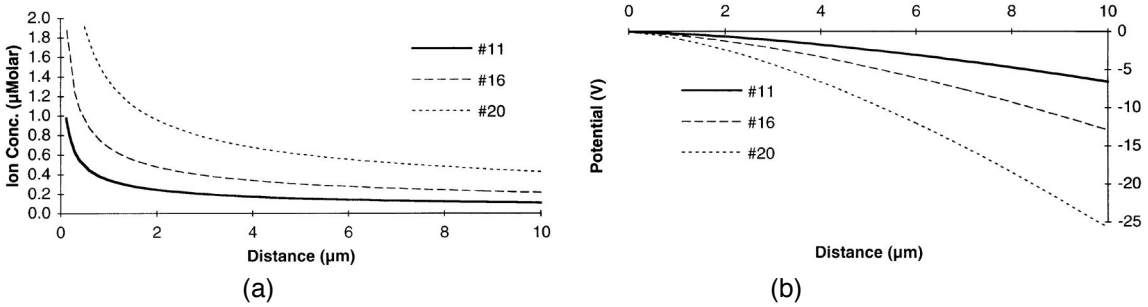

(a) (b)

Fig. 4.10 Concentration gradients (a) and potential gradients (b) in an unbalanced charge conduction layer. Note that the potentials here are expressed in Volts.

Table 4.6 Ion Depleted Region

	Trial 11	Trial 16	Trial 20
Current density (I)	0.32 A/m^2	1.25 A/m^2	5.0 A/m^2
Ionic Flux (J)	3.32 μMol/s•m^2	12.9 μMol/s•m^2	51.8 μMol/s•m^2
Hydrogen ion mobility ν_{H^+}	3.15x10^{-8} m^2/V•s		
$\left[\frac{2JF}{\nu_{H^+}\varepsilon\varepsilon_o}\right]^{\frac{1}{2}}$	0.31x10^{-9} V•m$^{-3/2}$	0.61x10^{-9} V•m$^{-3/2}$	1.21 V•m$^{-3/2}$

Matching Regions B & C — The assumptions for Region B lead to a zero ionic concentration at $x_B = 0$, in Region C the concentration of positive ions goes to infinity at $x_C = 0$. Clearly both of these cases are non-physical and there must be a transition from one region to the other at reasonable values of the ionic concentration. For the purposes of the analysis here, the two functions are matched where the electric field and electric field gradient are equal. This gives a function which is continuous in electric field but has a discontinuity in ionic concentration. The position of the match points in the coordinates of each region and the voltage gradients at the match points are given in Table 4.6.

An accurate solution would have to solve for electric field and ionic concentration in a transition region where both the concentration of unpaired positive ions and the concentration of negative chloride ions are both too large to ignore. An exact solution for this transition region is beyond the scope of this thesis, however, this region is relatively thin, less than a micron, with a voltage gradient on the order of 1,000 V/cm. An uncertainty of 25% in the voltage drop across this transition would only yield an error of ± 250 mV which does not affect the basic conclusions of this section.

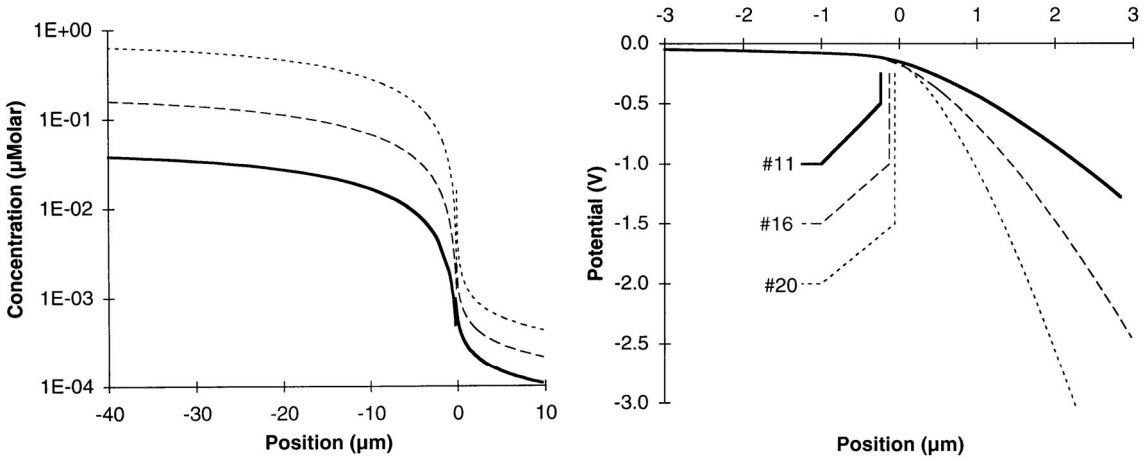

Fig. 4.11 Matching of Regions B & C. Position is indicated in Region B coordinates. Lines indicate position of transition. Note that ionic concentration is shown on a log scale.

Table 4.7 Matching Regions B & C

	Trial 11	Trial 16	Trial 20
Region B Position (x_B)	-0.24 μm	-0.13 μm	-0.06 μm
Region C Position (x_C)	0.12 μm	0.08 μm	0.01μm
Voltage Gradient	-1,080 V/cm	-1,690 V/cm	-1,060 V/cm

Summary of Conduction Without Convection — At constant current in the absence of convection it will take approximately one half second for a gradient layer to form at the cathode. This will cause a rise of 100 to 200 mV due to the increased resistance of the gradient layer. Once the gradient layer has formed it will move away from the cathode at 30 μm/s. After one second a 15 μm thick ion depleted layer will open between the gradient layer and the electrode. To maintain a constant current, the voltage in these three cases will have risen by 12, 24 and 47 V. In the highest current case, the voltage would reach the 1,000 V saturation of the current supply used in these experiments within 5 seconds.

This behavior is, in fact, never seen in a low viscosity electrolyte solution. The reason for this is the rapid transition to convective flow at the electrode. The nature of this transition to convection is the subject of the next section.

4.4.4 Conduction in the Solvent - Convection

Force on the Solvent - Without Convection — The only force available to drive convection on the micron scale of the electrochemical boundary layer is electrostatic force. Fig. 4.12 shows the body force on the fluid next to the cathode for the conductivity and current flux conditions of deposition 16 without convection. The body force on the fluid at any point is simply the product of the net electrostatic charge density per unit of solvent times the electric field at that point.

$$\boldsymbol{F} = qE \qquad [4.26]$$

The body force is a vector pointing toward the cathode, i.e. the solution is attracted to the cathode.

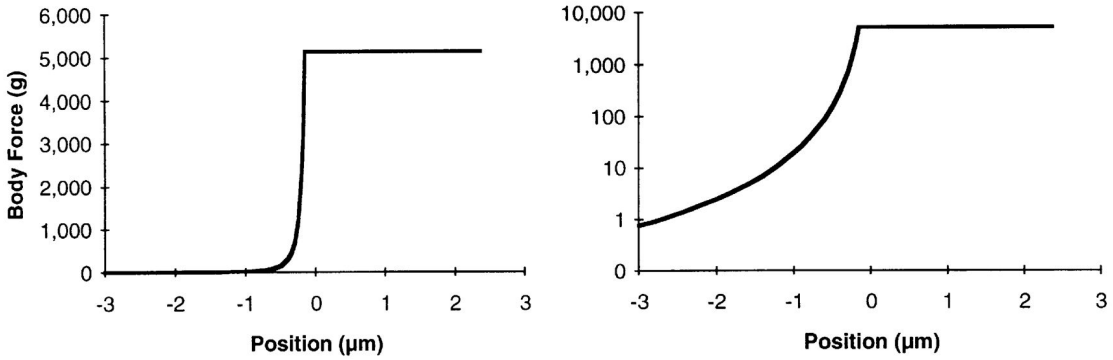

Fig. 4.12 Electrostatic body force on ethanol next to the cathode for current and conductivity conditions of Deposition 16. The force is given in multiples of the gravitational force on ethanol. Position is in reference frame for Region B. (a) linear scale, (b) Log scale.

In the gradient layer the electrostatic charge is calculated from the gradient of the electric field:

$$\frac{\partial^2 \phi}{\partial x^2} = \frac{q}{\varepsilon \varepsilon_o} \qquad [4.27]$$

in the gradient region the electrostatic charge and electric field both go up exponentially as the total ionic concentration drops. This gives a very rapid rise in the body force over the last few microns of the gradient layer.

In the unbalanced charge layer continuity gives the result that charge and electric field are inversely related, therefore their product, the body force, is constant.

Basis of Convective Instability — With the attractive force on the solvent rising toward the cathode, it is not immediately obvious why this layer should be convectively unstable. If this were a gravity/density gradient, this would be the definition of stability.

The fact that this layer is severely unstable to convection comes from the orders of magnitude difference in the transmission speed of changes in the solvent due to 1) electric field, 2) convection and 3) diffusion/migration, and in the response times of the

corresponding changes of the solvent 1) electrostatic charge/ionic flux, 2) fluid momentum, and 3) ionic concentration differences.

Changes in electric field are effectively transmitted instantaneously through the solvent. This results in a change in the direction and speed of ionic migration and therefore flux in the solvent. For our purposes here this change is also effectively instantaneous. Wherever there is a ionic concentration gradient there will also be a change in electrostatic charge. This only requires a small relative change in the position of positive and negative ions, and occurs on the scale of milliseconds. This charge then feeds back to modify the electric field in the solvent.

Convection can move parcels of solvent with different ionic concentration or chemical composition through the solvent as speeds from millimeters to centimeters per second. The time necessary for convection to begin will depend on the accelerating force per unit volume in the fluid. As shown in Fig. 4.12, the force on the fluid in this case reaches to several thousand times the force of gravity on that same unit of fluid.

Diffusion and migration are the slowest processes in the solution. The maximum diffusion speed in this problem is ≈3 mm/s in the highest concentration gradient regions. The maximum migration speed occurs for the positive ion in the charge depleted zone, reaching ≈5 cm/s. However, much more typical is the range of speeds in the charge balanced region of 30 μm/s up to 4 mm/s. This means that inhomogeneities in ionic concentration will be very slow to dissipate in comparison to electric field changes and convective motion.

Convective Instability - Example — Convection at the electrode will take the form of a vortex with fluid at one side moving toward the electrode and at the other moving away. To create a very simple conceptual and analytical model of this flow, the two sides of the vortex are replaced by two tubes, Fig. 4.14. One end of the tubes is open to the bulk solution while the other end terminates at the cathode. At the cathode end of the tubes there is a bridge which allows fluid motion from one tube to the other.

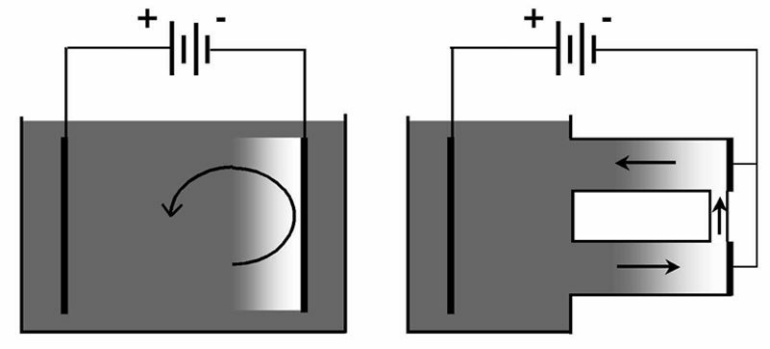

Fig. 4.13 A two dimensional circular vortex at the electrode (a) is modelled by two tubes hydraulically connected at the electrode surface (b).

To illustrate the forces driving convection the case shown in Fig. 4.14 is taken as a baseline case. In each of the tubes the gradient layer is assumed to have formed uniformly and moved away from the electrode by two and one half microns. A finite perturbation is then added. A one half micron layer of fluid from the depleted layer is moved instantaneously from tube B to tube A. Two cases at opposite extremes are then considered, constant current and constant voltage through each of the tubes.

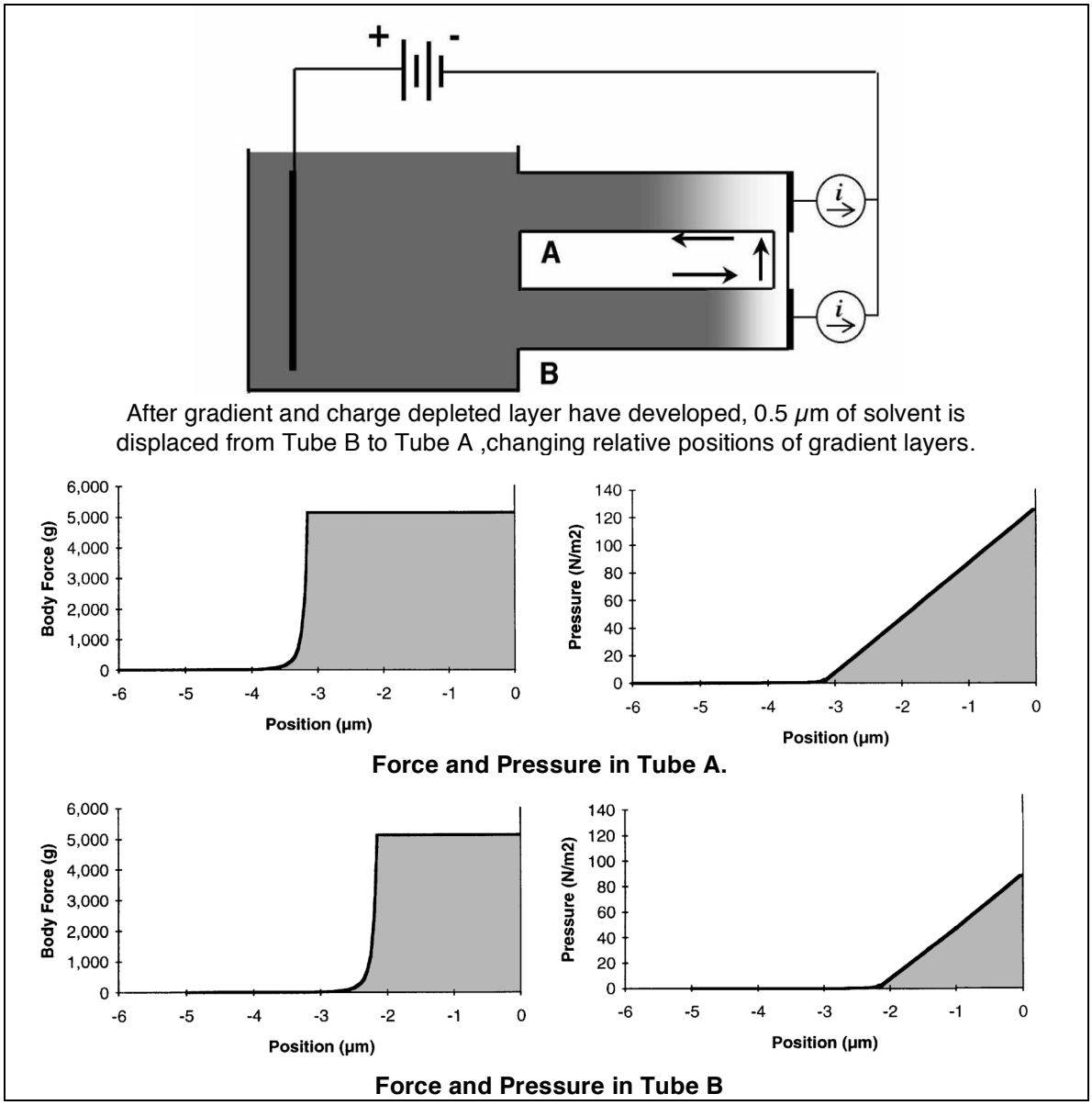

Fig. 4.14 If a constant current is maintained in each of the two tubes leading to the electrode, pressure forces will resist any flow between the tubes. In this case convection will be strongly damped.

The constant current case is the simplest and most intuitive. In this case the electrostatic body force on the solution remains the same, but in tube A the depleted layer is thicker. The integral of the body force from the bulk to the electrode gives the hydrostatic pressure at the electrode. With a thicker depleted layer, an identical body force is integrated over a longer distance, and the pressure at the electrode in tube A is higher than at the electrode in tube B. This would force the displaced fluid back into tube B until the depleted layers are the same thickness again. Thus in the case of a uniform current flux across the electrode surface, this layer would be stabilized against convection.

However, this intuitive case is not representative of the case in the unconstrained solution. The power supply will adjust so that the same total current is conducted through the solution, but there is no requirement that the current flux be uniform across the electrode surface. Given a uniform potential at the electrode and the much higher conductivity of the bulk solution relative to the gradient and depleted layers, these layers are best described as separating two equipotential planes.

Returning to the two tube example, when a portion of the depleted layer moves from tube B to tube A, the effective resistance of tube A increases dramatically while that of tube B drops equally dramatically. Using the hierarchy of effects laid out above, the first change will be in electric field, current flux, and electrostatic charge. The change in electrostatic charge and electric field will translate into an immediate change in body force and therefore hydrostatic pressure. The concentration profile in the gradient layer will initially be assumed constant, and the forces that would drive convection will be assessed.

In the base case when the gradient layer has moved away from the electrode by 2.5 μm, the total voltage drop over the 100 μm next to the electrode is 2.09 V. This is taken as the constant voltage for the following analysis. When one half micron of fluid is displaced from tube B to tube A, the current in tube A will drop by 33% while the current in tube B will increase by 55%. Although the total voltage drops are equal through each of the tubes, the electric fields are higher in tube B. The electric field gradients are also higher in tube B, which indicates higher net electrostatic charge. This higher electrostatic charge acted on by higher electric fields leads to much higher body forces on the solvent in tube B.

This is shown in the graphs in Fig. 4.15. The pressure at the electrode in tube B rises to 140 Pa from 110 Pa while the pressure drops to 80 Pa in tube A. In this case an initial disturbance will lead to a pressure difference that will drive the system further in the direction of the disturbance.

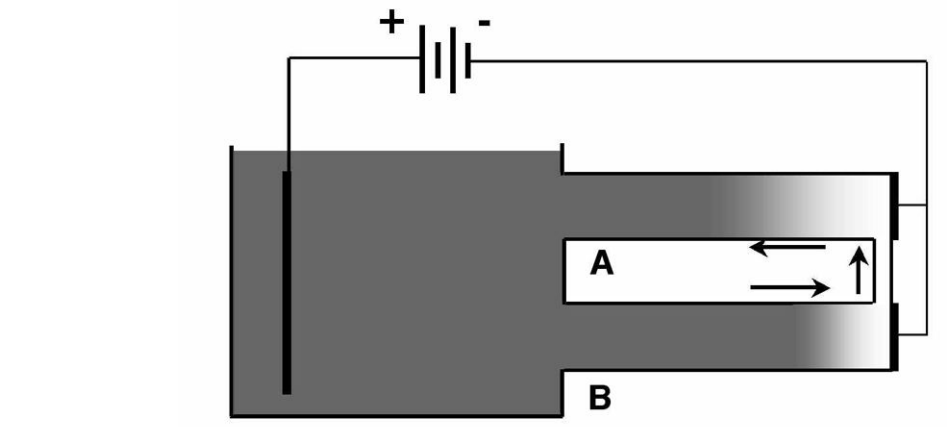

After gradient and charge depleted layer have developed, 0.5 μm of solvent is displaced from Tube B to Tube A ,changing relative positions of gradient layers.

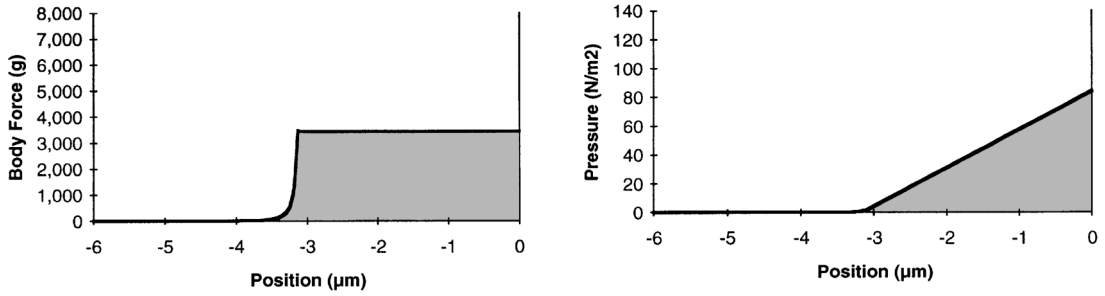

Force and Pressure in Tube A.

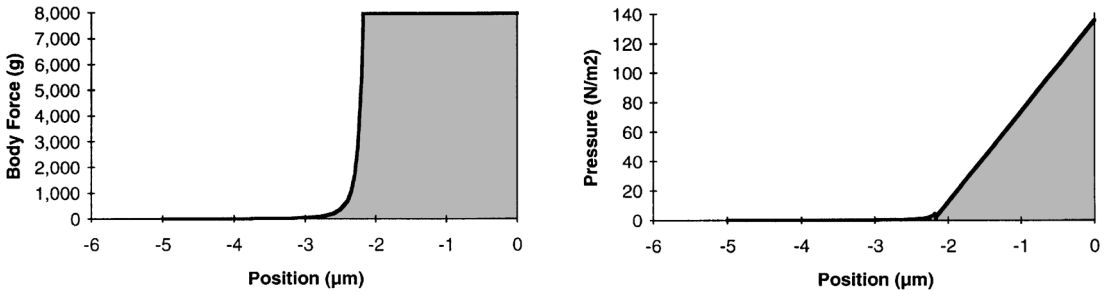

Force and Pressure in Tube B

Fig. 4.15 At a constant voltage, a small disturbance will lead to pressure forces which drive the system farther from equilibrium. This system is convectively unstable.

Once this instantaneous electrostatic/electrodynamic analysis is done it is now necessary to look at the slower responding phenomena, convection and diffusion. Convection is driven by pressure differences. In this case the instability of the charge depleted layer drives convection while convection increases the instability of the charge depleted layer. On the other hand, the increased conduction in tube B will cause the gradient layer to become steeper and recede faster from the electrode, with the opposite

occurring in tube A. Thus the change in speed of the gradient layers acts to dampen the instability.

In the two tube example of Fig. 4.15, the gradient layer in tube B would accelerate to 45 μm/s away from the cathode while slowing to 20 μm/s in tube A. This gives a relative speed of 25 μm/s.

To compare this to convection it is necessary to estimate possible convection speeds. This can be done by combining the pressure differential with an estimate of the mass to be accelerated. To get an order of magnitude estimate of the mass, a conservative estimate of an initial vortex size of 30 μm is taken. This would obviously include all of the depleted layer as well as the steepest portions of the gradient layer. This is then roughly approximated by making the two tubes in the above example 30 μm long. The pressure difference between the two tubes is 60 N/m^2 with a mass to be accelerated of 0.048 kg/m2. This gives an acceleration of 1,250 m/s^2. At this acceleration the convection speed would exceed the relative speeds of the gradient layers in 20 ns. If this pressure were stable over a distance of 0.5 μm the solvent would accelerate to 3.5 cm/s, more than one thousand times the speed of the gradient layers.

The example used here is somewhat exaggerated. It is unlikely that in a free solvent a several micron depleted layer would form. Because of the high instability of the these layers, it is far more likely that convection begins even before the gradient layer is fully formed. This is supported by current voltage measurements which show a simple linear resistance behavior when passing the limit current. Determining the actual point where convection begins is beyond the scope of the current discussion, however, this example gives a good example of the forces that develop in the absence of convection. This both serves as an illustration of the necessity of convection in the solvent without particles and background for the next section where the effect of particles is finally introduced.

Returning to the two tube example, convective motion will only proceed until the gradient layer comes up against the electrode in tube B. In this two tube example the system would quickly reach an equilibrium state with solvent flowing through the system at approximately 60 μm/s. Solvent flowing into tube B will exactly match the motion of the gradient layer relative to the solvent so that the gradient layer is stationary relative to the electrode. Virtually all of the current will be carried through this tube, with tube A filing up with ionically depleted solvent. The gradient layer will stabilize at a distance just far enough from the cathode that the electrostatic force on the solvent creates enough pressure to drive the convection.

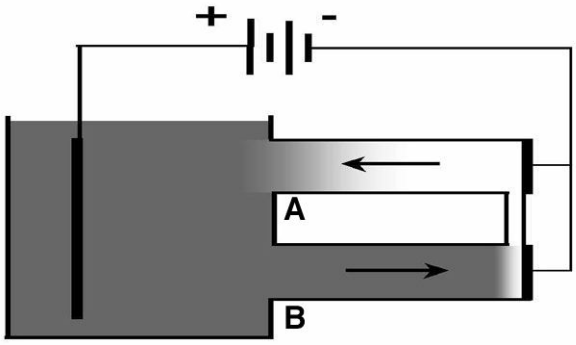

Fig. 4.16 Stable convection in two tube case. Almost all current will be carried by solvent in tube B while tube A fills with ion depleted solvent. The fluid will flow at a speed just sufficient to keep the gradient layer fixed relative to the electrode.

Stable Convection — The two tube example above is a case where geometric constraints on the system allow a stable convection pattern to develop. Having a fixed geometric constraint on the system on the same scale as the vortices is a condition for the formation of a stable vortex or system of vortices. These geometric constraints can be broken into electrode distance and pinning.

If the electrodes are close enough together that a single vortex between the electrodes provides sufficient transport to suppress the formation of additional vortices a stable system of vortices can form. This requires either the current be very low, leading to very slow vortex motion, or the electrodes be very close together. Examples of stable vortices between closely spaced electrodes are given in (**7, 8, 9**).

Fig. 4.17 gives an example from (**7**) of stable vortices forming between closely spaced electrodes. The anode is a transparent sputtered coating of conductive indium/tin oxide on glass. The cathode is platinum. The electrodes are parallel with a spacings of 175 and 120 μm in (a) and (b) respectively. The fluid is an electroluminescent rubrene electrolyte solution. The photographs are taken through the transparent anode looking at the cell perpendicular to the electrodes. The bright areas indicate where positively charged solution flows toward the cathode where electrochemical reduction causes it to luminesce, as shown in the schematic portion of Fig. 4.17. Note that the glowing areas occur at a spacing roughly 2x the interelectrode spacing, indicating a roughly circular crossection to the vortices.

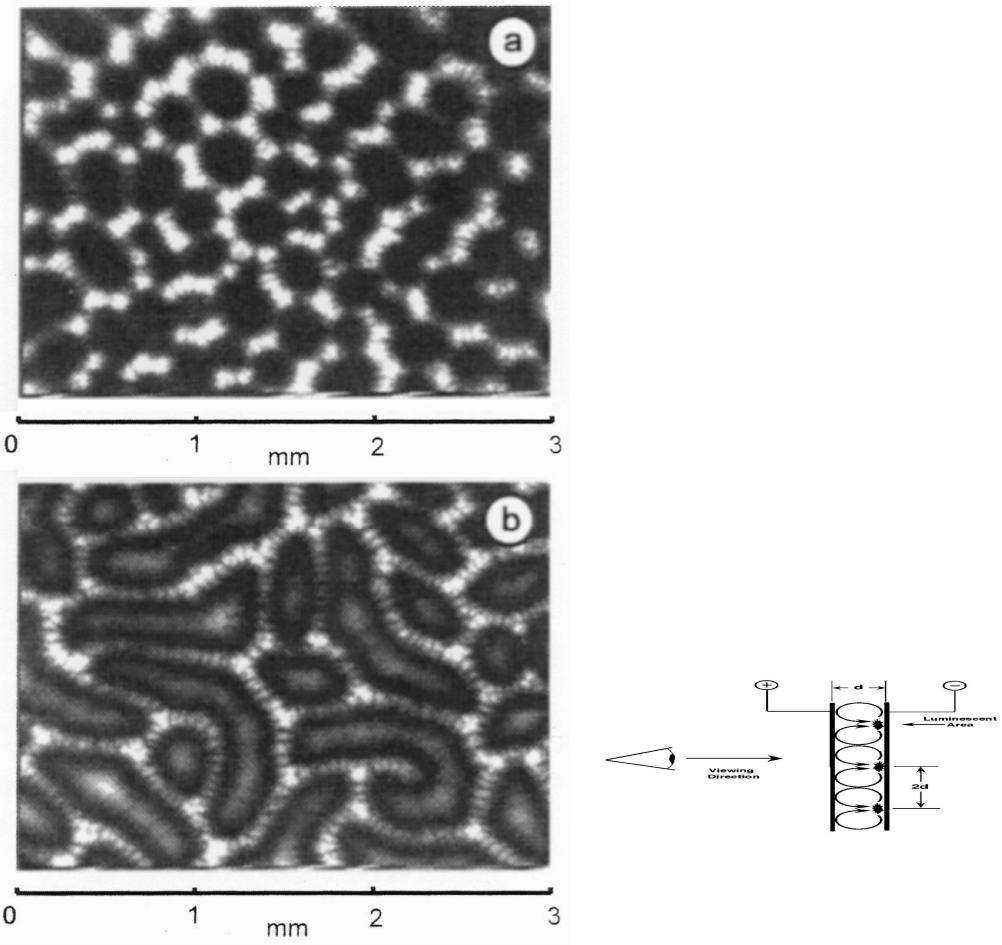

Fig. 4.17 Stable convective cells in DC conduction between closely spaced parallel electrodes, visualized using electroluminescent electrolyte photographed through transparent anode. Luminescent areas indicate flow impingement on the cathode. (a) Quasi-hexagonal arrangement of toroidal vortices, electrode spacing 175 μm, (b) Paired vortex tubes, white areas indicate flow impingement on the cathode, light areas indicate flow impingement on the anode, dark areas indicate flow parallel to the electrodes, electrode spacing 120 μm. From (**7**).

In Fig. 4.17(a) the vortices are essentially toroidal and arranged in a quasi-hexagonal pattern with fluid moving toward the anode in the center of the dark areas. These toroidal vortices represent the highest energy arrangement of vortices between two plates. The vortices in Fig. 4.17(b) show a slightly lower energy arrangement with the vortices arranged as parallel pairs of vortex tubes which connect back to each other at random distances.

Fig. 4.18 shows an entirely different system. This is a nematic liquid crystal between two glass plates being driven in conduction by an alternating current. The arrangement of multiple, parallel, counterrotating vortex tubes is an example of the lowest energy arrangement of stable vortices between two parallel plates.

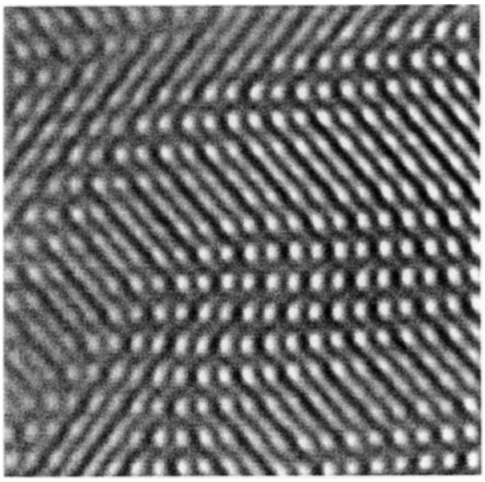

Fig. 4.18 Stable convective cells in AC conduction between closely spaced parallel electrodes, fluid is nematic liquid crystal solution as used for LCD displays, electrode spacing 26 μm, area shown is 497 μm square, the spacing between the parallel vortices is 18 μm. From (**8**).

There is an energy barrier between the quasi-hexagonal, toroidal vortex state and the parallel tubular vortex state, however, if there is sufficient instability in the system, it will evolve toward the parallel tubular arrangement. This transition can also be forced. If there is an overall flow of the fluid in one direction parallel to the electrodes, toroidal vortices will be stretched in the direction of the flow. This can cause the toroids to break and re-link to form long vortex tubes in the direction of flow. This can result in very commonly seen parallel ridge or deposition patterns during EPD where a larger convective flow directs the formation of parallel vortex tubes at the surface. A clear example of this is given in the photograph of the deposition of silver powder in Ch. 5.

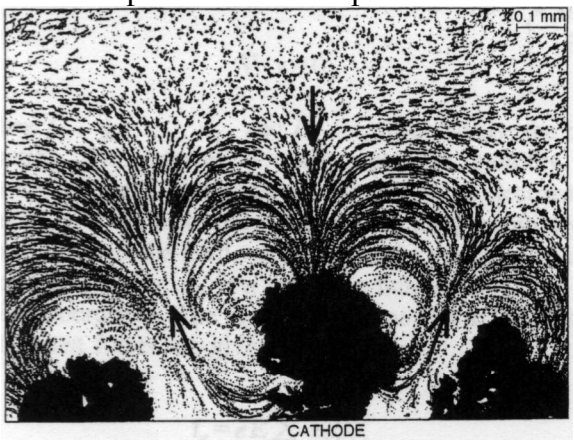

Fig. 4.19 Pinned convective cells From (**7**).

Stable vortices can also form around irregularities on the electrode surface. These can pin either the inflow or outflow of a vortex. An example of this is given in (**9**). Here growing filaments of copper focus electric fields on their tip and focus the inflow of fluid

to a specific point. This sort of pinning can also occur due to non-uniformities in the conductivity of the electrode or non-uniform accumulation of deposit forming on the electrode surface.

Free Convection — In the usual EPD cell the electrode is a uniform conductive surface, there is a large distance between the anode and cathode, and a current is used which is several orders of magnitude higher than the limit current for the cell. In this case circular vortices will form at the surface with the diameter and spacing on the same scale as the ionic concentration gradient layer. These vortices will increase ionic transport, but as the vortices themselves become ionically depleted they will grow out into the bulk solution. The resulting oval crossection of the vortices will not be stable and these vortices will break apart, merge and grow. The larger vortices will then provide more ionic transport to the surface. However, at some point the vortices will become large enough that they do not provide sufficient transport in the layer immediately adjacent to the electrode. Once again a steep ionic concentration gradient layer will form generating a new set of small vortices. In some cases a stable system can form where a large vortex transports ions in from the bulk and a set of small tubular vortices aligned with the larger vortex flow provide enhanced transport at the electrode surface. This is particularly common where the larger vortex is pinned by some inhomogeneity in the system. In other cases, particularly where the cell and electrode are uniform on the scale of the gradient layers, there will be a continuous, chaotic, "boiling" layer of vortices being generated, breaking, merging, growing, and re-generating.

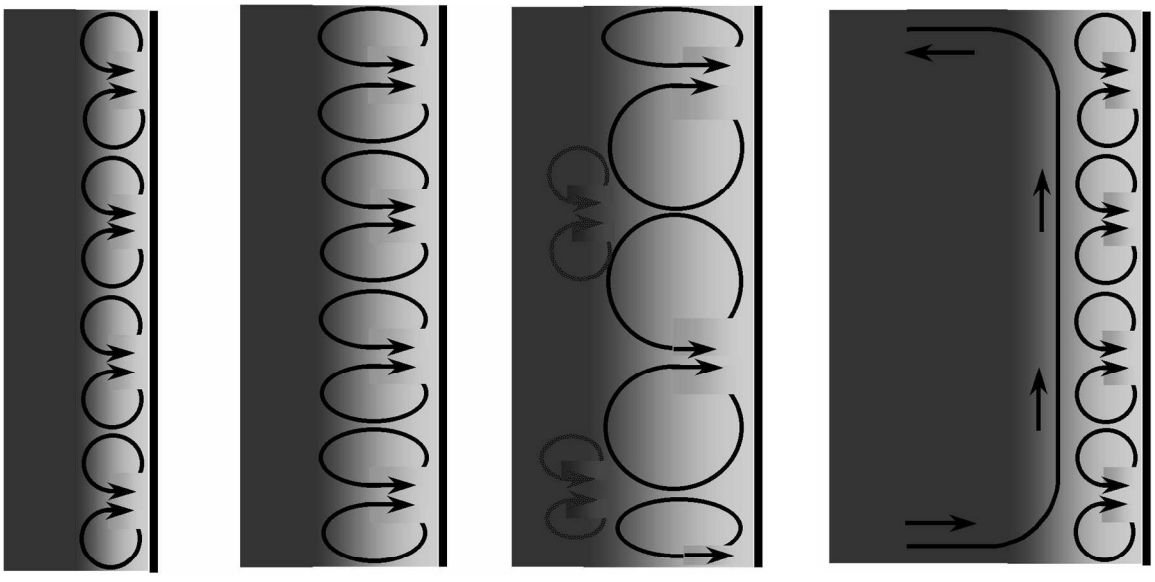

Fig. 4.20 Unstable convective cells.

4.4.5 Conduction in the Solvent - Effect of Particles

Having examined conduction without convection, the forces initiating convection, and the growth of convection, it should be clear the vital importance of ionic transport and ionic concentration changes in determining the behavior of a fluid in D.C. conduction. It is necessary to understand this first because of the somewhat surprising result that the most important effect of the addition of particles to this system is the change of ionic transport and the buffering of ionic concentration changes during D.C. conduction.

This result is counterintuitive because of the negligible effect the particles have on conductivity and conduction. As stated in Ch. 3, the difference in conductivity of a solution with 1 vol.% of particles either suspended or sedimented out was less than the margin of error in the conductivity measurement. Taking the net positive surface charge on the particles and the migration velocity of the particles in a D.C. electric field, the contribution to current flux in the bulk solution for the three cases here is 1.9, 0.4, and 0.06%.

However, when the total reversibly adsorbed HCl on the particle surfaces is considered, the picture is entirely different. The dissolved HCl in solution in these three cases is 0.045, 0.192, and 0.751 Mol/m^3. The available HCl on the surfaces of the suspended alumina is 0.865, 1.11 and 1.28 Mol/m^3. This means that, per unit volume, the amount of HCl which can desorb from the particle surfaces is 20, 6 and 2 times the HCl in solution. This applies to the molar flux of HCl as well. Taking the migration speed and concentration of the alumina particles in the bulk solution, the total flux of HCl carried by the particles is 11.7, 12.3 and 8.47 μMol/s•m^2 toward the cathode. This compares to the flux of dissolved chloride ions away from the cathode of 1.36, 5.32 and 21.3 μMol/s•m^2. Through the following analysis it should become clear how important the adsorption measurements of Ch. 3 are to understanding deposition in this system.

In this section particles that are stopped at the deposition electrode are only referred to as an accumulation of particles. Whether or how these particles form a deposition on the electrode is a subject for the next section. The effects of these particles on ionic gradients depend only on their presence, regardless of whether they have formed a rigid deposition or not.

4.4.5.1 Comparison of Trials #11 & #16

To begin with, the focus will be on deposition trial #'s11 and16. The objective will be to show why there is a stable linear voltage rise accompanied by deposition in trial #16 and no voltage rise or deposition in #11.

Bulk Migration — In the solution without particles, an ionic concentration gradient forms at the cathode as H^+ ions are consumed and Cl^- ions migrate away faster than they are replenished by diffusion from the bulk. With particles present, the migration of Cl^- ions away from the electrode will be countered by the electrophoretic migration toward the electrode of adsorbed Cl^- ions on the particles. In both cases #11 and #16, the flux of adsorbed Cl^- carried by the particles is greater than the migration of dissolved Cl^-. Wherever the particles are free to move by electrophoresis no large ionic concentration gradients would be expected to develop. Up to the front of accumulating particles at the electrode the ionic concentration in solution will be the same as the bulk.

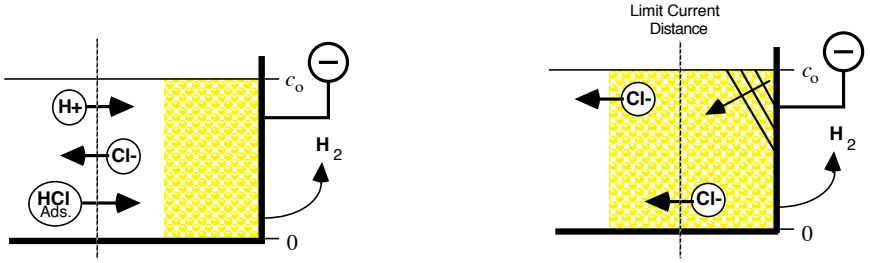

Fig. 4.21 In the bulk solution Cl^- migration is counteracted by electrophoretic motion of adsorbed HCl. At the cathode electrophoretic motion of the particles is stopped, but migration of Cl^- in solution continues.

Accumulated Layer — When they come up against the electrode, the electrophoretic motion of the particles stops. Where the electrophoretic migration is stopped, the flux of adsorbed Cl^- becomes zero while the migration of Cl^- in solution continues. It is in this area concentration gradients can develop.

Because there are no direct measurements of this layer, it is necessary to make some assumptions about the accumulation of particles at the electrode. In the bulk electric field of 13.9 V/cm in trial #11 the alumina particles will migrate at a speed of 13.5 μm/s. At the electrode the particles will accumulate at an estimated density of 20-25 vol. %. This gives an average interparticle separation of 80-90 nm. This estimated density is very approximate, and there will most likely be a density gradient through this accumulated

layer, however, the conclusions reached here will be valid for a wide variation in this density. At an average density of 25% the accumulated particle layer will grow at a rate of 0.375 μm/s, giving a total thickness of 45 μm over the 120 s of the deposition experiment.

In deposition trial #16 an accumulated layer density of 35% will be assumed. The reason for this higher assumed density will be given later. In the bulk electric field of 13.0 V/cm the particles will migrate at a speed of 11.0 μm/s, accumulating a 38 μm layer over the 120 s deposition time.

Assumed Gradient — Accurately modeling the development of these concentration gradients will likely require numerical simulation at some future date. However, by making some simplifying assumptions it is possible to establish a rough numerical criterion for what type of gradients will develop and when deposition of the particles will or will not occur. It is then also possible to qualitatively describe the development and shape of the concentration and potential gradients in this accumulated layer without the simplifying assumptions.

The greatest simplification can be made by replacing the actual non-linear adsorption isotherm with a simple linear adsorption for each of the cases. This is shown in Fig. 4.22.

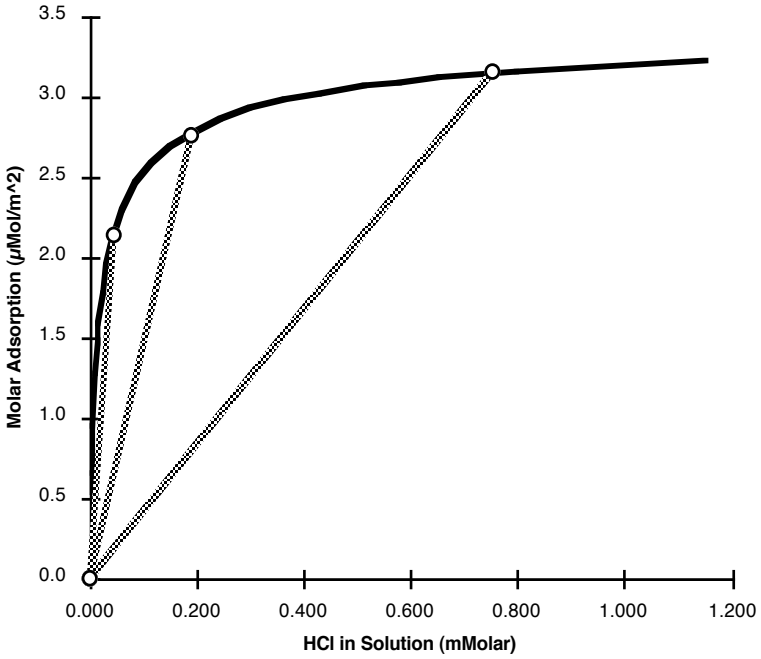

Fig. 4.22 Adsorption isotherm for HCl on alumina. Circles show the total adsorption for cases 11, 16 & 20. Lines show the linear adsorption assumption for each of the three cases.

The second assumption is that ionic concentration in solution is small relative to the adsorbed HCl in the accumulated layer. The implication of this second assumption is that desorption of HCl largely compensates for the consumption of H+ at the cathode and the migration of Cl- away. This means that the overall motion of the gradient layer will be slow relative to the movement of ions within the gradient layer. This then leads to the concept of the quasi-static, quasi-neutral gradient layer. In the Levich limit current case the migration of ions is blocked by the electrode at one end of the electrochemical cell, resulting in a constant ionic concentration at that point. In this case the desorption of HCl does not result in a fixed concentration but one that changes relatively slowly. Because of this slow change in concentration and therefore slow movement of the gradient layer, it approaches the behavior of a stationary gradient layer (quasi-static), and the analysis of Levich, given in section 2.2.8, can be applied. This means that a linear concentration gradient layer will form with a slope equal to the slope in the limit current case, declining from a point where the concentration is equal to the bulk solution to a lower concentration at the electrode.

The ionic concentration gradient in the accumulated layer will then develop as shown in Fig. 4.23(b). A gradient with a constant slope will form at the cathode and will move slowly away as the adsorbed HCl in the layer next to the electrode is desorbed and consumed. Only when the edge of the gradient layer has moved to the limit current distance from the electrode will the concentration at the electrode drop effectively to zero allowing a depleted charge conduction layer to form, and it is only the formation of a charge depleted conduction layer that can account for the large voltage rises seen in the deposition trials.

This analysis is then turned around to define a criterion for the formation of a charge depleted layer. A control volume is defined which is bounded on one side by the electrode and on the other by an imaginary plane at the limit current distance from the electrode. If the net flux of Cl- out of this volume is more than 1/2 of the Cl- within this volume then a charge depleted layer can be expected to form.

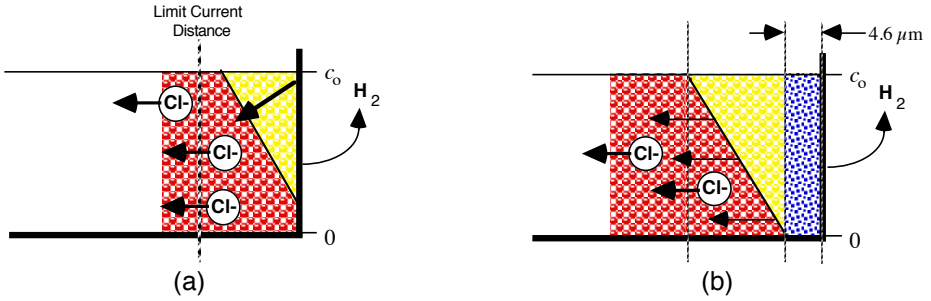

Fig. 4.23 (a) In deposition trial #11 the total Cl- flux out of the control volume is less than 1/2 of the total content. (b) Trial #16 gradient layer moves away from electrode creating ion depleted layer.

Applying this criterion to deposition trials #11 and #16 clearly shows the difference between the two. In #11 the limit current distance is 22 μm. Since electrophoresis of the particles over the course of this trial results in an accumulated layer of approximately

45 μm, the control volume can be assumed to be completely filled by particles at a volume density of 25%. This then gives a total content of HCl, both adsorbed on the particles and in solution of 476 μMol/m^2. The flux of dissolved Cl- out of this volume would be 1.36 μMol/s•m^2, or only 163 μMol/m^2 over the 120s of this trial. This is only 35% of the Cl in the control volume, therefore in this case the presence of reversibly adsorbed HCl on the surface of the particles will suppress the formation of a charge depletion layer. Little or no voltage rise would be expected. This is shown is Fig. 4.23 (a)

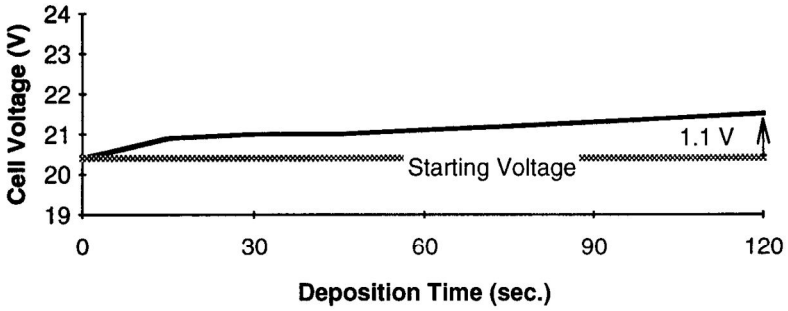

Fig. 4.24 Voltage rise during deposition trial #11 .

In the case of trial #16 the limit current thickness is 23 μm. Again this volume will be more than filled by particles due to electrophoresis during the deposition trial. This then gives a total content of HCl in the 23 μm control volume of 895 μMol/m^2. The molar flux of Cl- out of this volume is 5.32 μMol/s•m^2, or 628 μMol/m^2 over the course of the trial. This clearly exceeds the criterion set out above of 1/2 the molar contents of the control volume. In this case an ion depleted layer would be expected to develop. This is consistent with the 3.3 V rise actually seen during this deposition trial.

Assuming a constant gradient moves from the cathode, the total outward flux of Cl- ions could be accounted for by desorption from a 23 μm gradient layer and a 4.6 μm thick charge depleted layer. This 4.6 μm is calculated based on the 35 vol. % particle density assumption for the accumulated layer. If this 4.6 μm layer is consolidated to 60 vol. % by the high electric field in the depleted layer, the resulting layer would be 2.7 μm. This is only 20% less than the actual estimated deposition thickness of 3.3 μm.

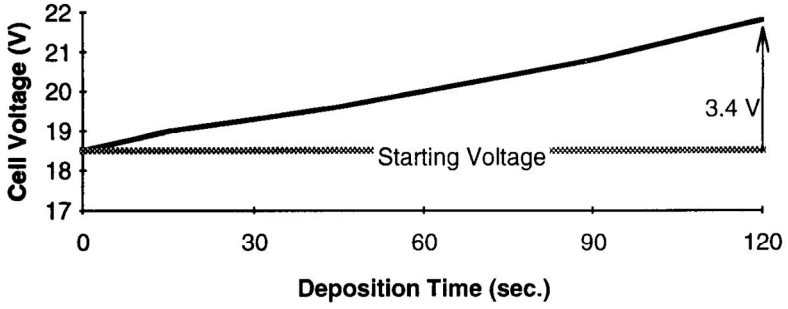

Fig. 4.25 Voltage rise during deposition trial #16 .

Actual Gradients — The one thing that does not fit in this picture is the early onset of the voltage rise in this deposition trial. According to the simple model above, it would take 84 seconds before 1/2 of the Cl- ions have migrated out of the control volume. This means that there should be an 84 sec. delay before the formation of an ion depleted layer with its accompanying anomalous voltage rise. However, as shown in Fig. 4.25, the voltage rise begins almost immediately and continues linearly through the duration of the deposition.

This can be accounted for by returning to the modeling of the adsorption isotherm. It is obvious by inspection that a simple linear model becomes a poorer and poorer representation of the actual adsorption/desorption behavior as the ionic concentration in solution increases. For the conditions of deposition trial #11 it is not unreasonable. However, for the conditions of trial #16 by the linear assumption 50% of the adsorbed HCl particles would desorb if the solution ionic concentration dropped by 50%. Based on the actual isotherm, in reality less than 10% would desorb by this point.

A very simple modification of the linear assumption can slightly improve the fit to the actual isotherm, but more importantly can illustrate one of the most important features of the concentration gradient in the presence of particles. The modification is as shown in Fig 4.26 below. It is assumed that there is zero desorption during the first 50% drop in solution concentration of HCl and the desorption is linear thereafter.

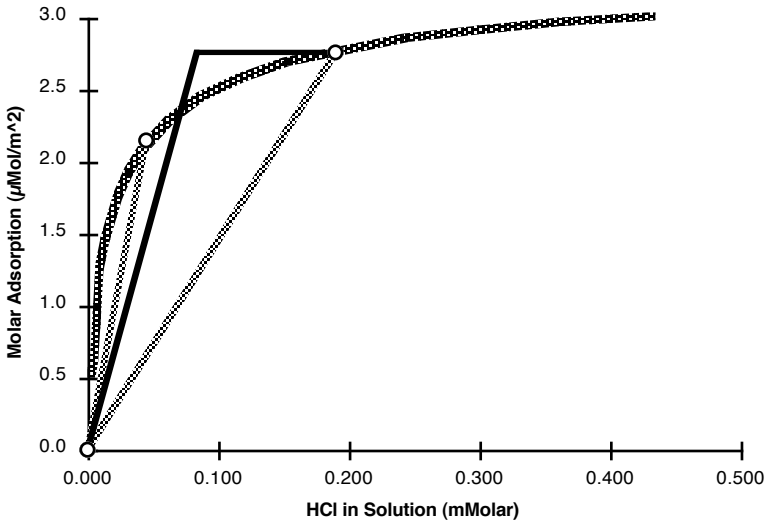

Fig. 4.26 Adsorption isotherm for HCl on alumina. Circles show the total adsorption for cases 11 & 16 Gray lines show the linear adsorption assumption. Black line is modified linear assumption for case 16.

The development of the gradient layers under this modified assumption would proceed as shown schematically in Fig. 4.27. When the current is turned on the concentration at the electrode will drop by 50%, which will be referred to as the 1/2 c_o point. Without buffering by desorption from the particles this will happen very quickly, on the order of a tenth of a second. Once HCl begins to desorb from the particles the 1/2 c_o point will move away from the electrode at a relatively slow rate. Because the current density has not changed the gradient between the 1/2 c_o point and the electrode will once again be the same as the quasi-neutral equilibrium gradient. The limit current distance is now between the 1/2 c_o point and zero at the electrode and is therefore 1/2 the previous distance, or 11.5 μm. One half the adsorbed HCl in this volume is only 112 μMol/m^2. This would be consumed in 21 seconds, after which an ion depletion layer would begin to form. As this quasi-static, quasi-neutral layer is forming, the gradient between the bulk solution and the 1/2 c_o point will flatten and broaden, asymptotically approaching a linear gradient between the 1/2 c_o point and the concentration at the opposite electrode. The development of this gradient can explain the voltage rise over the first few seconds before the voltage begins to rise due to the growth of the ion depletion layer.

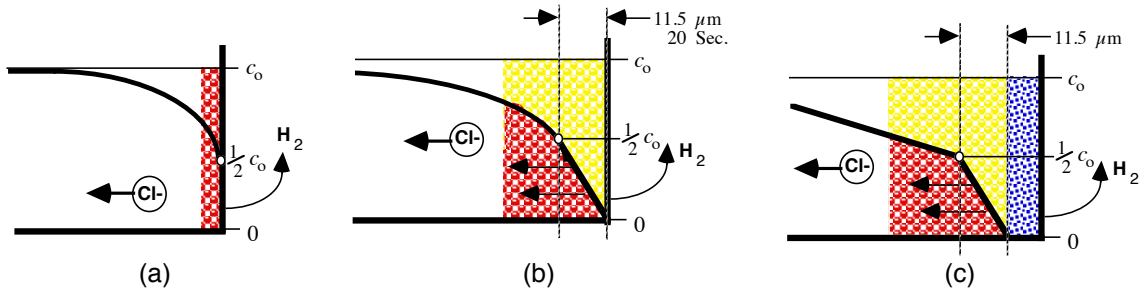

Fig. 4.27 Evolution of the concentration gradient layers under the modified desorption assumption of Fig. 4.x17 (a) the concentration at the electrode will quickly drop to 1/2 c_o (b) an 11.5 μm quasi-static, quasi-neutral gradient layer will slowly form. (c) the gradient layer will migrate opening up an ion depleted zone.

From looking at this modified assumption it is now possible to qualitatively describe the shape of the concentration gradients in the actual system. The key feature of the actual adsorption isotherm is that the desorption rate increases as the solution concentration decreases. At higher concentrations there is relatively little desorption. Most desorption occurs at low solution concentrations. The result is that most desorption coincides with the transition from quasi-neutral to unbalanced charge conduction.

Thus the actual gradients can again be separated into three regions: quasi-neutral, transition and ion depleted.

With particles present, the quasi-neutral region will no longer be characterized by a moving gradient but by an evolving gradient pinned at one end by desorption from the particles in the gradient region. This gradient will evolve in a similar manner to a thermal gradient in a homogeneous solid. The concentration will drop rapidly to a low level at the edge of the transition region and will evolve with time from an exponential drop near the transition layer toward a linear gradient across the cell. The electrostatic forces on the solvent in this region will be orders of magnitude less than the forces in the ion depleted region, but since the layer itself is orders of magnitude thicker it is just as likely to contribute to convection. The convection patterns will just be on a much larger scale - commensurate with the scale of the layer.

The transition layer is now larger and dramatically more important. This layer will be characterized both by unbalanced positive and negative ion concentrations, high voltage gradients and a majority of the desorption of HCl from the particles. The relatively slow motion of this layer is dictated by the desorption rate of HCl within the layer, and it is the motion of this layer which dictates the thickness of the ion depleted layer.

The ion depleted layer is regulated and stabilized by the transition layer. The role of particles in this layer is relatively minor. It appears from voltage measurements that the particles contribute just enough to conduction in this layer to offset the reduction in conductivity due to the physical blocking of the non-conductive particles. This contribution to conductivity could be either by catalyzing the auto-protolysis of the solvent or by promoting EHD convective transport within the pores.

4.4.5.2 Stabilization of Ion Depleted Layer

In discussing convection without particles it was shown that an ion depleted layer is very unstable to convection and no significant voltage rise due to an ion depleted layer is expected nor is found in actual experiments. However, the explanation for the voltage rise in these deposition trials depends on the formation of a stable ion depleted layer, therefore the presence of particles must stabilize the depleted layer. Here the vital role of the transition layer as outlined above becomes apparent.

The difference made by the particles can be illustrated by returning to the two tube example from above but now assuming the tubes to be packed with particles. Again the current is allowed to flow until a 2.5 μm ion depleted layer forms. If 0.5 μm of fluid is now displaced from tube B to tube A there will be virtually no change in the system. Since the quantity of HCl adsorbed to the particles is two orders of magnitude higher than the quantity of H^+ or Cl^- in solution, a motion of the fluid which leaves the particles in place

will have almost no effect. The ionic content of the solvent will be determined almost instantaneously by equilibrium adsorption/desorption in the pores between the particles. As long as the particles remain in place the position of the transition layer relative to the electrode will remain the same. This stabilizes the depleted layer against small, brief fluctuations in fluid motion.

However, it is possible to postulate a preponderate perturbation. Initially the particle density in the tubes is assumed to be 35 vol. %. The current is allowed to flow until a 3 μm depleted layer develops. If then in tube B the electrostatic force causes the particles in the ion depleted zone to suddenly consolidate to 52 vol. %, there will now be a 2 μm ion depleted layer in tube B and a 3 μm layer in tube A, the same situation as shown in Fig. 4.15. The electric field acting on the charged fluid will cause a hydrostatic pressure driving convection from tube B to tube A.

At this point the picture becomes more complicated and requires a combination of analysis, computer modeling and experiment to resolve. While there is an electro-hydrodynamic force driving convection, the viscous drag of the flow through the particle bed retards it. Higher voltage gradients in tube B will lead to a higher current flux. This means a faster migration of the transition region away from the electrode, and vice versa in tube A. Without particles the gradients move with the convecting fluid and can accelerate quickly toward or away from the electrode. With particles present, the location of the gradients are fixed by the particles and only move slowly in response to convective flows. This means that effect of diffusion and migration of ions can be on the same scale as the effects of convection. This also means that electric fields, diffusion and migration in the lateral direction can no longer be ignored.

It is clear from experimental results which show linear voltage rises accompanied by smooth uniform depositions that small perturbations are damped in the growth of these layers. This is direct evidence that within the particle layer viscous drag, adsorption/desorption and very high voltage gradients combine to allow migration and diffusion of ions to dominate over convective instability. Unfortunately, time does not permit the inclusion of a more complete analysis here, and the exact mechanisms and limits of this damping must be reserved for future discussion.

4.4.5.3 Deposition Trials #'s 16& 20

While the picture given above for deposition in trial #16 is complex, the evolution of the deposition process during trial #20 becomes even more so. In deposition trial #11 the accumulation of particles at the electrode suppressed the formation of a high voltage

gradient and no deposition occurred. In deposition trial #16 the flux of Cl- on the particles toward the electrode was higher than the migration of Cl- ions in solution away from the electrode. This means that high voltage gradients could only form within the accumulated particle layer. Adsorption equilibrium within this layer suppresses convective motion, and analysis based only ionic migration can account for the observed behavior. In deposition trial #20, on the other hand, the molar flux of Cl- ions in solution away from the cathode is 21.3 μMol/s•m^2 while the flux of Cl- on the particles toward the electrode is only 8.5 μMol/s•m^2. This means that the particles will neither suppress the formation of an ion depletion region, nor will they contain this region within the layer of accumulated particles at the electrode surface and thereby suppress convection.

Clearly, to account for the 18.9 V rise in cell voltage over the course of this deposition trial the particles must stabilize an ion depleted layer. However, without convection there would be a total flux of Cl- ions away from the electrode of 2500 μMol/m^2. The total Cl- quantity available in the region next to the electrode is only 1000 μMol/m^2. The remaining 1500 μMol/m^2 can only be accounted for by convective flows which wash Cl- ions from the bulk back toward the cathode.

Before entering into a description of the conduction layers in this deposition trial it is useful to review a combination of calculated and experimentally observed quantities. Based on the particle mobility in the bulk electric field of 14.1 V/cm, an accumulation of 31.7 g/m^2 of particles at the electrode would be expected. The weight of deposited particles after rinsing was 26.1 g/m^2 or 80% of the particles that would be expected to accumulate at the electrode. During rinsing, although it was not measured, a substantial overlayer of very loosely deposited material was removed. This appeared to be more than the 20% difference between the expected particle accumulation and the densely deposited layer. The densely deposited layer which could not be removed by rinsing will have a volume density of 50 to 60 %. This gives a thickness of 11 to 13 μm. Over the course of the deposition trial the voltage rose by 18.5 V. For the conditions of this deposition trial an 18.5 V potential difference would correspond to conduction through a stable ion depleted layer of 8 μm without particles present.

Ionic concentrations and concentration gradients will determine conductivity and mechanisms of conduction in the region next to the electrode. This in turn determines voltage gradients in the layer of particles accumulating at the electrode, which, in turn, determines the mechanism of deposition and consolidation of the particles. To describe the nature of the concentration gradients that develop during deposition #20 the following paragraphs will approach the system as a series of layers between the bulk suspension and the electrode.

The first layer is the fluid suspension outside the accumulated particle layer. Because there is a net flux of Cl- ions away from the cathode, the gradient layer will move away from the cathode faster than particles accumulate. This means that the gradient where the solution ionic concentration drops to very low values will continually try to move out of the accumulated particle layer into the fluid suspension. The fluid suspension, however, is convectively unstable in the presence of steep concentration gradients, therefore this layer will be in constant convection. Moreover, because this layer is not bounded nor are there any vortex pinning non-uniformities at the accumulating particle surface, this convection will be random and chaotic with vortices constantly forming, growing, merging, and re-forming. This means that at the surface of the accumulated particle layer the solution ionic concentration will be constantly fluctuating as an ion gradient attempts to migrate out of the accumulated layer and convection washes ions back in from the bulk solution.

At the surface of the accumulated layer is a low density particulate layer that serves as a buffer between the unstable convection of the fluid suspension and stable layers within the accumulated particle layer. When a convective flow moving toward the accumulated layer washes in solvent with a relatively high ionic concentration, the particles in the buffer layer will adsorb most of the extra ions before the flow can penetrate past the buffer layer into the accumulated layer. Where convection brings solvent with a higher ionic content up to the buffer layer there will be higher ionic and voltage gradients between the fluid suspension and the buffer layer. This will cause an increased local hydrostatic pressure which will cause the flow toward the electrode to spread laterally. The increased voltage gradient will also speed the outward migration of Cl- ions, depleting the ions which were adsorbed from the inward flow. Because of the steep slope of the adsorption isotherm at low solution concentrations, the total ionic concentration in this layer can fluctuate significantly while limiting solution ionic concentration to a very narrow range of values.

Behind the buffer layer is a transition layer in which the total concentration drops to the extremely low level that marks the beginning of the ion depleted conduction layer. Where the buffer layer is marked by continually varying ionic concentrations, the transition layer will be marked by a stable and steeply declining total concentration of HCl. In deposition trial #16 this transition layer will move outward at a speed dictated by the depletion of ions adsorbed to the particles in the accumulated layer. In this case, #20, the motion will be blocked by the buffer layer, which itself is tied to the motion of the boundary of the accumulated particle layer. The actual mechanism of this blocking is the backward diffusion of Cl- ions toward the cathode balancing the migration of Cl- away.

This means that the gradient in this case will be much steeper than in the case of deposition #16. Nevertheless, this layer still serves the same function as in deposition #16, which is to stabilize the boundary of the ion depleted conduction layer.

This ion depleted conduction layer is then the final layer. It is also the thickest and accounts for most of the voltage rise in during the deposition. The transition layer will be very thin and therefore there will be a sharp transition from the relatively moderate voltage gradients of quasi-neutral conduction to the extremely high voltage gradients necessary to drive unbalanced charge conduction in the ion depleted layer.

The primary difference between deposition trial #'s 16 and 20 is the mechanism regulating the thickness of the ion depleted layer. In deposition trial #16 the movement of the gradient layer is a function of ionic migration. In deposition trial #20 it is a function of the accumulation of particles. In both cases there will be a strong automatic leveling effect for the ion depleted layer.

In deposition trial #16 the thickness will be regulated by ionic flux. In any areas where the ion depleted layer is relatively thinner there will be a higher voltage gradient leading to faster outward migration of Cl- ions. This causes faster motion of the transition layer until the thickness of the ion depleted layer is evened out. Likewise thicker areas will be evened out by slower growth. In the conditions of this trial the automatic leveling effect only applies to the ion depleted layer. There is no mechanism to regulate the thickness of the accumulated particle layer. The total thickness of the particulate layer will be determined by convection and deposition cell geometry.

Under the conditions of deposition #20 there will be an automatic leveling effect for the entire deposition thickness. Because the motion of the transition layer is limited by the proximity of the surface of the accumulated layer, in areas where the total layer is thinner, the ion depleted layer will be thinner as well. This means that there will be a higher voltage gradient in the suspension attracting more particles to the thinner area.

4.4.5.4 Voltage Rise vs. Deposition Thickness

Throughout the previous discussion it was assumed that the anomalous voltage rise seen in the cases where a deposition formed was due to the formation of an ion depleted conduction layer. If this is correct then some correlation would be expected between an estimated ion depletion layer thickness and the deposition thickness.

The first step is defining what is the anomalous voltage. Deposition trials #5 through 9 had an average voltage rise of 0.4 V. Deposition trials # 10 & 11 showed the deposition of a monolayer of particles accompanied by voltage rises of 1.0 and 1.1V.

Based on these observations it will be assumed that 1 V of the voltage rise during deposition can be attributed to voltage necessary to drive a direct current through the solvent (often referred to as concentration polarization) and to voltage rise due to blocking of the electrode surface by deposited particles. The anomalous voltage is then taken as the voltage rise above one volt over the course of a deposition trial.

An ion depleted layer thickness can then be generated based on this anomalous voltage and the ionic flux density by using the equation for the potential drop across an unbalanced charge conduction layer, Eq. [4.23].

$$\phi = \phi_o - \frac{2}{3}\left[\frac{2JF}{\nu_{H^+}\varepsilon\varepsilon_o}\right]^{\frac{1}{2}} x^{\frac{3}{2}} \qquad [4.23]$$

The calculated thickness for each deposition trial from 12 to 21 is shown in Fig 4.28 as an 'x'. Superimposed on these calculated values are circular spots indicating the actual estimated deposition thickness based on a 60 vol. % density. The correlation is almost perfect for depositions 12 to 19. For depositions 20 & 21 the calculated ion depletion layer is 30% less than the actual estimated thickness.

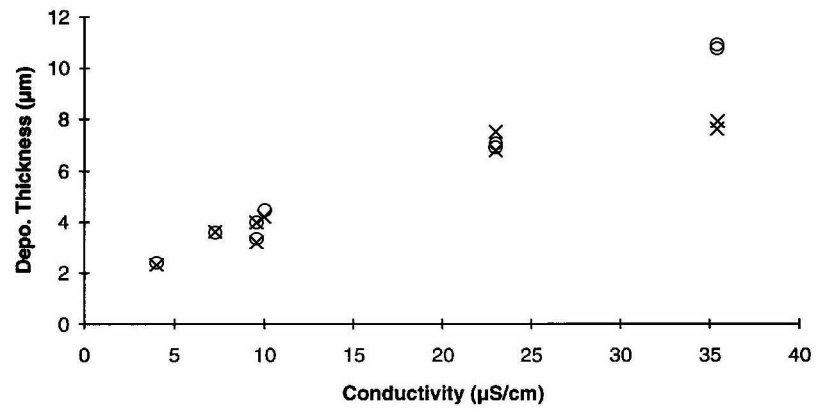

Fig. 4.28 X's are calculated ion depletion layer thicknesses, circles are deposition layer thicknesses based on experiment.

The correlation between the results of this calculation and the actual deposition thickness is actually much better than would be expected even if the theory were perfect. The depleted layer thickness calculation assumes unimpeded motion through pure solvent. In the deposition layer 60% of the volume will be occupied by non-conducting particles, leaving only 40 vol. % open porosity for ionic conduction. This should increase the resistance of the layer, leading to the expectation that the above calculation would give a higher thickness numbers than the actual deposition thicknesses. There are several possible explanations for this excess of accuracy. Determination of which explanation is correct will require further experimentation.

4.4.6 Deposition and Consolidation of Particles

Finally, the above discussion of conduction has provided sufficient background for address the putative subject of this chapter, the formation of a particulate deposition. All of the deposition trials made here began with an electrostatically stabilized suspension of particles. In some cases the repulsion force keeping the particles apart in suspension was overcome to yield rigid depositions of varying density and uniformity. The properties of these depositions can be accounted for by four mechanisms: 1. Electrostatic deposition, 2. Electrosedimentary deposition, 3. Convective deposition, and 4. Electrostatic consolidation.

Electrostatic Deposition —The definition of electrostatic deposition makes it appear to be one of the simplest mechanisms of EPD. In this case the force of the external electric field acting on an undeposited particle is sufficient to overcome the interparticle repulsion causing that particle to come into contact with an already deposited particle, thereby becoming part of the growing deposition.

This would be a simple mechanism if the DEBL around the particle was static. Unfortunately the diffuse layer is dynamic in several modes. It will polarize around the particle, it is pumped around the particle, and as it flows around the particle ions will be diffusing in and out of the layer. A quantitative understanding of how a deposited and undeposited particle come into contact and the electric field necessary to make this happen will most likely require computer simulation. Here there is only time for a very brief, but, hopefully, illuminating qualitative description.

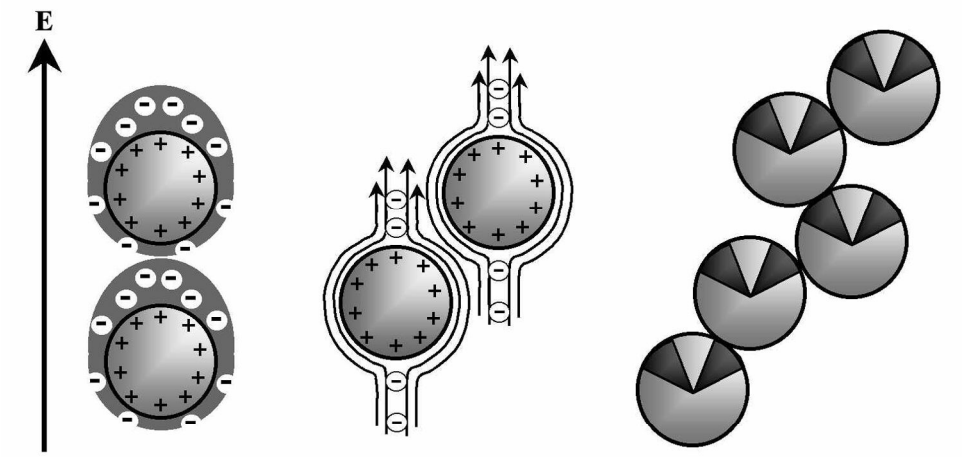

Fig. 4.29 (a) Polarization of a particle /boundary layer, (b) EHD convection make direct linear alignment unstable, (c) .

The first step is to begin with a single fixed particle surrounded by a diffuse electrostatic boundary layer. When an external electric field is applied the mobile ions in the diffuse layer will migrate to one side of the particle, creating an electric dipole. If this were a static dipole then a mobile particle would be expected to line up with the first particle on a line parallel to the electric field. However the ions in solution are mobile. The particle/diffuse layer dipole will attract ions from the solution at one end of the particle, the electric field will drive those ions in a layer of fluid around the particle, and they will diffuse outward on the other side. This creates an outward flow of solvent on the side of the particle away from the electrode. This then makes the position in a direct line with the electric field unstable for an approaching particle. At a position on a line perpendicular to the electric field there is no force to cause deposition. This means that between 0°, parallel to the electric field, and 90°, perpendicular to the electric field, there is a limited angular range where one particle will deposit on another. This type of deposition growth leads to very low density as angular chains and sheets of particles grow, blocking off considerable empty volumes between and below them.

The magnitude and importance of the polarization and EHD forces around a particle can be illustrated by looking at the electrophoresis of particles under the conditions of deposition trial #16. The electrostatic charge on an average sized (270 nm dia.) particle is 2.6x10-16 Coulomb. If polarization of the DEBL is ignored, the force on this particle due to the bulk electric field of 13 V/cm would be 3.4×10^{-13} Newton. If this force is balanced by a simple Stokes drag force, $6\pi\mu a u_\infty$, (μ= 1.07 mPa•s; a=135 nm) the particle's migration speed, u_∞, would be 126 μm/s. The actual speed based on the measured mobility is 11 μm/s. Thus the effects of EHD flows around the particle and polarization of the DEBL cause a 90% reduction in the migration velocity of the particle. This clearly shows the need for future work to consider the problem of the deposition of particles as a problem of electrohydrodynamics and not electrostatics.

Electrosedimentary Deposition —Electrostatic deposition becomes even more complicated as multiple particles are involved. The theory itself is very simple. The electric field will pull on a particle which itself will not deposit, however, the repulsive force will push on a particle closer to the electrode. Eventually the force on a large enough stack of particles will cause the particle closest to the electrode to deposit.

Unfortunately there are many problems with this very simple picture. The first is simply that the particles will not arrange themselves in a straight line. The undeposited particles will move relative to each other driven by electrostatic attraction, repulsion and

linking of EHD flows. It is possible that with thin boundary layers and low voltage fields the particles can be brought into a close packed arrangement where their movement is blocked. However, based on observations of various depositions it appears to be far more common that this layer remains low density and continues to behave as a fluid. Because of this, these particles need to be approached as dense colloidal layer rather than as individual particles.

The second complication is that at the same time as the electric field is pulling on the particles it is pushing on their DEBL's. This will cause a dielectric displacement reducing the electric field in this layer. The EHD flow of the DEBL's away from the electrode will also create a viscous drag force pushing the particles away from the electrode. This pushing and pulling points out a third complication with the simple view of the electrosedimentary mechanism. So long as this layer is charge balanced, the net electrostatic force on this layer will be zero. The same force that acts to attract the particles will act to repel the solvent around them. If there is to be a net electrostatic force on this layer it becomes a question of conductivity, conduction and ionic balance as was discussed above.

Although the net electrostatic force on this layer may be zero, this does not necessarily mean that the total force is. The pumping of the solvent in the DEBL's away from the electrode will create a hydrostatic pressure driving solvent the other way outside of the DEBL's to keep the volume constant. If the particles have become closely packed enough that this layer is effectively not fluid, this pressure can cause the innermost particles to deposit. The far more likely case is that the interaction of EHD flows around the particles will keep them from forming a closely packed arrangement. This layer will then still behave as a fluid, and any hydrostatic force that develops will drive convection rather than deposition.

With all of these confounding effects, the question then becomes, does this effect really exist? The answer is that it appears to exist, although the evidence for it is only indirect. Suspensions which have a calculated repulsion force greater than the force of the electric field on a single particle, can be deposited, and this can occur without a significant voltage rise which would indicate that a higher voltage gradient layer has formed. This mechanism appears to work only for suspensions which have a repulsion force only two or three times the force of the electric field and yields only low density depositions. The details of how this mechanism might work will require further experimentation and analysis.

Convective Deposition —This is the case where the hydrodynamic force of moving solvent can force particles into contact. If the solvent motion is perpendicular to the

surface, forcing particles straight into the deposition this can yield a dense, well packed deposition - similar to slip casting. If the flow is tangent to the surface particles will contact and deposit on high points on the surface leading to uneven growth and low density deposition. Unsteady flows will deposit particles in both modes leaving a mostly even but low density deposited layer.

Electrosedimentary Consolidation — Although exactly what happens during electrostatic deposition is unknown, once deposition has occurred and the accumulated particle layer is no longer fluid, this problem is transformed into the more familiar and tractable problem of conduction through a particle bed. Example analyses of this problem in the case of equilibrium conduction can be found in (**10, 11, 12**). The problem here is somewhat different given that fluid motion is blocked at one side of the particle bed, but otherwise the same factors apply to the analysis: electric field, surface charge density, and ionic content. The result is that there is a hydrostatic force on the entire layer as well as an electrostatic force on the particles in the layer, the magnitude of each being determined by the factors mentioned above. This combination of forces can consolidate what may begin as a very low density deposition. Since the sum of these forces will increase with depth into the deposition this can lead to a gradient of increasing density from the deposition surface to the electrode.

Ion Depletion Enhanced Electrostatic Consolidation — Part of the force acting on the particles in the electrosedimentary consolidation mechanism described above is an electrostatic force acting directly on the particles. An important part of the definition of that consolidation mechanism is that it occurs during equilibrium conduction. This is an important distinction because what happens during non-equilibrium conduction, specifically when an ion depleted layer begins to form and grow, is so dramatically different in nature and scale that virtually the only similarity is the application of the fundamental equations of electrostatics.

To appreciate the scale of the forces generated here it is helpful to return to the force calculations for a particle under the conditions of deposition trial #16. As mentioned above the force on the particle in equilibrium translation in the bulk electric field is 3.4×10^{-13} N, which is equivalent to 840 times the force of gravity on the same size particle. The viscous force due to EHD flow in the opposite direction is then approximately 770 G in the opposite direction, giving a net force moving the particle through the solution of 70 G.

This would seem like a fairly substantial force until a comparison is made to the force that can be generated in the ion depleted conduction layer. As a particle moves through the quasi-neutral gradient region into the transition region the HCl on the particle

will desorb, reducing the particle charge. However, as was shown in Ch. 3, in pure solvent the particle still has a significant positive charge of approximately $4x10^{-17}$ coulomb. Fig. 4.30(a) shows the potential gradient next to the electrode after an approximately 3 μm charge depleted layer has developed. This shows the extent to which the potential gradient changes from the 13 V/cm of the bulk suspension. Fig. 4.30(b) then shows the force that this electric field exerts on an average sized particle in this layer. One item to note is that in the charge depleted layer there will be no counter ions, therefore there will be no electrostatic boundary layer or EHD pumping of fluid away from the electrode to counter the direct electrostatic force. 100% of this electrostatic force goes into compacting the particles in this layer. The second item to note is the sharp rise in the force on the particles. Although the actual shape of the voltage gradient in the transition region has not been solved for here, it is clearly much less than a micron and is, in this case, on the same scale as the particles themselves. Despite the uncertainty about the exact shape of the transition region, it is possible to state that over a distance of two to three times the average particle diameter, the force on the particles will go up by an order of magnitude. This means that there can be a very sharply defined edge between a highly compacted deposition layer and an undeposited accumulated particle layer or a loose, low density deposited layer. Add to this the automatic leveling effect mentioned above and this mechanism can account for the thin, densely packed depositions with exceptionally uniform thickness that are frequently observed to be the product of a deposition accompanied by a linear voltage rise.

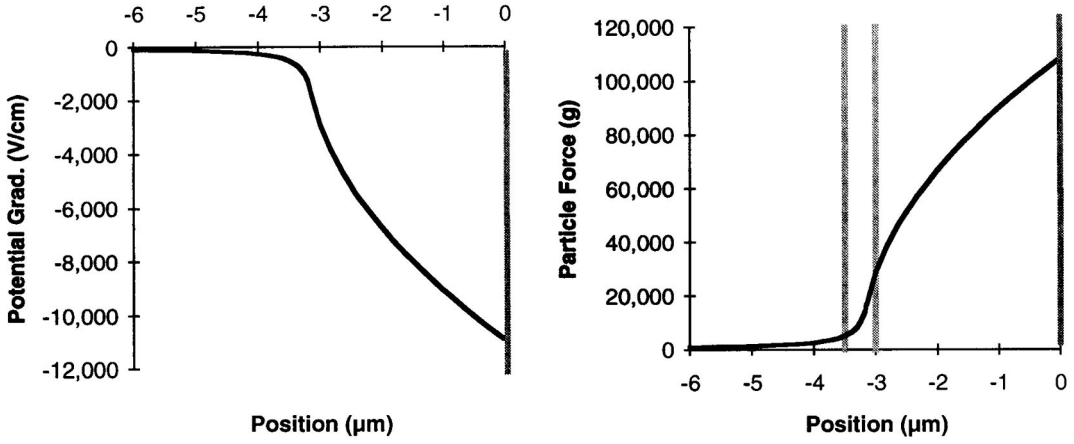

(a) (b)

Fig. 4.30 (a) Potential gradient with 3 μm depleted layer for conditions of deposition trial #16, 0 position indicates electrode surface; (b) Electrostatic force on an average size particle in multiples of standard gravitational force on the same particle. Gray bars indicate approximate location of transition layer.

4.4.7 Description of Experiment

Finally it is now possible to return to the description of what results were obtained in this series of deposition trials with the object of offering a description of why these results were obtained. In light of the above discussion, the three categories used to group the depositions as shown in Fig. 4.3 will now be extended to four, with deposition trial #'s 20 and 21 treated as a separate category.

Deposition Trials 1-4 — This set of trials was performed on a suspension with no added acid. As discussed in Ch. 3, the particles develop a positive 60 mV surface potential due to the dissociative adsorption of ethanol molecules and desorption of ethoxide ions. Due to the uncertainty of the actual ionic strength in the solution, the particle interaction force calculations are not shown here. However, knowing that the DEBL is thick and that the surface potential is relatively high allows two conclusions; a high surface potential means the energy barrier to floccing due to random motion is high and the thick boundary layer means that this interaction energy will be spread over a long distance leading to a low repulsive force. This means that the particles are well stabilized against floccing due to random motion in the quiescent solution but there is very little repulsive force resisting floccing by hydrodynamic or electrostatic forces.

When the current is turned on in these suspensions the solvent will rapidly transition to convection at the cathode. With no surface adsorbed ions the particles will have little effect on the development of ionic concentration and voltage gradients in the system. This convection was visible as the ripple patterns in all of the depositions, but is most obvious in the first deposition. Here inflowing suspension in the center of the deposition electrode allows a deposition to form while the balancing outflow of solvent at the edges of the electrode wash particles away leaving those areas bare.

The depositions that occurred in these four trials likely occurred by a combination of all three deposition mechanisms mentioned above. Convective deposition is a likely cause of the ridge patterns seen in the depositions when they are rinsed, but convective deposition cannot occur without some deposition occurring first by some other mechanism. The only other mechanisms available are electrostatic and electrosedimentary.

While convection may account for some deposition it is more likely to result in particles being washed away from the surface. Based on the bulk electric field and mobility of the particles, if the solvent were motionless and 100% of the particles accumulating at the electrode deposited, the expected deposition weight would be 54 g/m^2. This is very close to the actual deposition weight achieved in trial #3 of 53 g/m^2. However, that weight is after rinsing off a weakly deposited overlayer which would have raised the total weight well above expected. In contrast, deposition trial #4 yielded a deposition weight of only 34 g/m^2 even without rinsing. The wide scatter in deposition

results in these four trials indicate the importance of the manner in which convection develops on the final deposition results.

After the particles have deposited on the surface of these depositions they appear to be subject to electrosedimentary consolidation. This would need to be confirmed by more careful future measurements of density gradients, but visual observation suggests that the deposition density increases continuously from the deposition surface to the electrode.

Deposition Trials 5-11 — This set of deposition trials was performed on a series of suspensions where progressively more HCl was added to the solution. In this range the majority of that added acid was adsorbed by the particle surfaces resulting in a large rise in the particle surface potentials. Enough of the HCl remains unadsorbed, however, that the free ionic content goes up and the DEBL thickness goes down. The higher potential creates a higher energy barrier to floccing by random motion, and the thinner diffuse layer means that this energy rise occurs over a shorter distance, meaning a much higher maximum repulsive force exists as well.

Even this dramatically increased stabilizing force could potentially be overcome if it were possible to develop the extreme voltage gradients associated with the transition and unbalanced charge conduction layers. However, under the conditions of these deposition trials the adsorbed HCl on the particles is too high and the current flux too low to allow these gradients to develop. The result is that no anomalous voltage rise occurred in this set of trials and do deposition occurred beyond a monolayer of particles.

(The deposition of a monolayer of particles noted in deposition trials 10 and 11 involves the deposition of positively charged particles onto a negatively charged electrode surface. Despite its simple description this is a surprisingly complex process, the discussion of which must be reserved for a future work.)

Deposition Trials 12-19 — Although total surface charge does not change significantly over this set of trials, because of the increasing ionic concentration of the solution the surface potential declines steadily as the DEBL gets thinner. These two effects lead to a decrease in both the total energy barrier to floccing and the maximum interparticle repulsive force. Nevertheless, in all of these suspensions the energy barriers and repulsive forces remain high and the suspensions will exhibit long term stability.

The most important change here from the previous set of deposition trials is the change in the ratio of conductivity to adsorbed HCl. In deposition trials 5-11 the quantity of HCl adsorbed to the particles rose much faster than the conductivity, so desorption from the particles was able to suppress the formation of an ion depleted layer. In this set of trials the adsorption is reaching saturation and the bulk of the added HCl goes to increasing the conductivity of the solvent. With this increase in conductivity comes an increase in the current flux. The flux of Cl- ions out of the accumulated particle layer is now sufficient to

deplete the adsorbed Cl- on the particles next to the electrode, allowing an unbalanced charge conduction layer to form. Particles within this layer are compacted to almost maximum random packed density by the electrostatic force in this layer. This creates the dense, uniform deposition layer that is not removed by rinsing. That this layer is created by an ion depleted conduction layer is shown by the extraordinary match between estimated ion depletion layer thicknesses based on voltage rise and actual deposition thicknesses over this conductivity range, as shown in Fig. 4.29.

The ratio of conductivity to adsorption has not risen to the point that the flux of Cl- ions in the bulk away from the cathode is greater than the flux of Cl- adsorbed to the particles toward the cathode. This means that the electrophoresis of particles is able to suppress the formation of steep concentration gradient layers in the bulk solution that would drive EHD convection. Once the particles stop moving in the accumulated layer at the electrode they no longer prevent the formation of a gradient layer, but the large quantity of HCl that the particles can adsorb and release provides a vital role in stabilizing the gradient layers against convection within the accumulated particle layer. The high voltage gradients and the ionic buffering action of the particles creates a strong automatic leveling effect for the charge depleted layer. This means that the dense deposited layer can be extremely uniform over a large area regardless of non-uniformities of the electric field in the bulk suspension.

The fact that the net flux of Cl- ions in the bulk solution is toward the cathode means that particles will accumulate at the electrode faster than they are compacted into a dense deposition layer by the growth of the ion depleted layer. In the case of deposition trial #16, based on the particle mobility and bulk electric field the total particle accumulation at the cathode would be expected to be 53 g/m^2. Given the likelihood that convective motion of the suspension is suppressed, this estimate is likely fairly accurate. Of this only 8.1 g/m^2 is converted into a high density deposition. The balance is either not deposited at all or forms a weak, low density deposit which is easily rinsed off.

The ratio of particle accumulation to deposition is a topic for future study, but the fact that a significant overlayer of particles (tens of microns) remains on the surface of the deposition electrode as it is removed from the deposition device and transferred to the rinse solution indicates that a significant portion of the accumulated particle layer does form a rigid deposition. The fact that it then easily rinses off indicates that this deposited layer has a very low density. Since the only two mechanisms for deposition in this layer are either electrostatic or electrosedimentary, it is possible to state that under these conditions, electrostatic stabilization with a DEBL thickness approximately 10% of the average particle radius, these mechanisms will not yield a densely packed deposition in the absence of the ion depletion enhanced electrostatic consolidation.

Deposition Trials 20-21 — Although the estimated stabilizing energy barrier in these suspensions is low, the suspensions appear very stable with no visible sedimentation occurring over eight hours standing after the deposition trials were completed.

The primary difference between these two deposition trials and the previous set is the net Cl- ion flux in the bulk solution. In the previous set of depositions the sum of the Cl- ion migration in solution and Cl- ion migration on the surface of the particles gave a net Cl- ion flux toward the cathode. In these two trials conductivity has outstripped adsorption and the net Cl- flux is now away from the cathode. This means that the particles will no longer contain the formation of steep gradient layers within the layer of accumulated particles at the electrode. The suspension outside of the accumulated particle layer will transition to convection.

The large voltage rises here show that this convection outside the accumulated layer does not prevent the formation and growth of an ion depleted layer. Since an ion depleted layer is extremely unstable in the absence of particles, there must be a layer of particles which acts as a strong buffer between the unstable convection of the fluid suspension and the depleted layer. This is likely due to the high energy of adsorption of the Cl- ion to the particle surface and the resulting difference between Cl- in solution and adsorbed Cl- of several orders of magnitude. This, in combination with high voltage gradients, allows migration to dominate convective transport creating an effective constant current density condition.

The total deposition weight was 26.1 g/m^2. In the absence of convection based on the particle mobility and the bulk electric field, an accumulation of 31.6 g/m^2 of particles would be expected. The weight of particles rinsed off of the deposition was not measured, but the quantity rinsed off appeared to be more than the 20% discrepancy between these two numbers. This would suggest that electroconvective deposition was taking place, with convective flow accounting for the additional particle transport to create a thicker overlayer. This would have to be confirmed by future experimentation.

The most significant discrepancy is shown in Fig. 4.28. Based on the observed voltage rise, the ion depleted conduction layer would be expected to be 8 μm or less, while the depositions are approximately 11 μm thick. If the dense deposition and the depleted layer are the same thickness this would imply a much higher than expected conductivity of this layer. Alternatively, part of the overlayer could be compacted to a sufficient density to resist rinsing. This could occur by electrosedimentary compaction, hydrodynamic compaction due to convective flows, or a high voltage gradient transition region in the buffer layer leading to electrostatic compaction. Determining which of these explanations is correct will require further experimentation and analysis.

4.5 Conclusions

The objective of this chapter has been to present a detailed analysis of a simple deposition. A system was chosen which is known to produce good deposition results while being simple, stable, robust and reproducible. Alumina/ethanol with HCl has proven to be such a system. As shown in Ch. 3 the surface charge is uniformly positive and determined by a robust equilibrium between the solvent and Cl- in solution. The suspension is stable over an easily measurable range of conductivities and has a window of conductivities where uniform, dense depositions can be reliably reproduced.

The analysis of conduction made here shows that at constant current without convection or suspended particles, voltage would be expected to shoot up rapidly as an ion depleted conduction layer grows at the cathode. In the absence of some other transport mechanism, ionic migration and diffusion cannot provide sufficient ionic flux to the electrode under the conditions of ionic quasi-equilibrium. To maintain current an unbalanced charge layer must form which can only be created by very high voltage gradients. However, this analysis also shows that this type of layer is highly unstable to convection. The fact that no anomalous voltage rise is seen under constant current conditions in these electrolyte solutions indicates that convection begins almost immediately after the current is turned on and before a fully depleted layer can form.

The addition of suspended alumina particles dramatically changes this picture of conduction by changing ionic transport in the solution and buffering ionic content changes at the electrode. As HCl is first added to the alumina suspension most will be adsorbed to the particle surfaces with little remaining in solution to increase conductivity. As the particle surfaces become saturated, more and more of the added HCl will remain in solution and conductivity will begin to rise faster than total adsorption. This leads to three conduction regimes in this alumina/ethanol/HCl suspension:

1. *Convection - suppressed; depletion layer - suppressed* — In the low conductivity case ionic flux in solution is small compared to the flux of adsorbed ions carried on the surfaces of the particles. This prevents significant concentration gradients from forming and suppresses EHD convection. The large reservoir of adsorbed Cl- in the accumulated particle layer at the electrode prevents the formation of a depleted layer over the time of this deposition.
2. *Convection - suppressed; depletion layer - stabilized* — In this higher conductivity case the net flux of Cl- ions in the bulk is still in the direction of the cathode suppressing bulk convection, but the higher ionic flux is sufficient to deplete the adsorbed ions in the accumulated layer at the electrode. An ion depleted conduction

layer will form. It will be stabilized by the adsorption/desorption of ions in the transition layer, and a significant linear voltage rise is observed.

3. *Convection -active; depletion layer - stabilized* —In this high conductivity case the flux of dissolved Cl- ions in the bulk away from the cathode is greater that the flux of adsorbed Cl- on the particles moving toward the cathode. This means that steep gradient layers can form in the bulk solution which initiate convection. Convection then provides the additional ionic transport necessary to maintain constant current in the cell. However, the buffering effect of particles in the accumulated layer at the electrode still allows an ion depleted layer to grow. The high response of adsorption to small changes in solution concentration at low concentrations means that the particles can stabilize an ion depleted conduction layer — even in the presence of fluctuating ionic concentrations at the surface of the accumulated particle layer due to unsteady convection in the bulk solution.

Finally, with a picture of ionic concentrations, voltage gradients and convection states, it is possible to address the forming of a particulate deposition. Three mechanisms were presented as ways that particles in suspension could be forced into contact in the accumulated particle layer at the electrode: electrostatic, electrosedimentary, and convective deposition. While these mechanisms alone were able to create a deposition which was rigid enough to be removed from the deposition solution and handled, these depositions were low enough density, and therefore low enough strength, that they could easily be rinsed off. The prerequisite for the formation of a densely packed deposition layer is the presence of an ion depleted conduction layer. It is only the extreme voltage gradients in this layer that exert sufficient force necessary to compact the particles to maximum density.

An additional benefit of this stabilized ion depleted layer is a strong automatic leveling effect. Because the voltage gradients in this layer are several orders of magnitude larger than in the bulk suspension, even a small irregularity in the thickness of this layer can lead to a large deflection of the bulk electric field, ionic flux and particle electrophoresis. All of these effects act to strongly damp any thickness variation in the dense deposited layer.

Since the ultimate objective of EPD is usually to produce just these uniform thickness, densely packed layers of the particulate material, all of the various effects that occur in this type of deposition are collected under the name, "Ion Depletion Enhanced - Automatic Leveling" deposition. Although the depositions made here were from an electrostatically stabilized suspension this is not exclusive. Any set of deposition mechanisms where the primary role of forming the dense deposited layer and defining its

thickness is played by a stabilized ion depleted conduction layer would be included in this category.

Designing a suspension for Ion Depletion Enhanced deposition — There are three basic requirements for a suspension to be suitable for this deposition forming mechanism:

1. Depletion of the electrolyte at one electrode during conduction.
2. Particles which have a surface charge which is uniformly opposite that of the depletion electrode at all electrolyte concentrations down to that of the ion depleted layer.
3. Strong adsorption of the electrolyte by the particle surfaces.

Although these conditions may at first seem onerous, given the wide variety of solvent/electrolyte combinations available there is no reason this deposition forming mechanism could not be applied to a variety of non-conductive particulate materials. Two additional examples of this type of deposition are given in Ch. 5; PZT in acetone and TiO_2 in ethanol, both with iodic acid, HI, as the added electrolyte.

Recognizing Ion Depletion Enhanced deposition — The unmistakable sign that this effect is occurring is a continuous linear voltage rise at constant current over the course of the deposition.

Future Work — Although there are many questions that can still be asked about this deposition forming mechanism, the above analysis highlights two particular research directions that would be of the most value in confirming and extending these results, one experimental and the other analytic. On the experimental side the objective would be to directly observe density gradients and structure of a deposition without either rinsing or drying, and if possible, without even removing from the deposition from the deposition suspension. Some of the options for preserving this as-deposited structure are: freeze drying, supercritical drying, or metal infiltration by electrodeposition. On the analytic side what is needed is a series of finite element models beginning from a simple one dimensional diffusion, migration, desorption gradient model to three dimensional models incorporating convection. These would help to identify the critical points between stability and convection and illustrate more clearly how the particle surfaces act to buffer and stabilize what is normally an extremely unstable ion depleted conduction layer.

Appendix A

Fuoss Onsager Conductance Equation

The Fuoss-Onsager conductance equation is the summation of all of the effects on spherical ions moving by electrophoresis in an applied electric field. These effects are:

Electrophoresis — An ion will move in one direction due the applied electric field, but this motion will be retarded by the viscous force of oppositely charged ions moving in the opposite direction.

Dielectric Relaxation — The application of an electric field will cause positive and negative ions to move relative to one another, creating a polarization which reduces the effective electric field in solution.

Osmotic Pressure — Polarization of an ion relative to the counter ions around it will change the distribution of osmotic pressure experienced by that ion.

Viscosity — Oppositely charged ions will strike each other more often than would occur by random motion of uncharged ions. This leads to an increase in the effective viscosity experienced by an ion.

The Fuoss-Onsager equation gets its particular form the integration of the first three terms of the power series expansion of the Boltzman factor e^{ξ}. This leads to a form $const. - \ln(x) + x + ...$ The terms in $c^{1/2}$ are a result of the analysis of relaxation and electrophoresis.

The analysis of completely dissociated electrolytes in high dielectric constant solvents yielded the 1955 Fuoss-Onsager equation (**1**):

$$\Lambda = \Lambda_o - Sc^{1/2} + Ec\ln(_1 c) + J(a)c$$

The variables in this equation are Λ_o, the molar limit conductivity, c, the ionic concentration, and a, the radius of closest approach of the ion pair. S, E, and J are all determined by fundamental constants along with the solvent viscosity and dielectric constant.

In 1965 Fuoss, Onsager and Skinner (**2**) made a full theoretical treatment to extend the formula to solutions of ionogens which are not fully dissociated into ions and low dielectric constant solutions where ions can associate into non-conducting pairs by electrostatic attraction. The primary additional term in this equation is γ, the fraction of dissociated ions. This is related to the association constant K_A by the mass action equation: $1 - \gamma = K_A c\gamma^2 f^2 \Lambda$. This then gives the form of the equation used in this thesis:

$$\Lambda = \Lambda_o - S(c\gamma)^{1/2} + E'c\gamma\ln(6E_1'c\gamma) + Lc\gamma - K_A c\gamma f^2\Lambda$$

Following is a presentation of the components of this equation as presented in (**2**). The use of this formula is then illustrated by the analysis of conductivity measurements made for HCl in 99.43% ethanol used in Ch. 3.

Molar Limit Conductivity Λ_o

This is the theoretical molar conductivity of the electrolyte at infinite dilution.

Onsager Limit Slope $-S(c\gamma)^{1/2}$

This is the tangent slope of the molar conductivity function at zero concentration.

$S = \alpha\Lambda_o + \beta$

$$\alpha = \frac{8.204 \times 10^5}{(\varepsilon_r T)^{2/3}} \qquad \beta = \frac{82.5}{\eta(\varepsilon_r T)^{1/3}}$$

Third Order Terms $E' c\gamma \ln(6E_1' c\gamma)$

$$E' = E_1'\Lambda_o - E_2'$$

$$E_1' = \frac{2.942 \times 10^{12}}{(\varepsilon_r T)^3} \qquad E_2' = \frac{0.433 \times 10^8}{\eta(\varepsilon_r T)^2}$$

Fourth order terms $Lc\gamma$

$$L = L_1 + L_2(b)$$

$$L_1 = 3.202E_1'\Lambda_0 - 3.420E_2' + \alpha\beta$$

$$L_2(b) = 2E_1'\Lambda_0 h(b) + 44E_2'/3b - 2E'\ln(b)$$

$$\mathrm{h}(b) = \frac{2b^2 + 2b - 1}{b^3}$$

$$ab = \frac{1.671 \times 10^{-3} \dfrac{esu^2 \cdot cm \cdot {}^\circ K}{erg}}{\varepsilon_r T}$$ Bjerrum parameter $b\dfrac{esu^2}{erg} = \dfrac{e^2}{a\varepsilon_r kT}$

Adjustment for Ionic Association $-K_A c\gamma f^2\Lambda$

$$f_\pm = \exp\left[\frac{-\kappa e^2}{8\pi\varepsilon_o\varepsilon_r kT(1+\kappa a_o)}\right]$$ Ionic activity correction factor.

$$\kappa = \left[\frac{2e^2cz^2}{\varepsilon_o\varepsilon_r kT}\right]^{\frac{1}{2}}$$ Debye parameter.

Variables

Fuoss and Onsager consolidated many constants into single numbers in their listing of formulas in (**2**). Unfortunately, even though these numbers are not unitless, they did not include units for these numbers. This makes the use of these formulas less than intuitive for the first time user. To help clarify this, the units that need to be used for the variables in this equation are listed here, based on information from the book by Fuoss and Accascina (**3**).

T	Temperature in °K
η	Viscosity in Poise (0.1 N•s/m^2)
Λ_o	Molar Limit Conductivity μS•Liter/Mol•cm
a	Radius of closest approach in Centimeters
e	Unit Charge 4.802×10^{-10} esu
c	Ionic Concentration in Moles/Liter

Example

Fig. A.1 below shows calibration data for the conductivity of HCl in ethanol with 0.57 wt.% water collected during the preparation of Ch. 3. Superimposed on the data points is a plot of the Fuoss and Onsager 1965 equation calculated using the data below. Plus and minus 1% boundary lines show the measurement accuracy as compared to theory.

η	0.01101 Poise
ε_r	24.3
Λ_o	52.4 μS•Liter/Mol•cm
a	3.58×10^{-8} cm
K_A	Unit Charge 4.802×10^{-10} esu

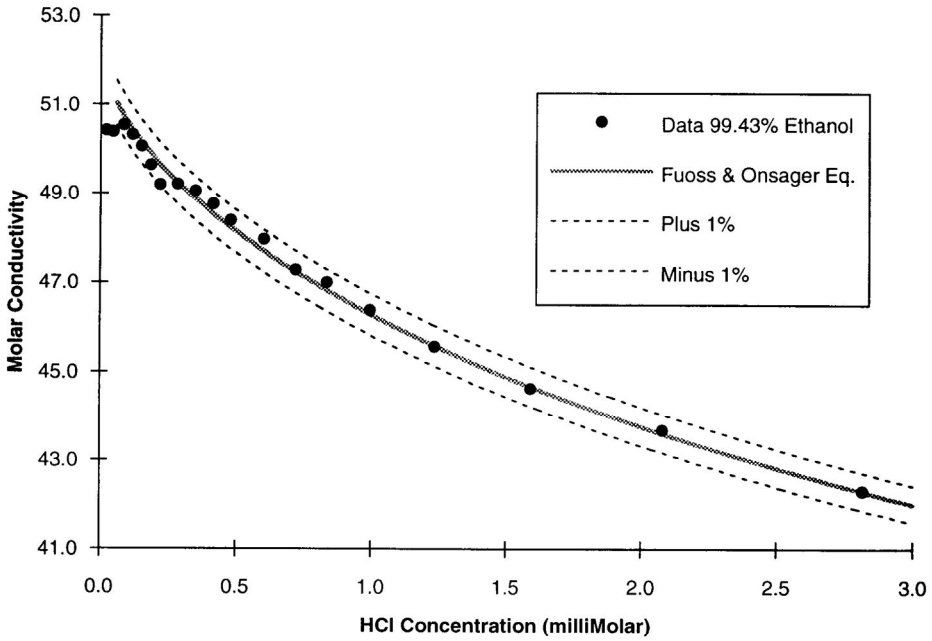

Fig. A.1 Fuoss-Onsager conductivity equation fit to data for the molar conductivity of HCl in 99.43 wt. % ethanol.

Appendix B

Determining potential in the quasi-equilibrium moving gradient layer.

This begins with the formula for total ion flux at any point and for the flux of chloride ions at any point in the gradient layer.

$$J = \left(D_{Cl^-} - D_{H^+}\right)\frac{\partial c}{\partial x} - \left(\nu_{Cl^-} + \nu_{H^+}\right)c\frac{\partial \phi}{\partial x} \qquad [4.10]$$

$$\frac{\nu_{Cl^-}}{\nu_{Cl^-} + \nu_{H^+}} J\frac{c}{c_o} = D_{Cl^-}\frac{\partial c}{\partial x} - \nu_{Cl^-}c\frac{\partial \phi}{\partial x} \qquad [4.11]$$

These were used in Ch. 4 to determine the following value for the concentration as a function of position in the gradient layer:

$$c = c_o - c_o \exp\left[\frac{J}{2c_o D_{H^+}}x\right] \qquad [4.18]$$

The first step in solving these equations for the potential gradient is to multiply Eq. 4.21 by $\frac{\left(D_{Cl^-} - D_{H^+}\right)}{D_{Cl^-}}$ to give:

$$\frac{\left(D_{Cl^-} - D_{H^+}\right)}{D_{Cl^-}}\frac{\nu_{Cl^-}}{\left(\nu_{Cl^-} + \nu_{H^+}\right)}J\frac{c}{c_o} = \left(D_{Cl^-} - D_{H^+}\right)\frac{\partial c}{\partial x} - \frac{\left(D_{Cl^-} - D_{H^+}\right)}{D_{Cl^-}}\nu_{Cl^-}c\frac{\partial \phi}{\partial x} \qquad [B.1]$$

This is then subtracted from Eq. 4.20:

$$\left[1 - \frac{\nu_{Cl^-}}{D_{Cl^-}}\left(\frac{D_{Cl^-} - D_{H^+}}{\nu_{Cl^-} + \nu_{H^+}}\right)\frac{c}{c_o}\right]J = \left[\frac{\left(D_{Cl^-} - D_{H^+}\right)}{D_{Cl^-}}\nu_{Cl^-} - \left(\nu_{Cl^-} + \nu_{H^+}\right)\right]c\frac{\partial \phi}{\partial x} \qquad [B.2]$$

The first diffusion/migration coefficient in the above equation can be simplified:

$$\frac{\nu_{Cl^-}}{D_{Cl^-}}\left(\frac{D_{Cl^-} - D_{H^+}}{\nu_{Cl^-} + \nu_{H^+}}\right) = \frac{\nu_{Cl^-} - \frac{\nu_{Cl^-}}{D_{Cl^-}}D_{H^+}}{\nu_{Cl^-} + \nu_{H^+}} = \frac{\nu_{Cl^-} - \nu_{H^+}}{\nu_{Cl^-} + \nu_{H^+}}$$

The second diffusion/migration coefficient term in square brackets in Eq. B.2 can also be simplified:

$$\frac{\left(D_{Cl^-} - D_{H^+}\right)}{D_{Cl^-}}\nu_{Cl^-} - \left(\nu_{Cl^-} + \nu_{H^+}\right) = \nu_{Cl^-} - \frac{\nu_{Cl^-}}{D_{Cl^-}}D_{H^+} - \nu_{Cl^-} - \nu_{H^+} = -2\nu_{H^+}$$

These can be substituted back into Eq. B.2 to give:

$$\left[1 - \frac{\nu_{Cl^-} - \nu_{H^+}}{\nu_{Cl^-} + \nu_{H^+}}\frac{c}{c_o}\right]J = -2\nu_{H^+}c\frac{\partial \phi}{\partial x} \qquad [B.4]$$

Re-arranging gives:

$$\frac{\partial\phi}{\partial x} = \frac{J}{-2\nu_{H^+}c}\left[1 - \frac{\nu_{Cl^-} - \nu_{H^+}}{\nu_{Cl^-} + \nu_{H^+}}\frac{c}{c_o}\right] = \frac{-J}{2\nu_{H^+}c_o}\left[\frac{c_o}{c} - \frac{\nu_{Cl^-} - \nu_{H^+}}{\nu_{Cl^-} + \nu_{H^+}}\right] \qquad [B.5]$$

Substituting in the previously determined value for c then gives the electric field as:

$$\frac{\partial\phi}{\partial x} = \frac{-J}{2c_o\nu_{H^+}}\left[\left(1 - \exp\left[\frac{J}{2c_oD_{H^+}}x\right]\right)^{-1} - \left(\frac{\nu_{Cl^-} - \nu_{H^+}}{\nu_{Cl^-} + \nu_{H^+}}\right)\right] \qquad [B.6]$$

Noting that the expression $-\left(\frac{\nu_{Cl^-} - \nu_{H^+}}{\nu_{Cl^-} + \nu_{H^+}}\right)$ can also be written as $\frac{2\nu_{H^+}}{\nu_{Cl^-} + \nu_{H^+}} - 1$, it is possible to separate Eq. B.6 into two terms:

$$\frac{\partial\phi}{\partial x} = \frac{-J}{c_o\left(\nu_{Cl^-} + \nu_{H^+}\right)} + \frac{-J}{2c_o\nu_{H^+}}\left[\left(1 - \exp\left[\frac{J}{2c_oD_{H^+}}x\right]\right)^{-1} - 1\right] \qquad [B.7]$$

This shows clearly that for large negative values of x the electric field will approach a constant number which is equal to the current flux divided by the conductivity of the solution, while the field rapidly approaches -∞ as $x \to 0$.

The electric field gradient can then be expressed using the chain rule as:

$$\frac{\partial^2\phi}{\partial x^2} = \frac{\partial}{\partial c}\left[\frac{-J}{c_o\left(\nu_{Cl^-} + \nu_{H^+}\right)} + \frac{-J}{2c_o\nu_{H^+}}\left[\frac{c_o}{c} - 1\right]\right]\frac{\partial c}{\partial x} \qquad [B.8]$$

Taking the derivative with respect to c :

$$\frac{\partial^2\phi}{\partial x^2} = \frac{J}{2\nu_{H^+}}\left(\frac{1}{c^2}\right)\frac{\partial c}{\partial x} \qquad [B.9]$$

The derivative of c as a function of x is then:

$$\frac{\partial c}{\partial x} = \frac{\partial}{\partial x}\left[c_o - c_o\exp\left[\frac{J}{2c_oD_{H^+}}x\right]\right] = -\frac{J}{2D_{H^+}}\exp\left[\frac{J}{2c_oD_{H^+}}x\right] \qquad [B.10]$$

Substuting this back into Eq. B.9 gives:

$$\frac{\partial^2\phi}{\partial x^2} = \frac{J^2}{4D_{H^+}\nu_{H^+}\left(c_o - c_o\exp\left[-\frac{J}{2c_oD_{H^+}}x\right]\right)^2}\exp\left[-\frac{J}{2c_oD_{H^+}}x\right] \qquad [B.11]$$

A slight re-arrangement yields the final form of the equation:

$$\frac{\partial^2\phi}{\partial x^2} = -\left(\frac{J}{c_o}\right)^2\frac{\exp\left[-\frac{J}{2c_oD_{H^+}}x\right]}{4D_{H^+}\nu_{H^+}\left(1 - \exp\left[-\frac{J}{2c_oD_{H^+}}x\right]\right)^2} \qquad [B.12]$$

The value of the potential as a function of position can then be determined by integrating Eq. B.7 :

$$\partial\phi = \left[\frac{-J}{c_o\left(\nu_{Cl^-}+\nu_{H^+}\right)} + \frac{-J}{2c_o\nu_{H^+}}\left[\left(1-\exp\left[\frac{J}{2c_oD_{H^+}}x\right]\right)^{-1}-1\right]\right]\partial x \qquad \text{[B.7]}$$

Using the following formula for the integration of the inverse exponential term:

$$\int\frac{dx}{1-\exp[kx]} = x-\frac{1}{k}\ln\left(1-\exp[kx]\right) \qquad \text{[B.13]}$$

gives an expression for the potential across the cell to the edge of the gradient layer;

$$\phi = \frac{-J}{2c_o\nu_{H^+}}\left[x-\frac{2c_oD_{H^+}}{J}\ln\left(1-\exp\left[\frac{J}{2c_oD_{H^+}}x\right]\right)-\left(\frac{\nu_{Cl^-}-\nu_{H^+}}{\nu_{Cl^-}+\nu_{H^+}}\right)x\right]+\phi_o \qquad \text{[B.14]}$$

By consolidating terms this becomes:

$$\phi = \frac{-J}{2c_o\nu_{H^+}}x\left[1-\left(\frac{\nu_{Cl^-}-\nu_{H^+}}{\nu_{Cl^-}+\nu_{H^+}}\right)\right]+\frac{D_{H^+}}{\nu_{H^+}}\ln\left(1-\exp\left[\frac{J}{2c_oD_{H^+}}x\right]\right)+\phi_o \qquad \text{[B.15]}$$

Using the Einstein relation for the ratio between difusion and migration (Eq. 4.3) brings this to the final expression:

$$\phi = -\frac{J}{c_o\left(\nu_{Cl^-}+\nu_{H^+}\right)}x+\frac{RT}{F}\ln\left(1-\exp\left[\frac{J}{2c_oD_{H^+}}x\right]\right)+\phi_o \qquad \text{[B.16]}$$

Here it becomes obvious that the first term is the linear voltage gradient driving conduction in the bulk solution with the second term being the additional voltage gradient necessary to drive the same ionic flux in the gradient region.

References

Chapter 3

1. Hamaker, H.C., and Verwey, E.J.W., "The Role of the Forces Between the Particles in Electrodeposition and Other Phenomena", *Trans. Faraday Soc.*, **36,** (1940) 180-185

2. H. Koelmans, and J.Th.G. Overbeek, "Stability and Electrophoretic Deposition of Suspensions in Non-Aqueous Media", *Disc. Faraday Soc.*, **18** (1954) 52-63

3. Malkin, E.S., and Dukhin, A.S., "Deposition of Colloidal Particles on an Electrode in an Alternating Electric Field", *Kolloid. Zh.*, **42,** (1980) 396

4. Sarkar, P., and Nicholson, P. S., "Electrophoretic Deposition (EPD): Mechanisms, Kinetics, and Application to Ceramics", *J. Am. Ceram. Soc.*, **79,**(1996) 1987-2002

5. Parks, G. A., *Chem. Rev.*,"The Isoelectric Points of Solid Oxides, Solid hydroxides, and Aqueous Hydroxo Complex Systems", **65,** (1965) 177-198

6. Romo, L. A., "Effect of C3, C4 and C5 Alcohols and Water on the Stability of Dispersions with Alumina and Aluminum Hydroxide", *Discuss. Faraday Soc.* **42,** (1966) 232-237

7. Lind, J.E. Jr., Zwolenik, J. J., and Fuoss, R. M., "Calibration of Conductance Cells at 25° with Aqueous Solutions of Potassium Chloride", *J. Am. Chem. Soc.* **81,** (1959) 1557-1559

8. Graham, J. R., Kell, G. S., and Gordon, A. R., "Equivalent and Ionic Conductances for Lithium, Sodium and Potassium Chlorides in Anhydrous Ethanol at 25°", *J. Am. Chem. Soc.*, **79,** (1957) 2352

9. Kay, R. L., "An Application of the Fuoss-Onsager Conductance Theory to the Alkali Halides in Several Solvents", *J. Am. Chem. Soc.*, **82,** (1960) 2099-2105

10. De Lisi, R., Goffredi, M., and Liveri, V. T.,"Effect of Water on Proton Migration in Alcoholic Solvents, Part 4.—Conductance of Hydrogen Chloride in Butan-2-ol and in Ethanol at 25°C", *J. C. S. Faraday I*, **72,** (1976) 436-447

11. Fuoss, R. M., Onsager, L., and Skinner, J. F., "The Conductance of Symmetrical Electrolytes. V. The Conductance Equation", *J. Phys. Chem.,* **69,** (1965) 2581-2594

12. O'Brien, R. W., and White, L. R., "Electrophoretic Mobility of a Spherical Colloidal Particle", *J. Chem. Soc. Faraday II*, **74,** (1978) 1607

13. Dukhin, A.S., Goetz, P.J., Wines, T.H., and Somasundaran, P., "Acoustic and Electroacoustic Spectroscopy", *Colloids and Surfaces A*, **173,** (2000) 127-158

14. Sawatzky, R. P., and Babchin, A. J., "Hydrodynamics of Electrophoretic Motion in an Alternating Electric Field", *J. Fluid Mech.*, **246,** (1993) 321-334

15. Henry, D. C., "Cataphoresis of Suspended Particles", *Proc. Roy. Soc. Lond. A,* **133,** (1931) 106

16. Loeb, A. L., Overbeek, J. Th. G., and Wiersma, P. H., *The Electrical Double Layer Around a Spherical Colloidal Particle*. MIT Press: Cambridge, Massachusetts, 1961

17. O. Popovych, and R.P.T. Tomkins, *Nonaqueous Solution Chemistry*. Wiley Interscience Publications, New York, 1981

18. Caldin, E. F., and Long, G., "The Equilibrium between Ethoxide and Hydroxide Ions in Ethanol and in Ethanol Water Mixtures", *J. Chem. Soc*., 3737 (1954)

19. Hunter, R. J., *Zeta Potential in Colloid Science, Principles and Applications*, Academic Press, New York, 1981

20. Isrealachvilli, J., *Intermolecular and Surface Forces, 2nd Edition*, Academic Press, New York 1992

Chapter 4

1. Sarkar, P., Huang, X. and Nicholson, P.S., "Electrophoretic Deposition and Its use to Synthesize YSZ/Al2O3 Micro-Laminate Ceramic/Ceramic Composites", *Ceram. Eng. Sci. Proc*., **14** (1993) 707-726

2. Graham, J. R., Kell, G. S., and Gordon, A. R., "Equivalent and Ionic Conductances for Lithium, Sodium and Potassium Chlorides in Anhydrous Ethanol at 25°", *J. Am. Chem. Soc*., **79,** (1957) 2352

3. Russel, W.B., Saville, D.A. and Schowalter, W.R. , *Colloidal Dispersions,* Cambridge University Press, Cambridge, (1989)

4. Laboratory Safety Manual, Department of Environmental Health and Safety, Penn State University.

5. Levich, Veniamin G., *Physicochemical Hydrodynamics,* Prentice-Hall, Englewood Cliffs, NJ (1962)

6. Chazviel, J.-N., "Electrochemical Aspects of the Generation of Ramified Metallic Electrodeposits", *Phys. Rev. A,* **42**[12], (1990) 7355-7367

7. Orlik, M., Rosenmund, J., Doblhofer, K., and Ertl, G., "Electrochemical Formation of Luminescent Convective Patterns in Thin Layer Cells", *J. Phys. Chem. B*, **102**[8], (1998)

8. Bisang, U., and Ahlers, G., "Bifurcation to Worms in Electroconvection," *Phys. Rev. E,* **60**[4], (1999)

9. Marshall, G., Mocskos, P., Swinney, H. L., and Huth, J. M., "Buoyancy and Electrically Driven Convection Models in Thin-Layer Electrodeposition", *Phys. Rev. E*, **59**[2], (1999)

10. Rice, C.L., and Whitehead, R., "Electrokinetic Flow in a Narrow Cylindrical Capillary", *J. Phys. Chem*., **69[**11], (1965) 4017-4024

11. Tavares, M.F.M., and McGuffin, V.L., "Theoretical Model of Electroosmotic Flow for Capillary Zone Electrophoresis", *Anal. Chem.,* **67**, (1995) 3687-3696

12. Wan, Q-H., "Effect of Electrical Double Layer Overlap on the Electroosmotic Flow in Packed Capillary Columns", *Anal. Chem.,* **69**, (1997) 361-363